THE UNIVERSITY *of* LIVERPOOL

A Study of Glueballs and Scalar Mesons in Lattice QCD.

Steven Miller

A Thesis submitted in accordance with the requirements of the University of Liverpool for the degree of Doctor of Philosophy.

Department of Mathematical Sciences

February 2005

Declaration

I hereby declare that all the work described in the thesis is the result of my own research activities unless reference is given to others. None of this material has been previously submitted to this or any other University. All work was carried out in the Theoretical Physics division of the Department of Mathematical Sciences during the period October 2001 to October 2004.

Acknowledgements

To kick things off, the most thanks goes to Alan Irving for supervising me on this long journey of discovery! He has always found the time to help me out and offer advice even though he is quite possibly the busiest man of all time. Two people without whom I would never have been able to write any code are Craig and Balint so special thanks must go to those two. I must also thank Tim for teaching me what field theory I know and Chris for his constant ribbing about how silly staggered fermions are.

I thank all the people whom I have shared an office with over the past three and half years for putting up with my bad habits and hangover fuelled rants and bad smells. I particularly thank Gav, Matt, Zbysh and Stewart for helping me obtain some of those hangovers. I will miss those long hard days spent in the pub watching the footy and snooker with Matt and Gav instead of working.

On a serious note I must pay tribute to Michelle and Mum for putting up with me at home and for never asking me to try to explain what I do to them. I dedicate this thesis to them.

Abstract

We present a study of the $J^{PC} = 0^{++}$ states in Lattice QCD. Gauge configurations generated by the MILC collaboration have been used to carry out our calculations. These have been generated using a Symanzik improved gauge discretization and an improved staggered fermion discretization.

To set the scene we introduce the reader to QCD and describe why and how we discretize the QCD Lagrangian. We then move on to consider staggered fermions and discuss in some detail the advantages and disdvantages of using this particular discretization procedure. The way that QCD is simulated on the lattice using supercomputers is also discussed.

The first 0^{++} state that we will meet is the scalar glueball. How we calculate the mass of this particle and the results of the calculation are presented along with a comparison to other results in the literature. The tensor glueball will also be be considered. We then discuss the 0^{++} mesons. Firstly we will consider the flavour non-singlet (a_0) meson and calculate the taste splitting which arises from the staggered discretization and also study the scalar correlator using fuzzed operators. As a by product of this calculation we are also able to study excited states of the pion.

The flavour singlet scalar meson will also be considered. We shall describe the stochastic methods employed to calculate the disconnected correlations that arise in the correlation functions of flavour singlet states. These disconnected correlations are combined with the connected correlator calculated in the non-singlet study to determine the flavour singlet mass. Along the way we will make links to other studies of scalar quantities and discuss the implications of our results.

Contents

List of Figures

List of Tables

Chapter 1

Introduction

There are four fundamental interactions which govern our understanding of the universe. They are the Electromagnetic, Weak, Strong and Gravitational interactions. The goal of theoretical physicists all over the world is to understand these interactions and also to develop a theory which describes all the interactions in what is called a Grand Unified Theory, or GUT. Attempts to do the latter have so far proved fruitless. What we do have today is the Standard Model [1] of particle interactions, which encompasses the Electromagnetic, Weak and Strong forces. The Standard Model is by no means believed to be the fundamental theory of particles interactions itself. Indeed it does not even contain any gravitational interactions, but represents a low energy approximation to a unified theory.

A large area of research today is based on looking for physics beyond the Standard Model and trying to fit gravity into these theories. There are two popular theories which are widely believed to explain physics beyond the Standard Model; Supersymmetry and String Theory. Since this thesis involves Standard Model physics, we shall not delve into these complicated theories. For a general introduction to these subjects, an enthusiastic reader is referred to recent lecture notes [2, 3].

As was touched upon earlier, the Standard Model contains theories which describe the Electromagnetic, Weak and Strong interactions. In fact, the Electromagnetic and Weak forces were unified into a single theory in the late 1960's and early 1970's [4, 5].

This unified theory is called the Electroweak gauge theory. The major breakthrough here was that this was a renormalizable theory, i.e. divergences and infinities which appear in the theory could be removed. This was important because previously the quantum field theories which described the Weak interactions were non-renormalizable. The fact that gauge theories were renormalizable led to a breakthrough in the theory of the strong interactions also and gave rise to QCD or Quantum Chromodynamics. This theory builds upon the quark model [6] of the Strong Interaction by introducing gauge fields into the picture. In this chapter we will discuss the quark model and then move on to discuss QCD.

1.1 The Quark Model

The quark model was introduced in the early to mid 1960's as a way of classifying and describing the large number of strongly interacting particles, called hadrons, that had been observed in particle accelerators and cosmic ray experiments. Earlier attempts at a quantum theory which described the hadrons [7], were plagued by problems due to a large coupling constant which meant that perturbative methods were unsatisfactory. As we shall see later this is still a cause of concern today. The major conceptual leap was the proposal that the observed hadrons were made up of another type of particle. These fundamental particles are called quarks [6, 8].

It was first thought that there were three types of quark, the up, down and strange quark. The different type of quarks are called flavours of quark. These quarks have spin $\frac{1}{2}$, fractional electric charge and have an $SU(3)$ symmetry. By considering different combinations of these quarks it was possible to explain all of the observed hadrons of the time. Hadrons were further broken down into two categories, the mesons and the baryons. Mesons consist of a quark and an anti-quark pair, whereas the baryons are made up of three quarks. This model also predicted the existence of other, as yet undiscovered, particles and their masses. When most of those predicted particles were discovered the quark model was accepted as being a valid model for describing hadrons.

The problem with the quark model was that the quarks themselves were not observable in any particle accelerator experiments. This made it difficult for people to believe in the quark model itself as the underlying theory for describing hadrons. One must ask what it is that holds these quarks together to form hadrons but does not allow the quarks to be observed as single entities. Also, quarks did not obey Fermi statistics and could not be put into a quantum field theory so as to explain these phenomena. However these problems were rectified after the advent of gauge theories. Quarks could now be described in a gauge theory along with a gauge field which holds the quarks together in hadrons. This theory is QCD.

1.2 QCD

To ensure that quarks obeyed Fermi statistics and the Pauli Exclusion Principle it was necessary for another quantum number to be assigned to them. This is what is called the colour of a quark. Colour can be thought of as a type of charge in an analogous way to electric charge, the difference being that we don't detect this colour charge. There are three different types of colour which are termed, somewhat unimaginatively, red, blue and green. Evidence that there are indeed three colours comes from the decay of a π^0 into two photons ($\pi^0 \rightarrow 2\gamma$). A theoretical calculation of the decay rate leads to an answer which is proportional to the number of different quarks, or colours of quark, that can contribute. Comparing this with the experimental number verifies that the number of colours is indeed three. A theory of three colours of quark can be described using $SU(3)$ symmetry.

So, we now can describe a theory of three flavours of quark with an $SU(3)_F$ symmetry, where each flavour of quark has three colours described by an $SU(3)_C$ symmetry, where the F and C subscripts stand for flavour and colour respectively. Quarks can change colour by exchange of another type of colour charged particle, called a gluon. Gluons are the force carriers of QCD, just as the photon is for QED [9]. There are eight different gluons which, as we shall see later, is a result of the fact that there are eight generators of the $SU(3)$ gauge group. The gluons carry a colour and an anti-colour charge, but no colour neutral gluon exists. When we come to describe QCD as a gauge theory, the gluons will be the gauge fields.

It is now known that hadrons are bound states of quarks and gluons. Indeed it is now widely believed that there are in fact six flavours of quark and not three. These extra three are the charm, top and bottom quarks. These quarks are needed to account for the now huge number of known hadrons. It is also known that hadrons are colour neutral. This means that a meson contains a quark of a certain colour and an anti-quark of the corresponding anti-colour. A baryon is made up of three quarks, one of each colour. This fact explains why the baryons do not violate the Pauli Exclusion Principle, as was earlier thought when the quark model described some baryons as consisting of three identical quarks.

Now that we know that the quark model with colour charge added to it gives an accurate description of the hadrons, we can build up a gauge theory of quarks and gluons, in an analogous way to the Electroweak gauge theory, in the hope that this will help us to understand the strong interaction. When building up the Lagrangian for the theory we must make sure that it is invariant under local $SU(3)$ transformations. This is because colour is not an observable and as such any changing of colour should not be detectable in any observables. Since colour symmetry is an $SU(3)$ symmetry, then the Lagrangian must also exhibit $SU(3)$ symmetry.

The Lagrangian of QCD is

$$\mathcal{L} = -\frac{1}{4} F^a_{\mu\nu}(x) F^{\mu\nu}_a(x) + \sum_{i=1}^{6} \overline{\psi}_i(x)(i\not{D} - m_i)\psi_i(x). \tag{1.1}$$

Here the ψ and $\overline{\psi}$ are the quark and anti-quark fields, i labels the quark flavour and the m_i are the quark masses. Also,

$$\not{D} = \gamma^\mu D_\mu, \tag{1.2}$$

where

$$D_\mu = \partial_\mu + igA_\mu \tag{1.3}$$

is the covariant derivative which ensures that the Lagrangian is invariant under the following local $SU(3)$ transformations;

$$\psi'(x) = \Lambda(x)\psi(x) \tag{1.4}$$

$$\overline{\psi'}(x) = \overline{\psi}(x)\Lambda^{-1}(x) \tag{1.5}$$

$$A'_\mu(x) = \Lambda(x)(A_\mu(x) - \frac{i}{g}\partial_\mu)\Lambda^{-1}(x). \tag{1.6}$$

The γ_μ are the Dirac Gamma matrices and the A_μ here are the gauge fields and are defined as

$$A_\mu = \frac{1}{2} A_\mu^a \lambda^a. \tag{1.7}$$

Here the λ^a are the Gell-Mann matrices, which are the generators of the $SU(3)$ group. There are eight of these matrices, from which it follows that that there must be eight of the A_μ^a matrices, which are the gluon fields. One should also say here that g is the coupling constant of QCD.

We have now defined all the variables in the second term of (1.1). This term describes the interaction between the quarks and gluons and it is relatively straightforward to see that it is invariant under the transformations (1.4 - 1.6). Let us now consider the first term of the QCD Lagrangian. $F_{\mu\nu}^a$ is the field strength tensor and is defined in the following way,

$$\begin{aligned} F_{\mu\nu}^a &= \partial_\mu A_\nu^a - \partial_\nu A_\mu^a + ig[A_\mu^a, A_\nu^a] \\ &= \partial_\mu A_\nu^a - \partial_\nu A_\mu^a - g f^{abc} A_\mu^b A_\nu^c. \end{aligned} \tag{1.8}$$

Looking at this one can see that the term $F_{\mu\nu}^a F_a^{\mu\nu}$ describes the interactions of the gluons with themselves. In particular it gives rise to three and four gluon interactions. This allows us to consider bound states of the gauge particles themselves in QCD. Such particles are called glueballs and we will discuss these in much greater detail later.

Now one has to consider how to go about calculating observables in QCD. In other gauge theories, such as QED, the usual procedure is to use Feynman's path integral approach [10] to calculate Greens functions and use perturbative methods to complete the calculation. This involves expanding the Greens functions in powers of the coupling constant of the theory. For QED this is an extremely useful calculational tool since the coupling constant of QED is $\approx 1/137$ at low energies. Therefore one only needs to expand the Greens functions to a very low order in the coupling to gain highly accurate results. In QCD this is not always the case because the QCD coupling constant is particularly dependant on energy. In particular, at low energies the coupling becomes large and we can no longer rely on perturbation theory to obtain accurate results. However, at high energies the coupling is small and perturbative methods are valid. One can illustrate this by considering the renormalisation group equation (RGE).

The RGE occurs as a result of the need to renormalize QCD. When calculating Greens functions it is usually the case that there are divergences that occur which can lead to physical observables becoming infinite. Obviously this is an unwanted feature of a theory. To avoid this phenomenon one can regularize the theory at a certain momenta and rescale the bare, or unobserved, quantities of the theory by a divergent quantity. So, the divergences of the theory are absorbed into unobserved parameters and the physical observables are now finite. The bare parameters of the QCD Lagrangian (1.1) are the A_μ^a, m_i, ψ_i and g. In some sense one has free reign when deciding how to rescale the bare parameters, but a condition is that physical observables do not depend on the renormalisation scheme. This means that a change in the momentum cut-off, μ, that we use in the regularisation is not reflected in the observables.

As such, any Greens functions one calculates in the renormalized theory should be invariant under changes in μ. This is reflected in the RGE

$$\mu \frac{d}{d\mu} G = 0, \tag{1.9}$$

where G is some Greens function. One can write $\frac{d}{d\mu}$ in terms of our bare parameters. For example,

$$\frac{d}{d\mu} = \frac{\partial}{\partial\mu} + \frac{\partial g}{\partial\mu}\frac{\partial}{\partial g} + \frac{\partial m}{\partial\mu}\frac{\partial}{\partial m}. \tag{1.10}$$

For the above argument about the coupling constant let us consider the term containing g. We define the following beta function,

$$\beta(g) = \mu\frac{\partial g}{\partial\mu}. \tag{1.11}$$

For small g one can expand $\beta(g)$,

$$\beta(g) = -g^3(\beta_0 + \beta_1 g^2 + \ldots). \tag{1.12}$$

One can now integrate (1.11) to find

$$\alpha_s(\mu) = \frac{1}{4\pi\beta_0 \ln(\mu/\Lambda_{QCD})} \tag{1.13}$$

to leading order, where

$$\alpha_s(\mu) = \frac{g^2(\mu)}{4\pi}, \tag{1.14}$$

Λ_{QCD} is the QCD momentum scale which is around 200 MeV and [11]

$$\beta_0 = \frac{1}{16\pi^2}(11 - 2n_f/3) \tag{1.15}$$

where n_f is the number of quark flavours.

Looking at (1.13) one can see that as the momentum increases then α_s decreases. In fact at extremely large momenta then the coupling is almost zero, i.e. QCD behaves as if it was a free field theory. This phenomenon is known as asymptotic freedom. When we are at sufficiently high energies that this is the case, perturbative methods are indeed sufficient for high accuracy calculations. However if one considers energies of around 2-3 GeV or below then it is easy to see that α_s is of $O(1)$ and as such any perturbative series will diverge. If one wishes to calculate hadronic quantities, such as masses, these are the energies one must work at and so there is the need for non-perturbative methods.

The above conclusions also make it plausible why quarks are never observed as single particles, but are always confined in bound states. At high energies, i.e. at short distances the quarks behave like free particles because of the small coupling constant. At larger distances, the coupling increases and so the quarks are confined within hadrons. At distances as large as hadron radii, the corresponding momenta is small enough that α_s becomes very large. Therefore it is more favourable for quarks to remain bound inside hadrons. The gluons are also confined as a result of this at small energies. It is believed that the gluons form a sort of string of glue which is bound to quarks at either end. If one pulls the two quarks apart, the attractive force between them increases and the resistive force in the gluon string increases. As the distance increases the string can snap creating another quark pair, which will bind to the ends of the broken string.

The second explanation for confinement presented here is a non-perturbative effect. It has been given the name string breaking and a lot of effort has gone into looking for string breaking effects [12]. The success of these studies has been varied, but if string breaking effects can be definitely seen and understood then we would have a non-perturbative explanation for why quarks are confined. The above explanation which was given as a result of the RGE is a perturbative one and is already hindered by the fact that the perturbative expansion is only valid at small coupling. However it still provides us with a useful illustration of why quarks are confined.

Since this thesis is concerned with the calculation of the masses of flavour singlet scalar quantities, such as the scalar glueball and also the scalar mesons, one is forced to work in the low momenta region of QCD. This means we have to find a way to study QCD non-perturbatively. An elegant way to do this is to work on a Euclidean lattice. This involves discretizing space-time and also the QCD Lagrangian and carrying out a Monte Carlo simulation. This area of theoretical physics is called Lattice QCD. For in depth discussions of Lattice gauge theories, the reader is referred to the following textbooks and lecture notes [13, 14, 15]. In the following chapters we will introduce the basics of Lattice QCD and describe how one carries out the simulations.

Chapter 2

Lattice QCD

This chapter is devoted to explaining the ideas behind Lattice QCD. In particular we will focus on why and how we discretise the continuum theory. The major problems one encounters in Lattice QCD will also be discussed.

2.1 Introduction

As touched upon in the previous chapter, perturbative methods for studying QCD are not applicable at low energies. We need a way to study QCD non-perturbatively and this is where the lattice steps in. By discretizing space-time onto a four dimensional Euclidean lattice we give ourselves a way of regularizing the theory non-perturbatively. If a lattice is made up of sites separated by a finite lattice spacing a, then wavelengths on the lattice must be at least $2a$. This automatically gives us an ultra-violet cut-off at a momentum of $\frac{\pi}{a}$, and therefore we have no infinities.

By working on a finite sized lattice one also reduces the number of degrees of freedom in our calculations from infinity to a finite number. Instead of having to consider the values of the gluon and fermion fields at all points in space-time, we now only have to consider these values at a finite number of points. This can still represent a huge number of degrees of freedom, depending on the size of the lattice but it does allow us to attempt to solve the QCD path integral numerically.

It is here that one notes the first two problems with the lattice that we need to worry about. We are studying a theory in an unphysical world where space-time is discrete and finite. By discretizing space time we are introducing discretization errors into our calculations. As we shall see later these are of order a^2 or even order a for different discretizations.

Also, because we are working in a finite box we must impose boundary conditions on our fields. Theses are usually periodic or anti-periodic. Because of the boundary conditions, when we compute observables on the lattice there will be a contribution from mirror states. This contribution is unphysical and does drop off exponentially with increasing physical lattice size. Reaching lattice sizes where these finite size effects can be neglected is very difficult if we wish to keep a small.

2.2 Discretizing QCD

To be able to study QCD on the lattice one must discretize the QCD action.

$$S = \int d^4x \Big(-\frac{1}{4} F^a_{\mu\nu}(x) F^{\mu\nu}_a(x) + \sum_{i=1}^{n_f} \overline{\psi}_i(x)(i\not{D} - m_i)\psi_i(x) \Big) \tag{2.1}$$

A method of doing so, encompassing the above ideas, was put forward by Wilson [16] in 1974. We should say here that there are no restrictions on how one discretizes the QCD action as long as the continuum action is recovered when we taking the limit $a \to 0$. Indeed we shall see in the next chapter that there are numerous different discretization methods used by different research groups around the world.

Of course the continuum QCD action is defined in Minkowski space and we are now working on a Euclidean lattice. We need to transform the Minkowski metric to a Euclidean one. This is done via a Wick rotation.

2.2.1 Wick Rotation to Euclidean Space

To calculate observables on the lattice we use Monte Carlo integration techniques [17]. The update step in the algorithm uses a probability weighting function equal to the exponential term in the partition function,

$$Z \sim e^{iS}. \tag{2.2}$$

Obviously one does not want to be dealing with complex probabilities, or with a weighting function which is larger than 1. Therefore we want the exponent to be real and negative.

By doing the Wick rotation to Euclidean space this condition is satisfied. We make the transformation,

$$t \to it, \tag{2.3}$$

and then the exponent in Z is now real,

$$e^{iS} \to e^{-S_E}. \tag{2.4}$$

Here S_E is the continuum Euclidean action.

2.2.2 The Fermion Matrix

When working on the lattice it is convenient to consider the gauge and fermionic parts of the action separately. This is because when calculating the partition function

$$Z = \int \mathcal{D}\overline{\psi}\mathcal{D}\psi\mathcal{D}A_\mu e^{-S_E}, \tag{2.5}$$

where

$$S_E = S_E^{gauge} + S_E^{ferm} = \int d^4x(-\frac{1}{4}F^{\mu\nu}F_{\mu\nu} - \overline{\psi}M\psi) \tag{2.6}$$

and

$$M = \not{D} - m, \tag{2.7}$$

numerically, one must integrate out the fermion fields. This has to be done because fermion fields are Grassmann quantities which are difficult to deal with in a numerical simulation due to their anti-commuting nature. Since the fields appear in the integral quadratically we can integrate them out as follows

$$Z = \int \mathcal{D}\overline{\psi}\mathcal{D}\psi e^{-\overline{\psi}M\psi} = \det M. \tag{2.8}$$

Our partition function now becomes

$$Z = \int \mathcal{D}A_\mu \det M e^{-S_E^{gauge}}. \tag{2.9}$$

M is called the fermion matrix. It is calculating the determinant of this matrix and also inverting it which is the most time consuming part of a lattice QCD calculation. The fermion matrix will be discussed in greater detail when we come to describe how to carry out our lattice simulations. For now we note that we can think about the gauge and fermion actions as separate quantities. Therefore one can proceed by first discretizing the gauge action and then considering the fermion action.

2.2.3 The Lattice Derivative

The final thing we must do before we attempt to discretize the QCD action is to define a discretized derivative operator. We replace the continuum derivative operator with a difference operator,

$$\partial_\mu \Psi(x) = \frac{\Psi(x+\hat{\mu}) - \Psi(x-\hat{\mu})}{2a} \tag{2.10}$$

where $\Psi(x)$ is an arbitrary field and $\hat{\mu}$ is the unit vector in the direction of μ multiplied by the lattice spacing.

2.3 The Discretized Gauge Action

When putting gauge fields onto our lattice we first note that a particle moving from a point x_1 to a point x_2 in a background gauge field will collect a phase factor. This is equal to the path ordered product

$$\mathcal{P} e^{ig \int_{x_1}^{x_2} A_\mu dx^\mu}. \tag{2.11}$$

On the lattice the shortest possible path any particle can take is to move from a site, x, to an adjacent site $x + \hat{\mu}$.

We are able to use these facts to define links on the lattice where the gauge fields live. A link, U_μ, is defined as

$$U_\mu(x) = e^{iagA_\mu(x)}. \tag{2.12}$$

These links join a lattice site, x, to the adjacent site in the direction μ. The links belong to the gauge group, in this case $SU(3)$, and transform under a local gauge transformation,

Λ, in the following way;

$$U'_\mu(x) = \Lambda(x) U_\mu(x) \Lambda^\dagger(x+\hat{\mu}). \tag{2.13}$$

The $\Lambda(x)$ must also be $SU(3)$ matrices.

We would like to be able to construct our action out of these simple links and of course our action must be gauge invariant. The only gauge invariant quantities which we can make from the links are traces of Wilson loops. These are closed, path ordered products of links. So, the simplest gauge invariant quantity on the lattice is just a 1×1 Wilson loop which we call a plaquette,

$$P_{\mu\nu}(x) = U_\mu(x) U_\nu(x+\hat{\mu}) U^\dagger_\mu(x+\hat{\nu}) U^\dagger_\nu(x). \tag{2.14}$$

If we perform a random gauge transformation on a plaquette and take the trace we see that it is indeed gauge invariant,

$$\mathrm{Tr} P'_{\mu\nu}(x) = \mathrm{Tr}(\Lambda(x) U_\mu(x) U_\nu(x+\hat{\mu}) U^\dagger_\mu(x+\hat{\nu}) U^\dagger_\nu(x) \Lambda^\dagger(x)) = \mathrm{Tr} P_{\mu\nu}(x). \tag{2.15}$$

We can expand equation (2.14), sum over all orientations and lattice sites and use the lattice derivative defined in (2.10) to find,

$$\sum_x \sum_{\mu<\nu} \mathrm{Tr} P_{\mu\nu}(x) = \sum_x \mathrm{Tr}(1 - ia^2 g F_{\mu\nu}(x) + \frac{a^4 g^2}{2} F_{\mu\nu}(x) F^{\mu\nu}(x) + O(a^6)). \tag{2.16}$$

From this we can see that we can construct a lattice action which in the continuum limit, gives us the correct gauge part of the continuum action. The most common way to do this is to use Wilson's original gauge action,

$$S^{gauge}_{Wilson} = \frac{6}{g^2} \sum_x \sum_{\mu<\nu} \mathrm{Re}\ \mathrm{Tr} \frac{1}{3}(1 - P_{\mu\nu}(x)). \tag{2.17}$$

Expanding this gives,

$$\frac{a^4}{4} \sum_x (F_{\mu\nu}(x) F^{\mu\nu}(x) + O(a^2)), \tag{2.18}$$

which in the limit $a \to 0$ is the continuum Euclidean gauge action.

From equation (2.18) we can see that our discretization procedure for the gauge part of the QCD action has resulted in $O(a^2)$ discretization errors. We can reduce these errors by including other Wilson loops in our action. This will be talked about in greater detail in the next chapter.

2.4 The Discretized Fermion Action

Now that we have a suitable form for the gauge action we need to put fermions onto our lattice. To do this we simply assign a fermion field, $\psi(x)$, to each site of the lattice. These fermion fields transform under local gauge transformations as follows

$$\psi'(x) = \Lambda(x)\psi(x), \tag{2.19}$$

$$\overline{\psi'}(x) = \overline{\psi}(x)\Lambda^\dagger(x). \tag{2.20}$$

It is now possible to see that we can construct another quantity on the lattice which is gauge invariant, namely some path ordered product of links connecting a $\overline{\psi}$ at one end and a ψ at the other.

At a first glance one may think it is relatively easy to discretize the fermion action,

$$S_E^{ferm} = \int d^4x \overline{\psi}(\not{D} - m)\psi. \tag{2.21}$$

Here we have suppressed the quark flavour index. If we replace the ∂_μ in $\not{D}$ with the lattice version (2.10) we obtain,

$$\overline{\psi}\gamma^\mu \partial_\mu \psi = \frac{1}{2a}\overline{\psi}(x) \sum_\mu \gamma^\mu (\psi(x+\hat{\mu}) - \psi(x-\hat{\mu})). \tag{2.22}$$

This is not gauge invariant however. We must construct our action out of gauge invariant quantities so we must use the paths described earlier, that is to include links. Our action now looks like,

$$\frac{1}{2a}\overline{\psi}(x) \sum_\mu \gamma^\mu (U_\mu(x)\psi(x+\hat{\mu}) - U_\mu^\dagger(x-\hat{\mu})\psi(x-\hat{\mu})). \tag{2.23}$$

As in the case for the gauge action, we can expand this expression to obtain

$$\overline{\psi}(x)\gamma^\mu(\partial_\mu + igA_\mu(x))\psi(x) + O(a^2). \tag{2.24}$$

This is indeed the continuum fermion action, up to $O(a^2)$ corrections. It also shows that the difference operator with links included (2.23) is a lattice version of the continuum covariant derivative.

Thus we have arrived at the naive lattice fermion action,

$$\begin{aligned} S^{ferm}_{naive} &= a^4 \sum_x (m\overline{\psi}(x)\psi(x) \\ &+ \frac{1}{2a}\overline{\psi}(x)\gamma_\mu(U_\mu(x)\psi(x+\hat{\mu}) - U^\dagger_\mu(x-\hat{\mu})\psi(x-\hat{\mu}))) \end{aligned} \tag{2.25}$$

so called as it is the simplest fermion action that we can write down. Again we have introduced $O(a^2)$ discretization errors into our action, which we would like to be able to remove. We can improve on these errors as will be discussed later. However, we have a more pressing problem with this fermion action, that of fermion doubling.

2.5 Fermion Doubling

In the limit of vanishing quark mass we want our theory to describe one flavour of quark. However if we use (2.25) as our quark action then we have a theory describing sixteen flavours of quark. This can be seen if we look at free field quark propagators in momentum space.

In the continuum the free quark propagator is

$$G_{cont}(p) = \frac{1}{m + i\gamma^\mu p_\mu}, \tag{2.26}$$

which one can easily see has one pole in the $m \to 0$ limit. Let us now consider the free quark propagator on the lattice. Free quarks on the lattice are described by (2.25) with all the gauge links set to be equal to the identity matrix. In momentum space the lattice free quark propagator is

$$G_{latt}(p) = \frac{1}{m + \frac{i}{a}\sum_\mu \gamma_\mu \sin(ap_\mu)}. \tag{2.27}$$

It is easy to see that this has sixteen poles in the zero quark mass limit. When we take the continuum limit we interpret this as a doubling of the number of quark flavours from one to $2^d = 16$.

Obviously we don't want these extra flavours and we must try to construct an action which doesn't have the doublers as a feature. However we must be careful when doing so that we don't destroy any of the other properties of the action such as chiral symmetry, locality of interactions and translational invariance. This has proved to be very difficult to achieve and in fact the Nielson-Ninomiya No-Go theorem [18] states that we can't write down a lattice action which has the three above properties and has no doublers.

2.6 Summary

In this chapter we have introduced the basic ideas of lattice QCD. We have also formulated the simplest possible lattice action and shown that this action is flawed. However, we believe that we can control these flaws reasonably well and make improvements to action which reduce these flaws. These improvements will be the topic of the following chapter.

Chapter 3

Beyond The Naive Formalism

There are numerous ways in which one can improve our naive formalism as long as we regain the correct QCD action in the continuum limit. We will adopt a strategy similar to that in the previous chapter in that we will first deal with the gauge action and then the quark action.

3.1 Improved Glue

In section 2.3 it was shown that the naive discretization of the purely gluonic piece of the QCD action introduces $O(a^2)$ discretization errors. One can correct for the $O(a^2)$ errors following the lead of Symanzik's work on lattice scalar field theory [19]. Expanding the Wilson gauge action (2.17), the $O(a^2)$ correction term is [20, 21],

$$\begin{aligned} & r_1 \sum_{\mu,\nu} \mathrm{Tr}(D_\mu F_{\mu\nu} D_\mu F_{\mu\nu}) \\ + \quad & r_2 \sum_{\mu\nu\sigma} \mathrm{Tr}(D_\mu F_{\nu\sigma} D_\mu F_{\nu\sigma}) \\ + \quad & r_3 \sum_{\mu\nu\sigma} \mathrm{Tr}(D_\mu F_{\mu\sigma} D_\nu F_{\nu\sigma}). \end{aligned} \tag{3.1}$$

These are dimension six operators, which can be cancelled out by adding some linear combination of six link Wilson loops to the action.

There are only three different six link Wilson loops that can be constructed. They are the planar 2×1 rectangle, $R_{\mu\nu}$, the non-planar 2×1 loop, $L_{\mu\nu\sigma}$, and the $1 \times 1 \times 1$ parallelogram, $C_{\mu\nu\sigma}$. Adding a combination of these to the action improves it on the classical level. To correct for quantum effects one can also tadpole improve [22] the action. This involves a re-weighting of each link by a factor of $\frac{1}{u_0}$, where u_0 is the mean value of the links in a simulation and is usually calculated by taking the fourth root of the expectation value of the plaquette,

$$u_0 = \langle \frac{1}{3} \mathrm{Re}\ \mathrm{Tr} P_{\mu\nu} \rangle^{\frac{1}{4}}. \tag{3.2}$$

Tadpole improvement has the effect of reducing the contributions from ultraviolet divergences caused by tadpole loops, which appear in Lattice QCD because of the way gauge fields are represented on the lattice. Consider the link operator,

$$U_\mu(x) = e^{iagA_\mu(x)} = 1 + iagA_\mu(x) - \frac{1}{2}a^2 g^2 A_\mu^2(x) + O(a^3 g^3). \tag{3.3}$$

If the two gluons in the $O(a^2 g^2)$ term are contracted, ultraviolet divergences are generated which cancel the powers of a and so do not disappear in the $a \to 0$ limit. These divergences are responsible for the poor match between lattice quantities and continuum quantities in perturbation theory [22]. The re-weighting $U \to \frac{U}{u_0}$ partially compensates for the divergences, resulting in better agreement between lattice and continuum perturbation theory.

A fully improved pure gauge lattice action can be constructed combining the two ideas described above. The coefficients of each Wilson loop in the improved action have been calculated in [23]. In this work it was remarked that the third term in (3.1) can be removed by making a change of variable,

$$A_\mu \to A_\mu + a^2 \alpha_s f(\alpha_s) \sum_\nu D_\nu F_{\nu\mu}. \tag{3.4}$$

This has the effect that only two Wilson loops need to be added to the action to achieve $O(a^2)$ improvement.

Along with the leading $O(a^2)$ errors the Wilson Gauge action also has sub-leading discretization errors of $O(\alpha_s^n a^2)$. The $O(\alpha_s a^2)$ correction can be cancelled by including a term proportional to α_s in the coefficients of $R_{\mu\nu}$ and $C_{\mu\nu\sigma}$ in the action. The $O(\alpha_s a^2, a^2)$

tadpole improved gauge action is then,

$$\begin{aligned} S_{imp}^{gauge} &= \frac{10}{g^2}\sum_x \Big(\sum_{\mu<\nu} \mathrm{ReTr}\frac{1}{3}(1-P_{\mu\nu}(x)) \\ &- \frac{1}{20u_0^2}(1+0.4805\alpha_s)\sum_{\mu\neq\nu}\mathrm{ReTr}\frac{1}{3}(1-R_{\mu\nu}(x)) \\ &- \frac{1}{u_0^2}0.03325\alpha_s \sum_{\mu<\nu<\sigma}\mathrm{ReTr}\frac{1}{3}(1-C_{\mu\nu\sigma}(x))\Big), \end{aligned} \tag{3.5}$$

where

$$\alpha_s = \frac{-4\ln u_0}{3.0684}. \tag{3.6}$$

This action now has discretization errors of $O(\alpha_s^2 a^2, a^4)$.

3.2 Fermion Formalisms

As previously mentioned there are a number of popular fermion discretizations which take us away from the naive action. They are Wilson fermions [24], Kogut-Susskind or staggered fermions [25], domain wall fermions [26] and overlap fermions [27]. They all have their advantages and disadvantages alike.

The Wilson fermion action has no doublers, but the term added to the action to remove the doublers breaks chiral symmetry. Also the discretization errors are now $O(a)$. The errors can be removed by the addition of the clover term [28], but we still have no chiral symmetry. Staggered fermions retain a $U(1)$ chiral symmetry, but the action still possesses four doublers. This action will be discussed in greater detail later.

Domain wall fermions and overlap fermions evade the Nielson-Ninomiya theorem and so these actions give us chiral fermions with no doublers. The domain wall fermion uses a fifth dimension to do so and the overlap fermion operator utilises the Ginsparg-Wilson relationship [29] to have an exact lattice chiral symmetry. Both these fermion actions are extremely expensive to simulate so have not been used much in dynamical simulations. As computer power increases however, we expect these actions to become more prominent in future simulations.

3.3 Unimproved Staggered Fermions

As touched upon before, we can reduce the number of doublers in our theory and still retain a $U(1)$ chiral symmetry. This is achieved by using staggered fermions, which were introduced in the mid 1970's by Kogut and Susskind [25, 30]. We define staggered fermions, χ, using the following spin diagonalization transformations,

$$\begin{aligned} \psi(x) &= \Omega(x)\chi(x) \\ \overline{\psi}(x) &= \overline{\chi}(x)\Omega^{\dagger}(x) \end{aligned} \tag{3.7}$$

where

$$\Omega(x) = \prod_{\mu=1}^{4} (\gamma_\mu)^{x_\mu}. \tag{3.8}$$

Substituting these transformations into (2.25) gives us the unimproved staggered fermion action,

$$\begin{aligned} S_{stag} &= \sum_x (m\overline{\chi}(x)\chi(x) \\ &+ \frac{1}{2}\sum_\mu \overline{\chi}(x)\alpha_\mu(x)(U_\mu(x)\chi(x+\hat{\mu}) - U_\mu^{\dagger}(x-\hat{\mu})\chi(x-\hat{\mu}))) \\ &= \sum_{x,y} \overline{\chi}(x) M_{xy}\chi(y) \end{aligned} \tag{3.9}$$

where M is the unimproved staggered fermion matrix

$$M_{xy} = m\delta_{xy} + \frac{1}{2}\sum_\mu \alpha_\mu(x)(U_\mu(x)\delta_{x,y-\hat{\mu}} - U_\mu^{\dagger}(x-\hat{\mu})\delta_{x,y+\hat{\mu}}) \tag{3.10}$$

and

$$\alpha_\mu(x) = \Omega^{\dagger}(x)\gamma_\mu\Omega(x+\hat{\mu}) = (-1)^{\sum_{\nu<\mu} x_\nu}. \tag{3.11}$$

Looking at (3.9), one can see that we have no Dirac matrices in our action. Instead, we now have the Kogut-Susskind phases, α_μ. These phases do not have spin indices and our action for the χ fields is diagonal in spinor space. The four spin components of χ are essentially the same and so we can forget about three of them, thus reducing the fermion doubling problem by a factor of four. We now have an action which in the continuum limit describes four degenerate flavours of fermion.

How we interpret these extra flavours and how we deal with them in simulations will be discussed later but first we consider an important symmetry of the unimproved staggered action.

3.3.1 Axial Symmetry

The major reason why staggered fermions are preferred to Wilson fermions in some simulations is the fact that we have an axial $U(1)$ symmetry. This survives the discretization process because the staggered $\not{D}$ is anti-hermitian. The action (3.9) is invariant under the following transformation [31],

$$\begin{aligned} \chi(x) &\rightarrow e^{i\theta\epsilon(x)}\chi(x) \\ \overline{\chi}(x) &\rightarrow e^{i\theta\epsilon(x)}\overline{\chi}(x), \end{aligned} \tag{3.12}$$

where,

$$\epsilon(x) = (-1)^{\sum_\mu x_\mu}. \tag{3.13}$$

In the continuum limit this invariance becomes a flavour non-singlet axial symmetry and shields the quark mass from an additive renormalisation. This enables us to retain the chiral properties of our quarks. Therefore the staggered formalism becomes more desirable when light quark effects dominate the dynamics of the system.

So far all seems rosy in the staggered garden. We have reduced the doubling problem by a factor of four. We have reduced our simulation costs by a factor of four, because we only have one Dirac index to worry about instead of four, and we have a nice symmetry which preserves the chiral properties of our quarks. However, things are not as they seem. We run into quite a big problem when interpreting our four doublers.

3.3.2 Tastes of Staggered Fermions

We call our four extra flavours of fermion tastes, so as to distinguish them from the physical flavours [32]. So, for every physical flavour we say that the staggered discretization produces four tastes. This may not be too big a problem if the tastes all behave as exact copies of each other, but this is sadly not the case. Interactions with the gauge fields break the taste symmetry. We can think about this in momentum space.

A fermion which has momentum close to zero can emit or absorb a gluon which has momentum of around $\frac{\pi}{a}$. Therefore the fermion will now have momentum of around $\frac{\pi}{a}$. It is now a doubler and so has changed taste. These taste changing interactions result in mass splittings in the particle spectra. If one considers the pseudoscalar particles for example, the sixteen particles produced by the four tastes of fermions have vastly different masses (see [33], for example). Only one of these particles becomes massless in the zero quark mass limit. It is this fact which is the major disadvantage of using staggered fermions in QCD simulations.

One can also think about tastes in position space, which will help us later when we come to construct hadronic operators. Our staggered fermion action describes fields which have one spin component per site as opposed to four. In the continuum we have to reconstruct fermions which have four spin components. To try to understand this we work in the hypercubic or $spin \otimes taste$ basis, following the work of [34].

The lattice is split up into 2^4 hypercubes. When taking the continuum limit it is one of these hypercubes which map onto a single point. The χ fields at the sixteen corners of the hypercube correspond to the four copies of Dirac fermions in the continuum. We recall that the χ fields are single component fields and so we can think of the sixteen χ's as the four identical spin components of the four tastes. At non-zero lattice spacing, the sixteen degrees of freedom in a hypercube are some mixture of spin and taste because of interactions with the gauge fields.

In this basis, we can construct quark fields which have definite spin and taste out of the χ fields in a hypercube and write our action (3.9) in terms of these fields. Since we have split our lattice up into hypercubes, we associate a 4-vector, y, with the origin of each hypercube and introduce the set of sixteen vectors, η, which point to the corners of a hypercube. Sites on the lattice are now defined in terms of a hypercube and a corner:

$$x = 2y + \eta, \qquad 0 \leq y_\mu \leq \frac{L_\mu}{2} - 1, \qquad \eta_\mu = 0, 1. \tag{3.14}$$

Here L_μ is the number of lattice sites in the μth direction.

Quark fields are defined on our blocked lattice in the following way,

$$
\begin{aligned}
Q^{\alpha a}(y) &= \frac{1}{8}\sum_{\eta}\Gamma_{\eta}^{\alpha a}\chi(2y+\eta) \\
\overline{Q}^{\alpha a}(y) &= \frac{1}{8}\sum_{\eta}\overline{\chi}(2y+\eta)\Gamma_{\eta}^{\dagger\alpha a},
\end{aligned}
\tag{3.15}
$$

with spinor index $1 \leq \alpha \leq 4$, taste index $1 \leq a \leq 4$ and

$$
\Gamma_{\eta} = \prod_{\mu=1}^{4}(\gamma_{\mu})^{\eta_{\mu}} \tag{3.16}
$$

Inverting the expressions in (3.15), we obtain

$$
\begin{aligned}
\chi(2y+\eta) &= 2\sum_{a,\alpha}\Gamma_{\eta}^{\dagger\alpha a}Q^{\alpha a}(y) \\
\overline{\chi}(2y+\eta) &= 2\sum_{a,\alpha}\overline{Q}^{\alpha a}(y)\Gamma_{\eta}^{\alpha a}
\end{aligned}
\tag{3.17}
$$

Substituting these expressions into (3.9) and setting the U_{μ}'s equal to one leads to

$$
\begin{aligned}
S &= (2a)^4\sum_{y}\{m\overline{Q}(y)(\mathbf{1}\otimes\mathbf{1})Q(y) \\
&+ \sum_{\mu}\overline{Q}(y)[(\gamma_{\mu}\otimes\mathbf{1})\triangle_{\mu} + a(\gamma_5\otimes t_{\mu}t_5)\Box_{\mu}]Q(y)\}
\end{aligned}
\tag{3.18}
$$

where $t_{\mu} = \gamma_{\mu}^{*}$ and we have used the first and second derivatives on our blocked lattice defined in the following way,

$$
\triangle_{\mu}Q(y) = \frac{1}{4a}(Q(y+\hat{\mu}) - Q(y-\hat{\mu})) \tag{3.19}
$$

$$
\Box_{\mu}Q(y) = \frac{1}{4a^2}(Q(y+\hat{\mu}) + Q(y-\hat{\mu}) - 2Q(y)). \tag{3.20}
$$

For a more complete derivation of the action in this basis the reader is referred to the seminal paper [34] or the more detailed description given in [14].

The notation introduced in (3.18) means that we take the direct product of the γ matrices acting in spinor space and the t matrices acting in taste space, hence the name *spin*$\otimes$*taste* basis. Looking at (3.18) we can see that the mass term and the first derivative term are diagonal in taste space whereas the second derivative term is not. It is the $\gamma_5\otimes t_{\mu}t_5$ term which mixes the tastes at non-zero lattice spacing and leads to mass splittings in the particle spectra. This term carries an extra factor of a relative to the other two terms in the action and so disappears in the $a \to 0$ limit. This can be slightly misleading in that one may think that taste symmetry breaking is an $O(a)$ effect, when in fact it is an $O(a^2)$ effect. The $O(a)$ term appears as an artifact of the non-symmetric way the fields are spread across a hypercube in [34]. When averaging the fields symmetrically one can show that the taste violating term is indeed an $O(a^2)$ term [35].

So, the taste violating term disappears in the limit of zero lattice spacing, taste symmetry is restored and our action does indeed describe four degenerate flavours of fermion in the continuum. However, we don't have the luxury of working at zero lattice spacing and the taste breaking effects are not negligible at the lattice spacings at which we work. In the pseudoscalar channel these effects are particularly dramatic. We can improve our action so that the mass splittings seen in the pseudoscalar spectrum are reduced. The focus is usually on the pseudoscalars because the effect of taste changing in other channels is much smaller.

3.4 Improved Staggered Fermions

A lot of work went into trying to improve taste symmetry breaking in the latter part of the 1990's [36, 37, 38, 39, 40]. These studies led to an $O(a^2\alpha_s)$ tadpole improved action that is commonly used in dynamical staggered fermion simulations today. This action is called the *Asqtad* action [39]. This action is a further improvement on the Naik action [41], which improved the quark dispersion relation but did not address the problem of taste symmetry breaking.

The motivation for the way the action is improved stems from the fact that it is interactions with high momentum gluons which are responsible for taste changing. If we can suppress the coupling of quarks to gluons of momentum $p \approx \frac{\pi}{a}$ then we should be able to reduce the effects of taste changing interactions. At tree level this can be achieved by replacing the link variables in (3.9) by so called fattened links. Doing so smooths the gauge fields and lowers the effective ultraviolet cut-off of the gluons [42].

The first attempt to do this involved using the simplest possible fat link, U_μ^F you could think of [36]. This involves replacing a link by a sum of itself and the six three link paths, or staples, connecting the two sites at either end of the original link,

$$U^F_\mu(x) = \frac{1}{1+6w}[U_\mu(x) \quad + \quad w\sum_{\nu\neq\mu}(U_\nu(x)U_\mu(x+\hat{\nu})U^\dagger_\nu(x+\hat{\mu}) \\ + \quad U^\dagger_\nu(x-\hat{\nu})U_\mu(x-\hat{\nu})U_\nu(x-\hat{\nu}+\hat{\mu}))] \tag{3.21}$$

where w is the staple weight. Using this fat link in the action improved the taste symmetry breaking between the two pions considered in [36] by a factor of two.

This was improved on by a further factor of 40% in a later study [37]. In this work a fat link which involved staples of up to length nine links long was used. It was pointed out in [40] that the nine link staples are unnecessary and staples of length up to seven links are sufficient to cancel all tree level couplings to gluons with momentum of $\frac{\pi}{a}$ in one direction and hence the tree level taste changing interactions. This work also showed that at extra five link planar path needed to be added to the fat link to correct for an $O(a^2)$ error introduced by the discretization procedure.

The most thorough numerical study of different fat links was performed by members of the MILC collaboration [39]. Here they studied the effects of using staples of various lengths, including the third nearest neighbour coupling Naik term of [41], the Lepage term [40] and tadpole improvement. They found that the best action for reducing taste symmetry breaking using these techniques is the so called Fat7tad action. This action uses a fat link consisting of three, five and seven link staples weighted with tadpole improved coefficients. However, they concluded that the Asqtad action, which is the Fat7tad action with the Naik and Lepage terms added, was the most sensible improved staggered fermion action even though taste symmetry violations are slightly larger than for Fat7tad. This is because of the improved rotational symmetry and no $O(a^2)$ errors. This action was also shown to greatly improve the scaling behaviour of the ρ and nucleon masses when compared with other improved and unimproved staggered actions [43].

Improving the action gains us a great deal. As well as reducing taste symmetry breaking effects it also reduces the leading discretization error from $O(a^2)$ to $O(a^2\alpha_s^2)$. When combined with the Symanzik improved gauge action (3.5) the Asqtad action is a lattice QCD action which is correct up to $O(a^4, a^2\alpha_s^2, a^2 N_f\alpha_s)$ corrections. The reduction of the discretization errors allows us to work at coarser lattice spacings than with unimproved and other improved actions. Simulating at coarser lattice spacing is computationally less expensive and also allows one to have a larger physical volume using the same sized lattices as in other simulations.

Of course one would still like to simulate at small lattice spacings and have a large physical volume. The relative cheapness in the cost of computation with staggered fermions compared with other discretizations also means that it is more feasible to simulate QCD on larger, finer lattices using this action.

3.5 Further Improved Staggered Actions

During the last few years there have been some exploratory studies into improving the staggered fermion action even further and trying to eliminate taste changing interactions even more. In particular the HYP [44] and Fat7⊗Asqtad[1] actions [45] reduce taste violations significantly more effectively than the Asqtad action.

The HYP action is an attempt to non-perturbatively improve taste symmetry. The non-perturbative interpretation of taste violations is that since each spinor and taste component of a fermion sit at different corners of a hypercube, they all experience different gauge links. Fluctuations of the links in a hypercube cause the different components to behave like separate fields and so lead to taste symmetry breaking. The idea of the HYP action is to minimize the fluctuations of the links within a hypercube so that the different fermion components experience similar gauge environments, hence reducing taste violations.

In practice this is done by creating a fat link with three successive steps of APE smearing [47], with a projection back onto $SU(3)$ after each step. The procedure is modified so that the fat link only contains contributions from links that belong to the same hypercubes as the original unsmeared link. It has been shown [45] that this action out-performs the Asqtad action by a factor ~ 2 when it comes to taste symmetry breaking.

[1] The Fat7⊗Asqtad action has recently been renamed as the Highly Improved Staggered Quark (HISQ) action [46].

Following in the spirit of the Asqtad action, the Fat7⊗Asqtad uses the same link fattening techniques as in [39]. You make the Fat7 links in the usual way followed by a re-unitarization step. The Fat7 links are then used to construct the Asqtad action as opposed to the usual way of using the original unsmeared links. To avoid extra unwanted taste changing effects creeping in as a result of the large number of links in the paths involved in the successive smearing steps, a re-unitarization step is performed on the Fat7 links before the Asqtad smearing step.

The Fat7⊗Asqtad action has also been shown to do better by a factor of ~ 2 than the original Asqtad action concerning taste breaking. The results for this action and the HYP action are comparable but it is claimed that for ease of computation, Fat7⊗Asqtad is the better action to use. It does indeed seem that if simulations using staggered fermions are to continue in future that this action may be the one to use.

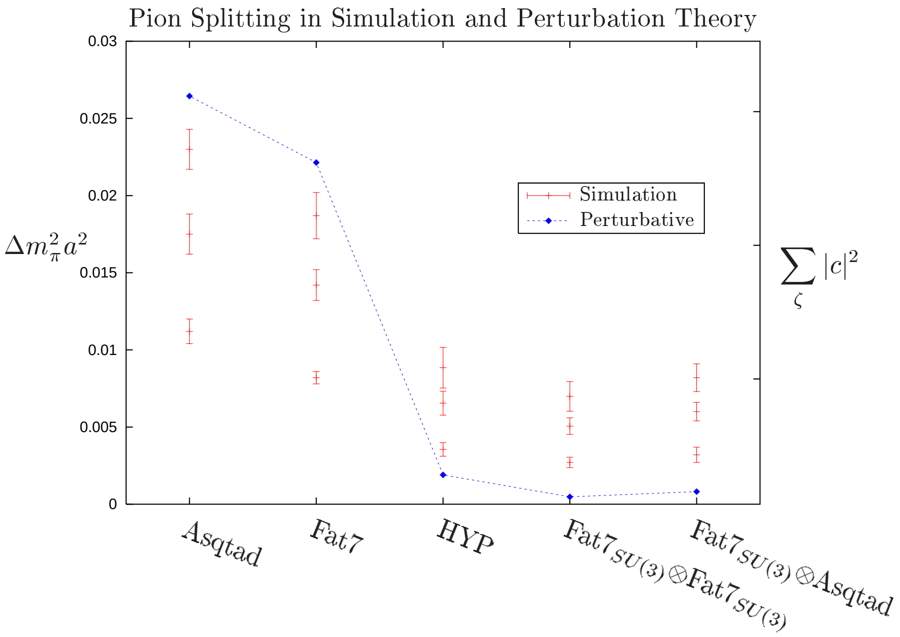

Figure 3.1: Pion Mass Splittings.

Figure 3.1 [48] shows the effects of using different valence quark actions on a quenched background. The plot includes two measures of taste violation, a perturbative estimation, $\sum_\zeta |c_\zeta|^2$ [45], and a numerical estimate, $\Delta m_\pi^2 a^2$, where

$$\Delta m_\pi^2 a^2 = a^2(m_\pi^2 - m_G^2). \tag{3.22}$$

Here m_G is the mass off the Goldstone pion and m_π is the mass of one of the non-Goldstone pions. One can clearly see that further improving the action gains you a great deal when it comes to taste symmetry breaking.

3.6 Summary and Thesis Outline

Up to now the basic ideas behind lattice QCD have been introduced. The problems of putting QCD on a lattice and regaining the correct continuum limit have been discussed. It has also been shown that discretization errors can be compensated for by improving the action. What has not been discussed yet is how we actually carry out our lattice simulations.

Since this thesis is concerned with calculations that have been made using the Asqtad fermion action along with the Symanzik improved gauge action, how QCD is simulated using this action will be discussed in the next chapter. How one deals with the different tastes of fermion in the vacuum will be dealt with here. Once this has been discussed the rest of the thesis will be concerned with the $J^{PC} = 0^{++}$ states in QCD. In Chapter 5 we will consider the scalar glueball and the effect of dynamical fermions on the glueball mass.

Following on from that, the 0^{++} mesons will be studied. Chapter 6 will deal with how the operators which create the states we are interested in are constructed. Tastes will be revisited again here also. The two different techniques involved in calculating the two contributions to the flavour singlet meson correlator will be also be described here and we will discuss how one of these contributions is used to calculate the flavour non-singlet meson mass. In Chapter 7 we shall present the results of our calculations using fermionic operators and discuss the findings of the studies.

Chapter 4

Simulating QCD On The Lattice

4.1 Observables

The reason one wishes to simulate QCD on a lattice is to calculate in the low energy region, where perturbation theory is no longer applicable. The lattice enables one to calculate low energy quantities, such as hadron masses and matrix elements of hadronic operators, from first principles in a non-perturbative way. When calculating observable quantities on the lattice, one usually considers the vacuum expectation value of the operator of the particular observable,

$$< \Phi >= \frac{1}{Z} \int \mathcal{D}\overline{\psi}\mathcal{D}\psi\mathcal{D}U_\mu \Phi e^{-S_E}. \tag{4.1}$$

Here Z is the partition function,

$$Z = \int \mathcal{D}\overline{\psi}\mathcal{D}\psi\mathcal{D}U_\mu e^{-S_E}, \tag{4.2}$$

S_E is the Euclidean lattice action and Φ is some operator which, in general, depends on the ψ fields and the gauge links, U.

If we wish to calculate things like particle masses, one typically studies correlation functions,

$$C(t) = \sum_x \langle \Phi^\dagger(\mathrm{x}, t)\Phi(0)\rangle \tag{4.3}$$

where Φ is an operator which has the quantum numbers of the particle we are interested in. Usually one would like to calculate the ground state energy of a particular particle, from which one can calculate the particle's mass. However, a general operator will couple to all states with the given quantum numbers such as higher excited states and two or three particle states. We can write (4.3) as a linear combination of all possible states, n, with the quantum numbers of Φ. Inserting a complete set of energy eigenstates into (4.3) we have,

$$\begin{aligned} C(t) &= \sum_n \sum_x \langle 0|\Phi^\dagger(\mathrm{x},t)\frac{|n\rangle\langle n|}{2E_n}\Phi(0)|0\rangle \\ &= \sum_n \frac{\langle 0|\Phi^\dagger|n\rangle\langle n|\Phi|0\rangle}{2E_n}e^{-E_nt}, \end{aligned} \tag{4.4}$$

where E_n is the energy of the state n and we have normalised the states as $\langle n|n\rangle = 2E_n$. If one considers states with zero momentum then E_n simply becomes the mass of state n. For non-zero momentum one can use the dispersion relation to convert energies to masses.

In order to isolate the ground state of the considered particle one needs to study the large time behaviour of (4.4). At large t the larger mass excited states will contribute less to the sum due to the exponential factor. The hope is that if one can study the correlation function at large enough t the contribution to (4.4) from excited states will be negligible and one can reliably calculate the ground state mass. However due to large statistical errors at larger t, calculations at large t can become unreliable and we are forced to work at smaller t values than we would like. In this situation one cannot be sure that excited state contributions are negligible but improved operators with increased projection onto the ground state can be used. This will be discussed in later chapters.

4.2 Monte Carlo Ensembles

To calculate observables as described in the previous chapter, one must find a way of calculating integrals of the form of that in (4.1). Even though we have reduced this to a finite number of integrals by using a lattice, it is still a very large number of integrals. However, we do not need to calculate the full integral. One can use Monte Carlo integration techniques to approximate integrals like that in (4.1). Before we consider Monte Carlo methods let us return to the partition function with the fermion fields integrated out,

$$Z = \int \mathcal{D}U \det M(U) e^{-S^{gauge}(U)}$$

$$= \int \mathcal{D}U e^{-S^{gauge}(U) + \text{Tr }\ln M(U)}. \tag{4.5}$$

One can work in the so called quenched approximation of QCD, which amounts to ignoring the fermion determinant in the partition function, i.e setting $\det M = constant$. This has the effect of removing quark-antiquark pair production in the vacuum from our theory. In the past quenching was done because of the cost of computing the fermion determinant many times in a Monte Carlo simulation. Working in the quenched approximation can typically reduce simulation time by a factor of 1000 as compared with full QCD. However since one is ignoring the effects of virtual particles, results from quenched QCD typically differ from experiment by about $10-20\%$. With the increase in computing power over the last few years we no longer have to work in the quenched approximation but it is convenient to consider this approximation while trying to understand Monte Carlo methods.

Our integrals are now of the form,

$$\int \mathcal{D}U e^{-S(U)}, \tag{4.6}$$

where $S(U)$ is, for example, the Wilson action defined in (2.17). It is easy to see that large values of the action contribute little to the integral, while small values of the action dominate the integral. It is possible to approximate the integral using a weighted sum of configurations of the U fields. The weighting should reflect the fact that configurations of the gauge links which give small values of the action contribute more. By doing this, our expression for the expectation value of an operator now simply becomes an average of the value of the operator on each configuration of fields,

$$\langle \Phi \rangle = \frac{1}{N} \sum_{i=1}^{N} \Phi(\{U\}_i). \tag{4.7}$$

We call these configurations of links gauge configurations.

To ensure that the configurations are weighted properly, one uses the exponential term, $e^{-S(U)}$, from the partition function as the weighting function. To generate an ensemble of configurations, one can start with a random configuration and generate new configurations from it using a stochastic algorithm, thus forming a Markov chain of configurations. A requirement on the algorithm is that after a number of steps the system of configurations is in thermal equilibrium. Two conditions must be met to ensure equilibrium;

$$\sum_{\{U\}_j} P(\{U\}_i, \{U\}_j) = 1 \tag{4.8}$$

and

$$P(\{U\}_i, \{U\}_j)e^{-S(\{U\}_j)} = P(\{U\}_j, \{U\}_i)e^{-S(\{U\}_i)}, \tag{4.9}$$

where $P(\{U\}_i, \{U\}_j)$ is the transition probability of obtaining the configuration $\{U\}_i$ from $\{U\}_j$ after an application of the stochastic algorithm. One also has to make sure that the set of configurations generated and used for measurements like those in (4.7) are uncorrelated or statistically independent. This means that each configuration should have no recollection of any of the previous configurations.

One can ensure that the gauge configurations are uncorrelated by measuring the autocorrelation time of an observable, usually the plaquette, after every application of the algorithm. For a discussion of autocorrelations, see chapter 7 of [13] for example. By only storing a configuration after a number of applications of the algorithm which is larger than the autocorrelation time, one ensures that the configurations are statistically independent. The algorithm must also satisfy another condition, that of ergodicity. This means that every possible configuration can be generated from any other one with some finite probability. In other words, the algorithm must be able to access the whole of configuration space.

There are many algorithms one can implement to ensure that the detailed balance condition (4.9) is satisfied. An example is the Metropolis algorithm. Using this algorithm we take an initial configuration, $\{U\}_i$, and propose some change or update to this configuration. We then accept this new configuration, $\{U\}_j$, with probability,

$$P_{acc} = min(1, e^{-\Delta S}), \tag{4.10}$$

where

$$e^{-\Delta S} = \frac{e^{-S(\{U\}_j)}}{e^{-S(\{U\}_i)}}. \tag{4.11}$$

Therefore if the update results in a lower value of the action, the new configuration is always accepted. If the action increases as a result of the update then we accept with probability $e^{-\Delta S}$. This acceptance step is realised by generating a random number $r \in [0,1]$ and accepting the new configuration if $r < e^{-\Delta S}$.

This algorithm is very inefficient however. Let us consider the two extreme choices we could make for our update. One could choose to update one link at a time. This means one has to randomly sweep through the lattice updating links and going through the accept or reject step a certain number of times before obtaining a new configuration. Updating one link at a time also causes problems if the action is non-local. One could also decide to update all the links at once, but this would mean a very small acceptance rate since changes in the action would tend to be large. Ideally one would like an algorithm which could allow for global updates and have a high acceptance rate.

An example of such an algorithm is the Hybrid Monte Carlo (HMC) [49] algorithm. This algorithm uses the Metropolis accept or reject step along with a molecular dynamics based algorithm for updating the gauge fields. The molecular dynamics algorithm involves introducing a conjugate momenta field, π_i, and constructing equations of motion by integrating a discretized version of Hamilton's equations. The integration is carried out using the Runge-Kutta, or so called leapfrog, method as described in [14, 49]. By iterating the resulting equations over a number of time-steps, where one has introduced a new time variable τ which we call simulation time, new configurations are generated. By introducing this finite time step, one introduces a step size error into the calculation. Introducing a Metropolis acceptance step at the end of the time evolution eliminates the step size error. We now have a satisfactory algorithm for generating quenched gauge configurations but must now consider how to generate so called dynamical gauge configurations.

4.3 Simulating with Dynamical Fermions

Up to now it has been convenient to consider the quenched approximation. However, one would like to simulate QCD with a more realistic vacuum structure where we have taken into account virtual quark loop effects. This means we must calculate the fermion determinant in our update steps. This is the most time consuming part of a Lattice QCD calculation since the size of the matrix is typically of the order $10^6 \times 10^6$. One must ask the question whether one can use the methods outlined above to generate dynamical gauge configurations.

The integrals one would like to calculate are of the form,

$$Z = \int \mathcal{D}U e^{-S(U)+\mathrm{Tr}\ \ln M(U)} = \int \mathcal{D}U e^{-S(U)+\ln\ \det M(U)}. \tag{4.12}$$

Since the fermion fields, which are Grassmann quantities, have been integrated out, the exponent of the partition function now only depends on the gauge degrees of freedom. Thus we have an effective gauge action,

$$S_{eff}(U) = S_g(U) - \ln\ \det M(U), \tag{4.13}$$

which can be used in the simulation. There are a few problems that need to be addressed though. Firstly, for this effective action to be used in a probability weighting function, $e^{-S_{eff}}$, one requires $\det M$ to be real and positive. In general this is not true however. To solve this problem it is usual to simulate with a matrix, Q, such that

$$\det Q = (\det M)^{N_f} \tag{4.14}$$

where N_f is the number of degenerate quark flavours one chooses to include. Using an even number of quark flavours ensures that $\det Q$ is real and positive.

Let us consider Wilson fermions, recalling that $S_f = \overline{\psi} M \psi$ describes one flavour of quark in the continuum limit. If one wishes to simulate with two degenerate quark flavours one can use the identity

$$(\det M)^2 = \det(M^\dagger M) \tag{4.15}$$

which shows that we can use the matrix $Q = M^\dagger M$ to describe the two flavour theory. By doing this one has re-introduced doubling into the theory, but in this case it is desirable as the up and down quarks are almost degenerate in the real world.

The problem with the cost of computing the fermion determinant also comes into play here. In the Metropolis acceptance step, one is required to calculate,

$$\Delta S_{eff} = \Delta S_g - \ln \frac{\det Q(U')}{\det Q(U)}, \tag{4.16}$$

where U' is the newly proposed configuration generated from U. It is implausible to calculate the ratio of determinants in a reasonable amount of time. One way to circumvent this problem is to use a complex scalar field, ϕ, which we call a pseudofermion field. Following [50] we can write,

$$\det Q = \int \mathcal{D}\phi^* \mathcal{D}\phi e^{-\phi^* Q^{-1} \phi}. \tag{4.17}$$

The partition function is now

$$Z = \int \mathcal{D}U \det Q(U) e^{-S_g(U)} = \int \mathcal{D}U \mathcal{D}\phi^* \mathcal{D}\phi e^{-S_g(U) - \phi^* Q^{-1}(U)\phi}. \tag{4.18}$$

We can now carry out our simulation with the effective action

$$S_{eff}(U) = S_g(U) + \phi^* Q^{-1}(U)\phi. \tag{4.19}$$

The computational cost has now transferred from the calculation of the determinant of the fermion matrix to the calculation of the inverse of the matrix. Since one is calculating $Q^{-1}\phi$, i.e the inverse of a matrix acting on a vector, one can use the conjugate gradient method to solve $Qp = \phi$ for p. While still time consuming, using this method is hugely more efficient than calculating determinants. One can now apply the HMC algorithm using the action (4.19) by introducing momenta fields conjugate to the pseudofermion fields as well as the gauge fields and proceeding as described in section 4.2.

Let us now return to the case of staggered fermions. The staggered fermion matrix describes four degenerate flavours or tastes of fermion, as was shown in section 3.3. Using the above method of simulating using $Q = M^\dagger M$, it may seem as though one would now be describing eight tastes of fermion. This is not the case though because the staggered $M^\dagger M$ only couples even sites to even sites and odd sites to odd sites. Furthermore the determinants of the even and odd site submatrices are equal. This means that one can avoid the doubling of species by using a pseudofermion field which is only defined on even (or odd) sites. Even so, using the HMC algorithm or another pseudofermion based algorithm such as the Φ algorithm [51], we are still only able to simulate a theory with four degenerate fermions.

Ideally one would like to calculate with 2+1 flavours of quark in the vacuum, the "2" being the light quarks (u, d) and the "1" being the strange quark. Therefore it is necessary to have an algorithm which enables simulation with an arbitrary number of quark flavours. Such an algorithm is the R algorithm [51]. This algorithm abandons the accept/reject step and also using pseudofermion fields in the action. Instead, the fermion determinant is included in the effective action

$$\begin{aligned} S_{eff} &= S_g + \ln\,\det(M^\dagger M)^{\frac{N_f}{4}} \\ &= S_g + \frac{N_f}{4}\mathrm{Tr}\,\ln M^\dagger M. \end{aligned} \tag{4.20}$$

The factor of $\frac{1}{4}$ appears to account for the four tastes of staggered fermion per continuum flavour.

When setting up the equations of motion for this action one ends up needing to explicitly calculate $(M^\dagger M)^{-1}$ instead of $(M^\dagger M)^{-1}\phi$. To get around this problem a noisy estimate is used in place of the inverse fermion matrix. This means that we have an inexact algorithm which also has step size errors due to the lack of an accept/reject step. The errors are $O(\delta\tau^2)$, where $\delta\tau$ is the step size. However, the big plus point for this algorithm is that one can simulate with 2+1 flavours of light quark. Simulating the two light quark flavours amounts to taking the square root of the fermion determinant, while simulating the strange quark requires the fourth root of the fermion determinant. In short, one takes fractional roots of the fermion determinant to remove the unwanted extra tastes from the theory.

There are some issues about whether this is a sound thing to do. There are concerns that using a fractional root trick may violate unitarity and locality. These arise from the fact that one may not be able to write down a local one flavour fermion action which has determinant equal to that of the fourth root of the staggered fermion action. Until it is proven one way or the other whether this is possible, the debate will be ongoing. For interesting discussions on the topic the reader is referred to [52] and [53]. There has been some recent progress in this area however. It has been shown [54, 55] that it is possible to construct a local lattice action which is equivalent to the one flavour free staggered fermion action, which is encouraging. These works need to be extended into the fully interacting theory in the future to settle the debate once and for all.

The gauge configurations used in this thesis were produced by the MILC collaboration using the improved gauge action (3.5) and the Asqtad fermion action. The simulations were carried out using the R algorithm. The sets of configurations used are listed in table 4.1. The ensembles listed in the top part of the table (sets A-D) have a lattice spacing of $\sim \frac{1}{8}$fm, while those listed in the bottom part (E-F) have a lattice spacing of $\sim \frac{1}{11}$fm. The results of hadron spectroscopy calculations using these configurations can be found in [56, 57].

Ensemble	β	$am_{u,d}$	am_s	No. of configs
A	6.81	0.03	0.05	564
B	6.79	0.02	0.05	483
C	6.76	0.01	0.05	658
D	6.76	0.007	0.05	448
E	7.11	0.0124	0.031	514
F	7.09	0.0062	0.031	505

Table 4.1: Simulation parameters.

4.4 Error Analysis

Any lattice QCD simulation will have errors associated with it. These errors can be both statistical and systematic. Statistical errors arise because of the finite number of gauge configurations one has access to. Systematic errors are due to the fact one typically carries out a fit to the lattice data or some extrapolation to zero lattice spacing or physical quark mass. For example, when carrying out a fit a systematic error is induced by the choice of fit region. Observables can be highly sensitive to the fit region and one must be careful when choosing fit regions. Also, the functional forms used to carry out extrapolations are usually truncated to some order in a, giving a systematic error due to the error in calculating a. In some cases the systematic errors are small compared with statistical errors in which case they can be neglected.

There a number of techniques one can use to estimate the statistical error on some lattice measurement. Let us consider the value of some primary observable on the lattice, O_i, where a primary observable is something which depends on the field variables only.

Here $i = 1, ..., N$ and N is the total number of configurations on which one made a measurement. The mean value of O is,

$$\overline{O} = \frac{1}{N} \sum_{i=1}^{N} O_i \tag{4.21}$$

and the variance of the measurements is given by,

$$\sigma^2 = \frac{1}{N} \sum_{i=1}^{N} (O_i - \overline{O})^2. \tag{4.22}$$

If the measurements are independent, which is the case if the gauge configurations are uncorrelated, then the error on $\overline{O}$ is given by

$$\epsilon = \frac{\sigma}{\sqrt{N-1}}. \tag{4.23}$$

In reality though the measurements one makes are usually correlated. These correlations can lead to errors being underestimated. To take the correlations into account it is usual to group blocks of successive measurements together into so called bins and use the bin averages as measurements. To determine the size of the bins one measures the autocorrelation time of the observable. By choosing bin sizes that are larger than the autocorrelation time, one ensures that the bin averages are uncorrelated. The error can then be estimated using the above equations, replacing N by $\frac{N}{N_{bin}}$, where N_{bin} is the size of the bins.

When it comes to considering secondary observables, which are functions of the primary observables, a more sophisticated technique is needed to obtain a good error estimate. One usually determines the value of a secondary observable as a function of the average of the primary observables. This means that one is not calculating the value on each configuration and averaging, so the above method for estimating the error is not applicable. The two common methods used for estimating the error on a secondary observable, for example the mass of a particle determined from correlators, are the jackknife and bootstrap methods.

The jackknife method involves eliminating one configuration from the full set of configurations and making a measurement of the mass on the remaining subset. This is done in all possible ways. The result is that we have N jackknife samples each containing $N-1$ configurations. One ends up with N different estimates for the mass and the error on the mass, calculated using the full set of configurations, is determined from the variance of these jackknife estimates.

In a bootstrap analysis one builds up a sample of N configurations randomly from the full set of configurations. This means that a particular configuration could appear in sample many times or not at all. One does this N_{bs} times, where N_{bs} is the chosen number of bootstrap samples, and makes a measurement on each sample. As in the jackknife analysis the error on the measurement using the full set of configurations is determined using the variance of the N_{bs} measurements.

4.5 Introduction to Fitting

Before one can carry out the error estimation methods described above one must ask how the secondary observables are actually calculated. Again, let us consider how we calculate the ground state mass of a particle. One first measures the correlation function (4.3) of an operator which couples to the particle we are interested in. One must then fit the data to some fit function to determine the mass of the particle. The fit function one uses to calculate particle masses is that defined in (4.4). If our operator has zero momentum we can write this in the form,

$$C(t) = A_0 e^{-m_0 t} + A_1 e^{-m_1 t} + A_2 e^{-m_2 t} + \dots, \tag{4.24}$$

where m_0 is the ground state mass, m_1 is the mass of the first excited state and so on.

One must decide how many terms of the series to include in the fit function. Given limited statistics and in some cases poor quality data it is difficult to get a good quality fit if one includes too many terms. If there is a good signal to noise ratio in the correlators at large enough t that the excited state contribution is small then it is usual to perform a single exponential fit to

$$C(t) = A_0 e^{-m_0 t}. \tag{4.25}$$

However if we are restricted by a poor signal at large t then the contribution from the first excited state to the correlator may not be negligible. In this case we would perform a two exponential fit,

$$C(t) = A_0 e^{-m_0 t} + A_1 e^{-m_1 t}. \tag{4.26}$$

These arguments can be extended if we are interested in the first or higher excited states. In general, if one is interested in the nth state it is a good idea to include $n+1$ exponentials in the fit function.

Another choice one has to make is over what values of t one should perform the fit. If we are performing a single exponential fit we have to be sure that, at the values of t used, the excited state contribution is negligible. At the same time we have to be sure that the data matches onto the fit function satisfactorily. A way one can determine the range of t to fit to is by calculating,

$$\chi^2 = \sum_t \left(\frac{f(t) - C(t)}{\epsilon(t)}\right)^2, \tag{4.27}$$

where $f(t)$ is the fit function used, $C(t)$ is the value of the correlator measured and $\epsilon(t)$ is the error on the correlator. This gives an indication of how well the data agrees with the fit function. By minimising χ^2 with respect to the fit parameters one ensures the best quality fit. What this means in practice is that one varies the minimum and maximum values of t used in the fit and uses the values which give a reasonable value of $\chi^2/d.o.f$, where $d.o.f$ is the number of degrees of freedom in the fit, as the chosen time region. A reasonable value of $\chi^2/d.o.f$ is usually deemed to be ≈ 1.

Up to now all that has been considered are correlations of operators with themselves, whose fit functions can be considered to be simple exponential forms. Later on we will have to consider matrices of correlations and correlations of operators which will not give rise to simple exponential forms. The details of the individual fits carried out in this work will be described at the relevant times.

Chapter 5

The Light Glueball Spectrum

5.1 Introduction

There have been a large number of calculations of the glueball spectrum in pure gauge Lattice QCD. Two of the more recent calculations [58, 59] have measured a large number of glueball states lying below 4 GeV. The two lightest states are a scalar, with quantum numbers $J^{PC} = 0^{++}$, and a tensor, with $J^{PC} = 2^{++}$. For this work the former is the important state as explained earlier. However, an attempt will also be made to calculate the mass of the tensor state. It is widely accepted that these two states have masses of around 1500-1700 MeV and 2200-2400 MeV respectively in the continuum limit of the quenched approximation.

In the real world however, QCD is not described by the quenched approximation. In the past it has been favourable to work in the quenched theory due to the high computational cost of simulating dynamical quarks. Nowadays this is less of a problem with the advent of multi tera-flop machines. An interesting question which maybe can now be addressed is that of what effect the dynamical quarks have on the glueball spectrum. This has been attempted using improved [60] and unimproved [61] Wilson fermions.

For the case of the scalar glueball, things get very interesting. There is experimental evidence of three flavour singlet resonances around the scalar glueball mass. These are the $f_0(1370)$, $f_0(1500)$ and $f_0(1710)$. The quark model predicts only two flavour singlet $\overline{q}q$ states, i.e. a meson which contains a quark and anti-quark of the same flavour, in the scalar nonet. A popular conjecture is that the three observed states are produced by mixing of the light scalar glueball and the flavour singlet $\overline{q}q$ states. Lattice mixing models have been studied in the quenched approximation before [62, 63], however the conclusions of these studies are not in total agreement. By working with dynamical fermions it is possible to measure the effects of this mixing directly.

The phenomenological interpretation of these states is that the $f_0(1500)$ is the most likely candidate for the scalar glueball [64]. This conclusion is reached from the consideration of experiments where the f_0 mesons have been seen. The $f_0(1710)$ has been found to decay strongly into $K\overline{K}$, which would suggest that the $f_0(1710)$ is made up of $\overline{s}s$. The $f_0(1500)$ is not observed in $\gamma \to K\overline{K}$ or $\pi\pi$ which would point to it not being a $\overline{q}q$ meson. The $f_0(1500)$ is also found to be strongly produced in gluon rich environments such as central collisions, which would point to it being mainly made up of glue. Using quark model arguments it is assumed that the $f_0(1370)$ is the $\overline{u}u + \overline{d}d$ state of the scalar nonet. This is also backed up the fact that the $f_0(1500)$ is produced in gluon rich environments and so is more than likely not the $\overline{u}u+\overline{d}d$ state. There is also a lighter flavour singlet state, the $f_0(980)$. This particle has a mass which is too small to be considered as a glueball candidate however and may even be a four quark state [65].

5.2 Analysis

5.2.1 Configurations

Since glueball masses are reasonably large, the lightest being around 1.5 GeV, they are difficult to determine from correlators because of the fast drop off of the correlation function (4.4) due to the large exponent. We also have the problem that the signal to noise ratio of glueball operators is notoriously poor. All this points to us requiring a huge number of configurations to be able to confidently calculate glueball masses. Indeed quenched calculations of glueball masses typically involve a few thousand configurations. Looking at table 4.1, one can see that the largest ensemble available to us is around 650 configurations. We must ask ourselves whether we can reliably calculate even the lightest glueball masses on ensembles of this size.

In an earlier work [60], using configurations generated with two flavours of dynamical Wilson fermions, it has been shown that you can indeed reliably calculate glueball masses on such modest sized ensembles. Therefore we can hope to gain some reasonable results from these data sets. An attempt has been made to calculate the scalar and tensor glueball masses on all six ensembles listed in table 4.1. One cannot be too confident of a continuum result because of the fact we are only working at two different lattice spacings. We may be able to determine something about the effect of decreasing light quark mass on the glueball masses. One thing that should be an advantage to us over some other calculations is the use of a Symanzik improved gauge action.

5.2.2 Methods for Determining Masses

To calculate masses of glueball states on the lattice it is necessary to study correlations of operators which are irreducible representations of the cubic group [66]. As was stated earlier we only consider the scalar and tensor glueball states, so we construct the representations A_1^{++} and E^{++}. These are realised by using spatial Wilson loops only. Following in the spirit of an earlier work [67] and on the advice of one of those authors, square Wilson loops of differing sizes are used.

One of the goals in constructing these operators is to maximise the overlap onto the ground state wavefunction of the particular glueball we wish to study. This is realised by first APE smearing [47] and then Teper blocking [68] the spatial links. We use two levels of smearing which replaces an original link with a sum of itself and its spatial staples. The blocking step is a procedure similar to smearing, but which effectively increases the lattice spacing by a factor of two. We use three levels of blocking, which allows us to construct four square Wilson loops of different sizes. Using no blocking we construct smeared plaquettes of width a. Implementing the blocking we construct 'blocked plaquettes' of average width

$2a$, $4a$ and $8a$, the widths being determined by the blocking level. The operators used are,

$$\mathcal{O}_i^{A_1^{++}}(t) = \mathrm{Tr}\sum_{\mathrm{x}}\left(\Psi_{12}^i(\mathrm{x},t) + \Psi_{23}^i(\mathrm{x},t) + \Psi_{31}^i(\mathrm{x},t)\right) \tag{5.1}$$

$$\mathcal{O}_i^{E^{++}}(t) = \mathrm{Tr}\sum_{\mathrm{x}}\left(\Psi_{12}^i(\mathrm{x},t) - \Psi_{23}^i(\mathrm{x},t)\right) \tag{5.2}$$

$$\mathcal{O}_i^{\prime E^{++}}(t) = \frac{1}{\sqrt{3}}\mathrm{Tr}\sum_{\mathrm{x}}\left(\Psi_{12}^i(\mathrm{x},t) + \Psi_{23}^i(\mathrm{x},t) - 2\Psi_{31}^i(\mathrm{x},t)\right) \tag{5.3}$$

where the Ψ_{xy}^i are blocked plaquettes in the x, y plane and $i = 0, .., 3$ is the blocking level.

When constructing our correlators we need to take into account the fact that, at zero momentum, the scalar glueball has the same quantum numbers as the vacuum. Therefore we subtract a disconnected piece from the scalar correlator. With our set of operators we studied the 2×2 correlation matrices

$$C_{ij}(t) = < \mathcal{O}_i^\dagger(t)\mathcal{O}_j(0) > - < \mathcal{O}_i >< \mathcal{O}_j > \tag{5.4}$$

for the A_1^{++} representation and

$$C_{ij}(t) = < \mathcal{O}_i^\dagger(t)\mathcal{O}_j(0) > \tag{5.5}$$

for the E^{++}. This was done for all six possible combinations of i and j with $i < j$. One can calculate effective masses from ratios of correlators. Since

$$C \sim e^{-amt}, \tag{5.6}$$

we can define an effective mass as

$$am_{eff}(t) = -\ln\frac{C(t+1)}{C(t)}. \tag{5.7}$$

In practice these correlators do not only contain contributions from the ground state of the particular glueball but also from heavier excited states,

$$C \sim \sum_\alpha e^{-am_\alpha t}. \tag{5.8}$$

Here $\alpha = 0, 1, ..., N$ labels the state, with $\alpha = 0$ being the ground state, $\alpha = 1$ being the first excited state and so on. As the excited states are heavier, their contribution to the correlators falls off more rapidly than the ground state contribution and we shouldn't have a problem extracting the ground state mass (see section 4.1). Unfortunately because of the poor signal to noise ratio, the correlators have been swamped by the noise before we can get far enough out in t so that the contribution from excited states has died away.

One can attempt to address this problem by using the variational method [62] to form a linear combination of operators which has an increased projection onto the ground state. This method involves maximising

$$u_i C_{ij}(t) u_j \tag{5.9}$$

subject to

$$u_i C_{ij}(t-1) u_j = constant. \tag{5.10}$$

This gives us the generalised eigenvalue equation

$$C_{ij}(t) u_j^{\alpha} = \lambda^{\alpha} C_{ij}(t-1) u_j^{\alpha}. \tag{5.11}$$

One can solve this to find the eigenvalues, λ^{α}, and the variational eigenvectors, u^{α}. Using these it is possible to form a new basis,

$$\overline{C}_{00}(t) = u_i^0 C_{ij}(t) u_j^0, \tag{5.12}$$

with maximum projection onto the ground state. To set the variational basis we chose to use $t = 0$ and 1. This is because the errors on $C_{ij}(t)$ are smallest at these values of t. This means we are solving (5.11) to the maximum precision allowed by the data.

A choice was made to only consider 2×2 correlation matrices and to interpret the eigenstates as the ground state and first excited state. This was made on the belief that contributions from higher excited states are small, even for the small t values at which we are forced to work. Also, for this work one is only interested in the ground state and to introduce higher excited states would not gain us anything in the calculation of the ground state mass. We use the variational eigenvectors to form linear combinations of our operators. We then choose as our glueball operator the combination that gives us the best overlap onto the ground state and the most stable effective mass plot. To do this one solves

$$(C_{ij}^{\beta})^{-1}(1) C_{ij}^{\beta}(0) u_j^{\alpha\beta} = \lambda^{\alpha\beta} u_j^{\alpha\beta}, \tag{5.13}$$

where β labels the variational basis of operators and runs from one to six[1]. The operators in each basis are tabulated in table 5.1.

β	$\mathcal{O}_1^\beta$	$\mathcal{O}_2^\beta$
1	$\mathcal{O}_0$	$\mathcal{O}_1$
2	$\mathcal{O}_0$	$\mathcal{O}_2$
3	$\mathcal{O}_0$	$\mathcal{O}_3$
4	$\mathcal{O}_1$	$\mathcal{O}_2$
5	$\mathcal{O}_1$	$\mathcal{O}_3$
6	$\mathcal{O}_2$	$\mathcal{O}_3$

Table 5.1: Operators in each variational basis. The bases are the same for the scalar and tensor representations.

Since the eigenvalues λ^α are related to masses in the following way,

$$\lambda^\alpha = e^{-m_\alpha}, \tag{5.14}$$

the eigenstate with the largest eigenvalue corresponds to the ground state. Therefore λ^0 is the largest eigenvalue. We use the corresponding eigenvectors, u^0, to construct the linear combinations

$$\tilde{\mathcal{O}}^\beta = \sum_{i=1}^{2} u_i^{0\beta} \mathcal{O}_i^\beta. \tag{5.15}$$

These operators have an increased projection onto the ground state, when compared with the original operators, and it is these one studies to obtain ground state masses. We can then make a choice about which of the six operators to finally use for our final estimate, taking into consideration a number of factors. This will be discussed in section 5.3.

We should now consider the effect of choosing $t = 0$ and $t = 1$ to set the basis. In [69] it was shown that for improved gauge actions, physical positivity is violated. A result of this is that correlation functions of gluonic operators can gain a negative contribution due to the violation. These negative contributions disappear at some value of t, which depends on the coefficients of the extra terms in the action [70]. Therefore if we can extract our masses at large enough values of t these contributions should have no effect in

[1]One should note that β is not summed over here, it is merely a label.

our calculation. However, as we have already discussed, the signal to noise ratio for the glueball correlators is very poor which means we are forced to consider small values of t and in particular we have used $t = 0$ and $t = 1$ to set the variational basis.

These unphysical contributions can lead to small or negative eigenvalues in the correlation matrices. This leads to problems for the variational method, which relies on the positivity of the correlation matrices. This was considered in [70], where evidence was found of these unphysical contributions. Two methods were proposed to try to get rid of the contributions by discarding the eigenstates corresponding to the small and negative eigenvalues. One involved projecting the correlation matrices into an eigenspace corresponding to large eigenvalues and the other involved projecting into the space corresponding to the largest eigenvalue only, with both methods giving consistent results for the 0^{++} mass. The second of these methods is same as the method we have employed here. This gives us confidence that we are avoiding these contributions as much as possible and indeed we did not find negative eigenvalues when solving the generalised eigenvalue equation (5.11) at $t = 0$ and $t = 1$. However, we should keep in mind that positivity violation may lead to problems in calculating glueball masses using configurations generated with improved gauge actions, especially when using a large basis of operators as in [70].

5.2.3 Non-Zero Momentum

We can repeat our calculation using operators which have non-zero momentum. This is done in an effort to reduce the statistical errors on the masses and also to improve our estimate of the mass itself. For the scalar case there is also the bonus that a boosted scalar operator does not couple to the vacuum. Therefore one does not have to subtract a vacuum expectation value from the correlators and so hopefully the correlators will be less noisy.

There are problems introduced when we consider heavier states of non-zero momentum. Because the boosted representations can mix, the correlation function of a particular operator will be contaminated by contributions from lighter states. This is not a problem for the scalar but it is for the tensor. To circumvent this problem one could explicitly subtract the scalar contribution from the tensor correlators or construct an operator which is orthogonal to the boosted scalar state. However, for reasons to be explained in more detail later, we choose not to consider the tensor state with momentum.

To construct our non-zero momentum operators, we perform a Fourier transform on the Ψ^i_{xy} introduced earlier. For the scalar the operator is

$$\mathcal{O}_i(\mathbf{P}, t) = \sum_{\mathrm{x}} \Big(\Psi^i_{12}(\mathrm{x}, t) + \Psi^i_{23}(\mathrm{x}, t) + \Psi^i_{31}(\mathrm{x}, t) \Big) e^{\frac{2\pi i}{L}\mathbf{P}\cdot\mathrm{x}} \tag{5.16}$$

where L is the spatial extent of the lattice. We only consider states with $\mathbf{P.P} = 1$, that is states with momentum $\frac{2\pi}{L}$ in one of the spatial directions and zero in the other two. We follow through the analysis in the same way as for the zero momentum case. However, instead of effective masses we now end up with effective energies for our glueball states. We use [60] the lattice dispersion relation

$$a^2 E^2_{eff}(t, \mathbf{P}) = a^2 m^2_{eff}(t, \mathbf{P}) + \sum_{\mu=1}^{3} \sin^2 \left(\frac{2\pi P_\mu}{L} \right) \tag{5.17}$$

to convert the energies to estimates of the masses.

We could of course have used the continuum dispersion relation instead of the lattice version, which would mean using $(2\pi/L)^2\mathbf{P.P}$ rather than $\sin^2(2\pi P_\mu/L)$ in equation (5.17). However, we follow the methods employed in [60] where it is claimed that the lattice dispersion relation was found to be the better one to use in lattice Higgs models. For our purposes it does not really matter which is used because we are only considering states with $\mathbf{P.P} = 1$ and the spatial extents of our lattices are 20 and 28. This means that the difference between $(2\pi/L)^2$ and $\sin^2(2\pi/L)$ is negligible.

5.3 Improving the Mass Estimates

In the case of the scalar glueball we looked at the effective masses, calculated for each of the six variational operators. For the case of the coarse lattices listed in table 4.1 it was found that we could only calculate up to $m_{eff}(3)$ reliably. This was because the correlators had decayed into noise by $t = 5$. On the finer lattices we were able to calculate up to $m_{eff}(4)$. This limited range of t is to be expected because of limited statistics and a poor signal but does provide an improvement on not using a variational approach, where we could only calculate up to $m_{eff}(2)$ or $m_{eff}(3)$. It should be pointed out here that t is in lattice units, so what we really mean is t/a. Physically this means that $t = 3$ on the coarse lattices and $t = 4$ on the fine lattices correspond to almost identical physical distances of $3/8fm$ and $4/11fm$ respectively. So, for both lattice spacings, the signal has died away at the same physical distance but using a smaller lattice spacing means we have more points from which we can obtain a better estimate of the mass.

We also looked at the overlap of the operators onto the ground state. This can be estimated [67] using the following expression

$$|< \mathcal{O}|Glueball >|^2 = e^{-a\sum_{t=0}^{\infty}(m_{eff}(t)-m)}, \tag{5.18}$$

where m is a final estimate of the glueball mass. When making a choice of the operator to finally use, the main factor taken into account was how good were the plateaux in the effective mass plots. Looking at the overlap of the operators didn't really tell us much in practice. In an ideal world we would want to minimise $m_{eff}(1)$ and maximise the overlap, but given the limited statistics available for this work we found we were unable to do so and have a reasonable plateau. It was found that the best operator was given by using blocking levels 2 and 3, i.e. the operator labelled by $\beta = 6$ in table 5.1. As a result of our smearing, blocking and variational analysis we have projected out a large part of the contamination from the first excited state. One can reduce this contamination further and so increase the projection on to the ground state even more, as follows.

When doing our variational analysis we solved the generalised eigenvalue equation

$$C_{ij}^{-1}(0)C_{ij}(1)u_j^{\alpha} = \lambda^{\alpha}u_j^{\alpha}. \tag{5.19}$$

We can use the ratio of the eigenvalues, $\frac{\lambda^1}{\lambda^0}$, to reduce the contamination as follows. Our system was modelled as a two-state system, as mentioned earlier. For this model one can show that the ground state mass of the system is [71]

$$am = \frac{am_{eff}(t) - \frac{\lambda^1}{\lambda^0}am_{eff}(t-1)}{1 - \frac{\lambda^1}{\lambda^0}}. \tag{5.20}$$

This quantity is used for our final estimate of the ground state mass. The final values quoted for the masses in the scalar case are a weighted average of this quantity from $t = 1$

to $t = 3$ on the coarse lattices and $t = 1$ to $t = 4$ on the fine lattices, incorporating effective masses from both the zero and non-zero momentum analysis. The weighting was proportional to the inverse of the statistical error on the values of $m_{eff}(t)$. This weighting ensures that effective masses with smaller statistical errors contribute more to the final result than those with larger errors. The errors that were used in the weighting were calculated using a jackknife analysis while the final errors on the masses were calculated using a bootstrap error analysis with 100 bootstrap samples. We also checked the effects of binning the data, as described in section 4.4. It was found that binning the data into bin sizes of two and four had no significant effect on the jackknife errors on the scalar glueball effective masses and so we do not believe that we have underestimated our errors[2].

For the tensor glueball things get a lot worse. It was found that we could only reliably calculate effective masses from $t = 0$ to $t = 1$ on the coarse lattices and from $t = 0$ to $t = 2$ on the finer lattices. This was not entirely unexpected given the relatively small number of configurations and the larger mass of the tensor glueball. Since the operators defined in (5.2) and (5.3) couple to the same state it is unnecessary to consider them both and so a choice was made to use (5.2).

The analysis carried out for the zero momentum scalar was repeated for the tensor, even though we couldn't go out very far in t. We chose not to look at the non-zero momentum tensor state because of this fact combined with the problems mentioned earlier of contamination by the boosted scalar state. We argue that given these facts and the relatively low number of configurations, it would be difficult to extract any meaningful information from looking at a boosted tensor state. As in the scalar case, we use a weighted average of the quantity defined in (5.20) for our final estimate of the tensor mass. However, the time ranges one can utilize here are only $t = 0$ to $t = 1$ on the coarse lattices and $t = 0$ to $t = 2$ on the fine lattices. How good an estimate this gives is debatable given the small range in t we are able to work with.

[2]A MILC collaboration analysis found that binning the data had no effect on most of their hadron spectrum calculations on the configurations considered here. They did however bin the data into bin sizes of 4 when performing fits for the pseudoscalar mesons.

5.4 Results and Discussion

In this section we present plots of the effective mass calculations and give some results and conclusions.

5.4.1 The Scalar Glueball

Figures 5.1 - 5.4 show effective mass plots for the scalar glueball, calculated on the coarse lattices, while table 5.2 lists the final estimates of the mass given by the methods described in the previous chapter. On the plots the long dashed lines represent these mass estimates while the dashed lines show the bootstrap error on these quantities. The circles show the values of the effective mass calculated using 5.7. The error bar on the circles were also calculated using bootstrap. Table 5.2 also quotes a systematic error which comes from the choice of the minimum value of t that was used in the weighted averaging of (5.20). Figures 5.5 - 5.6 and table 5.3 show the same things for the finer lattices.

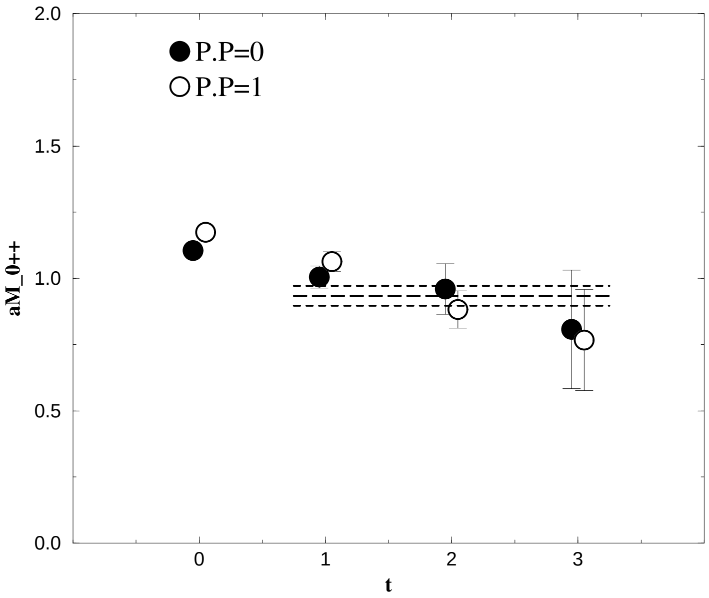

Figure 5.1: Scalar glueball effective mass plot for data set A.

The first thing one notices is that as the light quark mass decreases, the effective masses, as determined by the zero and non-zero momentum operators, begin to diverge

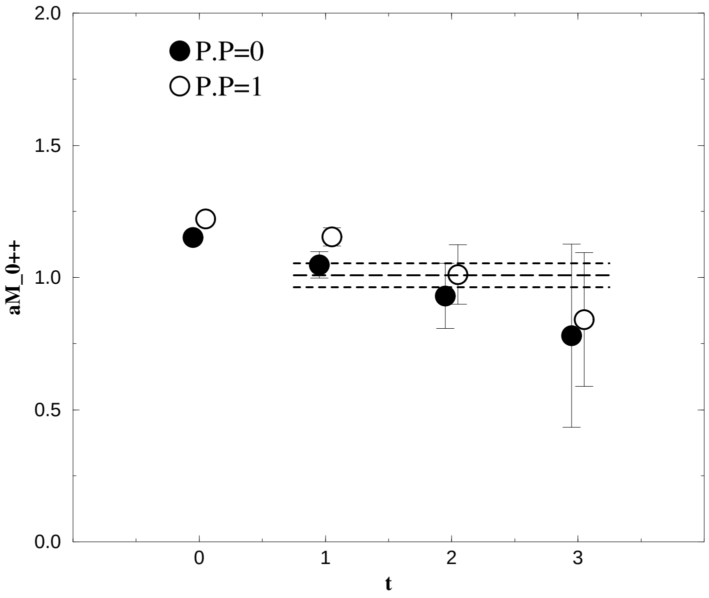

Figure 5.2: Scalar glueball effective mass plot for data set B.

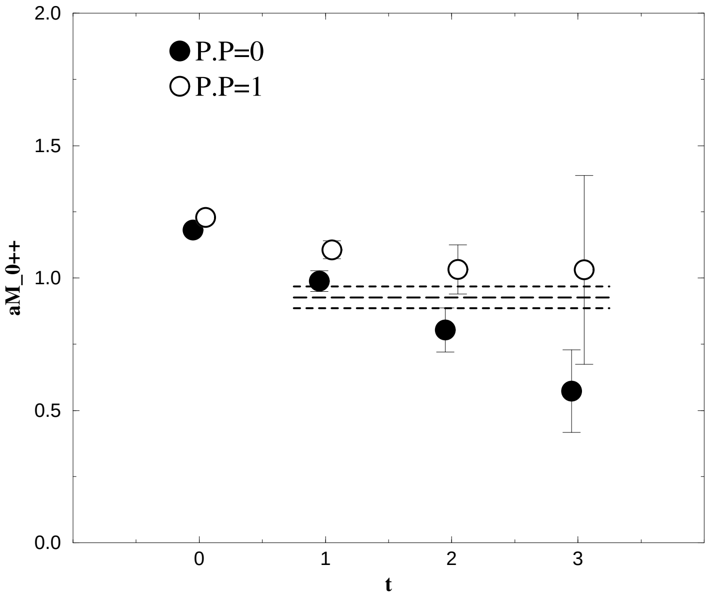

Figure 5.3: Scalar glueball effective mass plot for data set C.

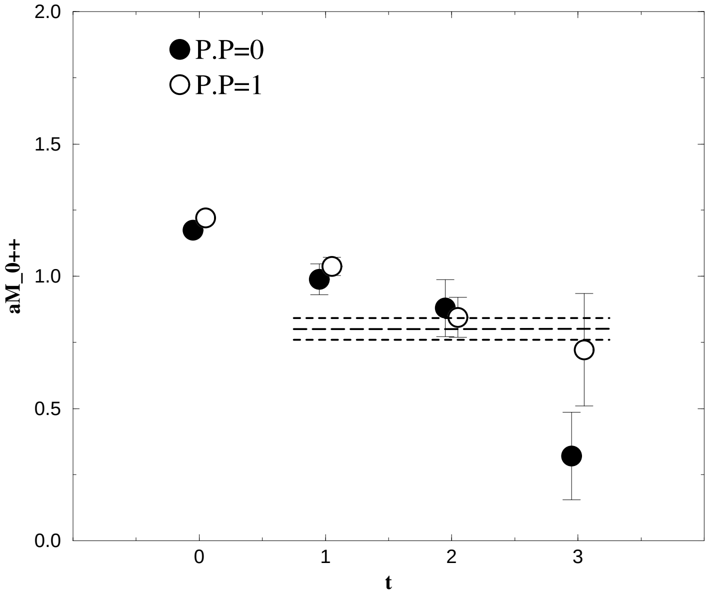

Figure 5.4: Scalar glueball effective mass plot for data set D.

Ensemble	$am_{0^{++}}$
A	$0.934(37)^{+0}_{-0.107}$
B	$1.009(45)^{+0}_{-0.132}$
C	$0.927(41)^{+0}_{-0.120}$
D	$0.801(41)^{+0}_{-0.188}$

Table 5.2: 0^{++} mass on the coarse lattices.

from each other. There is also a general trend that the effective mass is decreasing as we go out in Euclidean time. We must ask why this is happening. Since we are working with dynamical gauge configurations we should consider the effects of mixing with $\overline{q}q$ states. The scalar glueball can mix with flavour singlet scalar mesons and also two pion states. Mixing with the scalar meson will be considered in more detail later, as we shall be making measurements with scalar $\overline{q}q$ operators.

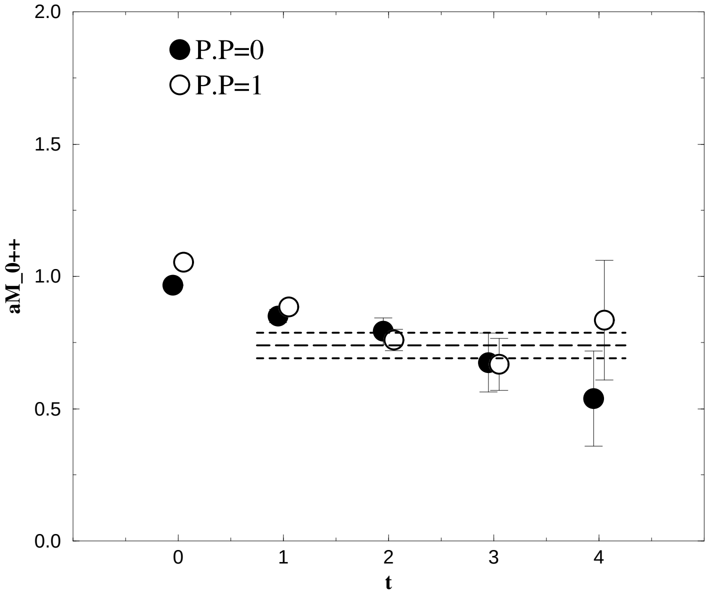

Figure 5.5: Scalar glueball effective mass plot for data set E.

Ensemble	$am_{0^{++}}$
E	$0.739(48)^{+0}_{-0.060}$
F	$0.716(54)^{+0}_{-0.061}$

Table 5.3: 0^{++} mass on the fine lattices.

For now, let us consider mixing with two pion states with overall momentum zero, i.e two pions of momentum $\pm\frac{2\pi n}{L}$, where L is the spatial extent of the lattice. The energy of such a state is given by (5.17). The simplest case here is where both pions have zero momentum, in which case the energy is just $2am_\pi$ and this is the threshold mass for the decay of a scalar meson into two pions. Therefore this is also the threshold for mixing of a scalar glueball with a two pion state. Looking at table 5.4, where the Goldstone

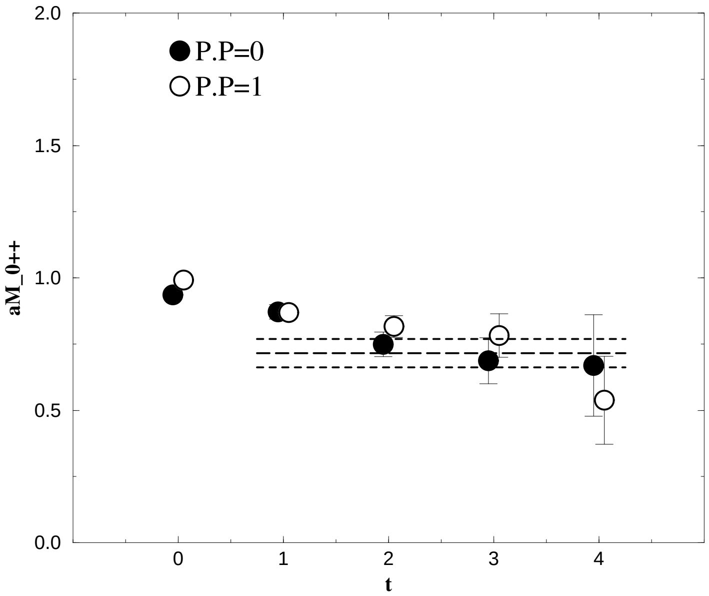

Figure 5.6: Scalar glueball effective mass plot for data set F.

pion masses are taken from [56, 57], one can see that twice the pion mass is less than our estimate of the glueball mass on all of the ensembles on which we made measurements. This could explain the behaviour of the effective mass plots.

Ensemble	$2am_\pi$	$am_{0^{++}}$
A	0.755	0.934(37)
B	0.623	1.009(45)
C	0.449	0.927(41)
D	0.378	0.801(41)
E	0.413	0.739(48)
F	0.296	0.716(54)

Table 5.4: Comparison of scalar glueball and two pion masses.

As the quark mass is decreased the two pion energy becomes much smaller than the scalar glueball mass, so one expects the effects of the mixing to be greater. This is because it becomes much more energetically favourable for the state to exist as two pions rather than a scalar glueball. A reason for the trend of decreasing effective mass as we move out in Euclidean time is that we are basically measuring a mixture of states. As we move out in t the smaller mass state begins to dominate. So at larger values of t, the two pion state could be expected to be more prominent, which could explain the behaviour.

One must also ask what effect the reduction in quark mass has on our estimate of the mass of the scalar glueball. On the coarse lattices the scalar glueball mass seems to be independent of quark mass within the statistical errors apart from on ensemble D, which has the lightest quarks. On the fine lattices the mass estimate is also independent of quark mass within the statistical errors. We can argue that mixing effects become more significant as we reduce the quark mass and so at larger quark masses the scalar glueball mass seems to be independent of quark mass. At smaller quark masses this may not be the case. It would be interesting to test this argument on either coarse or fine lattices with smaller quark masses or larger numbers of the original configurations.

Ideally one would like to have data at more values of t to use in the mass estimates. Since this is not the case one has to make do with the available data. This forces one to consider values of t where we cannot be sure, even after the variational analysis, that all excited state contributions are negligible. Indeed by choosing the minimum value of t to be at $t_{min} = 2$ rather than $t_{min} = 1$ results in a significantly smaller estimate of the scalar glueball mass. This is reflected in the systematic errors quoted in tables 5.2 and 5.3. We have shown that, as was found in [60], it is possible to extract reasonable results for the scalar glueball on relatively small, when compared to quenched calculations, numbers of configurations. Unfortunately, due to the lack of reasonable sized matched quenched ensembles, we can't say anything about the difference between the quenched and dynamical scalar glueball masses reported in [60].

What we can comment on is how our masses compare with other calculations of the scalar glueball mass. We have converted our mass values into physical units and plotted them against the square of the lattice spacing in figure 5.7. To convert our masses into physical units we have used the smoothed r_1/a values from [57] to get estimates of the masses in units of r_1, where r_1/a is calculated using the static potential [56]. We then use the value of r_1 in physical units, which is calculated via splittings in the Υ spectrum [73] to convert our numbers into GeV. The error bars are calculated by combining the errors

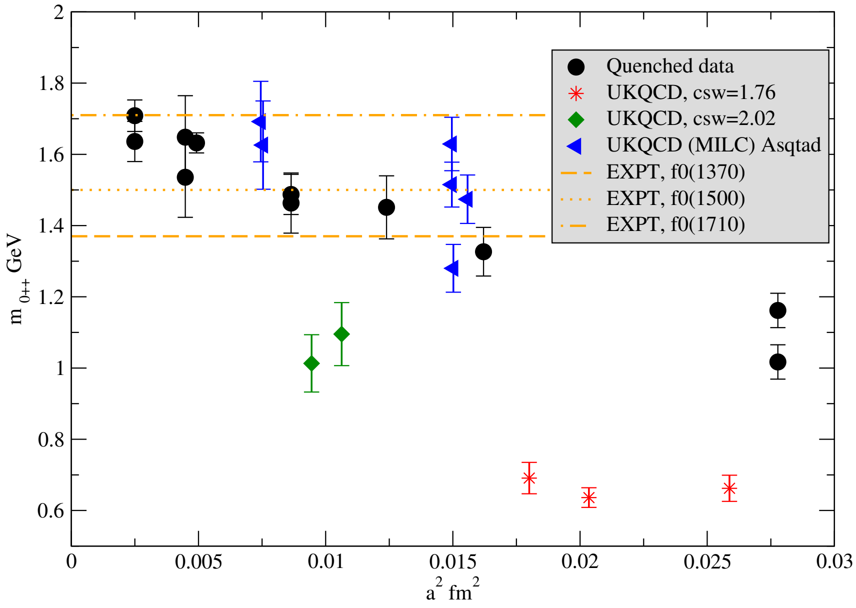

Figure 5.7: Scalar glueball masses from various simulations.

on the mass and the errors on r_1 in quadrature. Also on this plot are UKQCD calculations of the scalar glueball mass on quenched and dynamical clover configurations. One can see that our masses (the points represented by the left pointing triangles) are comparable with the quenched masses at similar lattice spacings, but quite a bit heavier than the dynamical clover masses. It should be pointed out here that the UKQCD lattices were not generated using an improved gauge action.

A tentative conclusion of [60] was that the difference in the mass of the scalar glueball in the quenched and dynamical clover theories was down to the effect of adding the clover term to the action and is not an unquenching effect. This conclusion is certainly supported by the results of our calculation. The effect of adding the clover term to the dynamical Wilson action is to enhance $O(a^2)$ corrections. This results in a smaller mass for the scalar glueball. Since our action is fully $O(a^2)$ improved, we do not suffer from these added corrections and so do not see a suppression in the scalar glueball mass. It would be interesting to compare these results with dynamical clover calculations that utilise an improved gauge action in the future. It may be that the improvement to the gauge action counteracts the enhancement of the $O(a^2)$ errors and the results would be comparable with the quenched results.

It would also be interesting to compare with an improved quenched calculation. One improved quenched calculation was carried out using anisotropic lattices in [59]. The smallest spatial lattice spacing considered in that work was $0.12fm$, which is comparable with the coarse lattices considered in this thesis. At that lattice spacing the scalar glueball mass was estimated to be $a_t m_{0^{++}} = 0.318(4)$, where a_t is the temporal lattice spacing. Since the anisotropy factor was 3 in that case, this would imply that $a_s m_{0^{++}} = 0.954(12)$, where a_s is the spatial lattice spacing. Converting this into units of r_0, where r_0 is the Sommer length scale [72], we get $r_0 m_{0^{++}} = 3.94(6)$. Our calculations on the coarse lattices are comparable with this number (see table 5.5), which is further evidence that unquenching may not have a significant effect on the mass of the scalar glueball.

Ensemble	$r_0 m_{0^{++}}$
A	3.67(16)
B	3.94(19)
C	3.57(17)

Table 5.5: 0^{++} mass in units of r_0 on ensembles A, B and C

In conclusion, it would seem that using dynamical quarks may or may not have an effect on the scalar glueball mass at finite lattice spacing, depending on which discretization procedure one uses. Looking at our results using staggered fermions we would argue that the dynamical quarks do not lead to a reduction in the mass, whereas using clover improved Wilson fermions does. However, the latter observation is probably because of the improvement procedure rather than dynamical quark effects. Of course, using light quarks does have an effect in that the channel for the decay of the scalar glueball into two pions is open. To make any concrete statements about whether this explains the behaviour of the effective mass plots, we would need to include the pion operators in the analysis. Calculations at another lattice spacing and increasing the statistics of the calculations considered here should clear up whether this behaviour is because of statistical limitations or discretizaton errors.

5.4.2 The Tensor Glueball

Since the signal for the tensor glueball was very poor we do not present individual effective mass plots for each ensemble. Instead the results for all the coarse lattices are plotted in figure 5.8 and the fine lattices in figure 5.9. We only have effective masses at two values of t to consider on the coarse lattices and three for the fine lattices, so there is not much one can conclude about the mass of the tensor glueball. Crude estimates of the mass are listed in table 5.6. These have been calculated using the method described in 5.3 and they are probably over estimates because of the inclusion of the effective mass at $t = 0$ in the calculation. The only thing one can really learn from this attempt to calculate the tensor glueball mass on these ensembles is that for a reliable calculation one would need a much larger number of configurations and maybe a smaller lattice spacing.

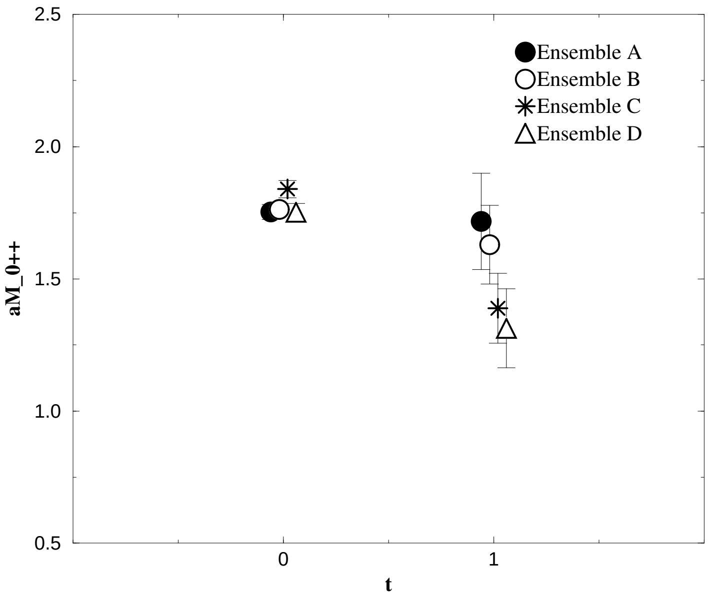

Figure 5.8: Tensor glueball effective masses for the coarse lattices.

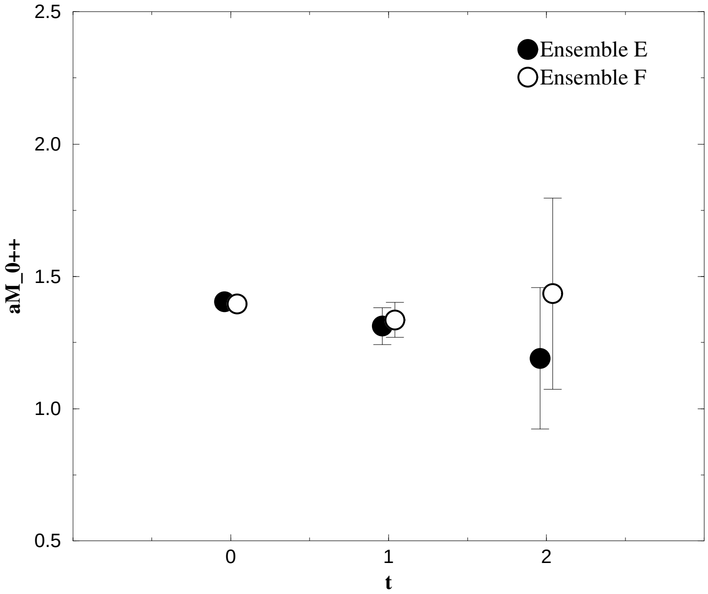

Figure 5.9: Tensor glueball effective mass plot for the fine lattices.

Ensemble	$am_{2^{++}}$
A	1.746(44)
B	1.736(43)
C	1.718(46)
D	1.639(50)
E	1.363(37)
F	1.380(34)

Table 5.6: Estimates of the tensor glueball mass.

Chapter 6

Mesons In The Staggered Formalism

6.1 Introduction

A meson is a colour singlet bound state of a quark and an antiquark. Different mesons are distinguished from each other by their quark content, charge and J^{PC} quantum numbers. For example a charged pion has quantum numbers $J^{PC} = 0^{-+}$ and contains an up quark and a down quark. The π^+ contains an up and an anti-down quark, whereas the π^- contains a down and an anti-up quark. On the lattice we can study mesons by studying operators that have the correct quark content and give the correct quantum numbers. Of course the major difference from the real world is that, in most lattice simulations, one treats the up and down quarks as being degenerate and as having unrealistically high masses. As computer power and algorithms improve it may possible to simulate at realistic light quark masses and to treat the u and d quarks separately. There are also complications with calculations involving the heavy quarks (c, b, t) on the lattice, which can be resolved by using alternative actions for the heavy quarks. We do not go into detail about these here because they are not relevant to this work. In this chapter we will describe how mesons consisting of light quarks are constructed on the lattice in terms of naive quarks and then make the extension to staggered quarks.

6.2 Flavour Singlet And Non-Singlet Mesons

The way one studies mesons on the lattice is to create a state with the required properties at some time t and let it propagate through the lattice until a time $t+\tau$, where we destroy the state by creating its anti-particle. In general a mesonic operator has the form

$$\mathcal{O}(\mathrm{x}, t) = \overline{\psi}_i(\mathrm{x}, t)\Gamma\psi_j(\mathrm{x}, t), \tag{6.1}$$

where Γ is some product of the Euclidean Dirac matrices, γ_μ, and i and j label the flavour of the quark. For now we shall just consider naive quarks. As was shown in section 4.1 one can calculate the mass of a state by studying the correlation function of the operator which creates that state. So for our general mesonic operator the correlation function is

$$\begin{aligned} C(\tau) &= \langle \mathcal{O}^\dagger(\mathrm{x}', t+\tau)\mathcal{O}(\mathrm{x}, t)\rangle \\ &= \langle \overline{\psi}_j(\mathrm{x}', t+\tau)\overline{\Gamma}\psi_i(\mathrm{x}', t+\tau)\overline{\psi}_i(\mathrm{x}, t)\Gamma\psi_j(\mathrm{x}, t)\rangle, \end{aligned} \tag{6.2}$$

where $\overline{\Gamma} = \gamma_4\Gamma^\dagger\gamma_4$.

To calculate this quantity we must perform integrals of the kind

$$\langle \overline{\psi}_{i,x'}\psi_{j,x'}\overline{\psi}_{j,x}\psi_{i,x}\rangle = \frac{1}{Z}\int \mathcal{D}\overline{\psi}\mathcal{D}\psi\mathcal{D}U_\mu \overline{\psi}_{i,x'}\psi_{j,x'}\overline{\psi}_{j,x}\psi_{i,x}e^{-S_E}. \tag{6.3}$$

This integral is an extension of the simpler integral

$$\langle \overline{\psi}_{i,x'}\psi_{j,x}\rangle = \begin{cases} M^{-1}_{xx'} & \text{if } i=j \\ 0 & \text{if } i \neq j \end{cases} \tag{6.4}$$

where $M^{-1}_{xx'}$ is an element of the inverse of the fermion matrix and $\langle \overline{\psi}_{i,x'}\psi_{j,x}\rangle$ is the quark propagator from a point x to a point x'. Looking at (6.4) one can see that we only get a non-zero value for the contraction of the fields if the quark and anti-quark are of the same flavour.

If we now reconsider (6.3), when performing the Wick contraction of the fields one must pair up the fields in all possible ways. There are two different cases one must consider here, the flavour non-singlet and flavour singlet cases. A flavour non-singlet meson is made up of a quark and an anti-quark of different flavours, whereas a flavour singlet meson is made up of a quark and an antiquark of the same flavour.

For the case of a flavour non-singlet meson, there are only two pairings of fields which will give a non-zero contribution according to (6.4). One can illustrate this explicitly by considering a meson containing an up and a down quark. An operator which creates such a meson is $\overline{\psi}_u \Gamma \psi_d$. Inserting this operator into (6.2), one wishes to calculate

$$\langle \overline{\psi}_{d,x'} \overline{\Gamma} \psi_{u,x'} \overline{\psi}_{u,x} \Gamma \psi_{d,x} \rangle, \tag{6.5}$$

where again $\overline{\Gamma} = \gamma_4 \Gamma^\dagger \gamma_4$. Carrying out the Wick contraction gives

$$-\mathrm{Tr}(M^{-1}_{d,xx'} \overline{\Gamma} M^{-1}_{u,x'x} \Gamma), \tag{6.6}$$

where the trace is over spin and colour. If we now turn our attention to a flavour singlet meson, for example a meson made of two up quarks with operator $\overline{\psi}_u \Gamma \psi_u$, one is now calculating

$$\langle \overline{\psi}_{u,x'} \overline{\Gamma} \psi_{u,x'} \overline{\psi}_{u,x} \Gamma \psi_{u,x} \rangle. \tag{6.7}$$

It is easy to see that there are now four ways of pairing up a quark and an antiquark so as to give a non-zero value of (6.4). Performing the Wick contraction gives

$$\mathrm{Tr}(M^{-1}_{u,x'x'} \overline{\Gamma}) \mathrm{Tr}(M^{-1}_{u,xx} \Gamma) - \mathrm{Tr}(M^{-1}_{u,xx'} \overline{\Gamma} M^{-1}_{u,x'x} \Gamma), \tag{6.8}$$

so one has two contributions to the correlators. There is a disconnected correlation,

$$D = \mathrm{Tr}(M^{-1}_{u,x'x'} \overline{\Gamma}) \mathrm{Tr}(M^{-1}_{u,xx} \Gamma), \tag{6.9}$$

and a connected correlation

$$C = -\mathrm{Tr}(M^{-1}_{u,xx'} \overline{\Gamma} M^{-1}_{u,x'x} \Gamma). \tag{6.10}$$

These correlations are illustrated in terms of quark lines in fig 6.1.

Of course, the way we have simulated QCD on the lattice means that the up and down quarks are degenerate. Therefore, the up and down quark propagators are equal. This means that the flavour non-singlet correlator (6.6) is the same as the connected part of the flavour singlet correlator (6.8). In general, if we wish to study a flavour non-singlet meson it is enough to study connected correlations and if we wish to study flavour singlet mesons we should include the disconnected correlation also.

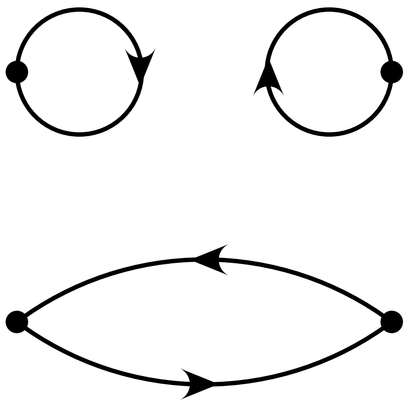

Figure 6.1: Diconnected and connected correlations represented diagrammatically in terms of quark lines.

If we consider the flavour singlet operators containing up and down quark fields, there are four correlations which are non-zero:

$$\langle\overline{\psi}_{u,x'}\psi_{u,x'}\overline{\psi}_{u,x}\psi_{u,x}\rangle \tag{6.11}$$

$$\langle\overline{\psi}_{d,x'}\psi_{d,x'}\overline{\psi}_{u,x}\psi_{u,x}\rangle \tag{6.12}$$

$$\langle\overline{\psi}_{u,x'}\psi_{u,x'}\overline{\psi}_{d,x}\psi_{d,x}\rangle \tag{6.13}$$

$$\langle\overline{\psi}_{d,x'}\psi_{d,x'}\overline{\psi}_{d,x}\psi_{d,x}\rangle \tag{6.14}$$

where we have set $\Gamma = 1$. Of these only two, namely the first and the last, have connected contributions. One can represent these correlations in a matrix which has eigenvalues C and $C + 2D$, where C and D are defined in (6.10) and (6.9) respectively, corresponding to eigenstates $\frac{1}{\sqrt{2}}(\overline{\psi}_u\psi_u - \overline{\psi}_d\psi_d)$ and $\frac{1}{\sqrt{2}}(\overline{\psi}_u\psi_u + \overline{\psi}_d\psi_d)$. This shows that one of the flavour singlet states consisting of these two quarks is degenerate with the flavour non-singlet state, and for the $\frac{1}{\sqrt{2}}(\overline{\psi}_u\psi_u + \overline{\psi}_d\psi_d)$ state we should calculate the quantity $C + 2D$.

We now know what quantities we need to calculate in order to construct meson correlators, namely quark propagators. These quark propagators are matrix elements of the inverse fermion matrix. One must now consider how to calculate the quark propagator.

6.3 Quark Propagators

The calculation of the quark propagator is a very time consuming part of lattice calculation. On the coarse lattices used in this thesis it involves the inversion of a 18432000×18432000 sparse, complex matrix. To calculate this exactly is a hugely expensive thing to do and so one proceeds in a different way. One usually creates a unit point source vector, ξ_x, and then solves the equation

$$M_{xx'}\phi_{x'} = \xi_x \tag{6.15}$$

using a method such as the conjugate gradient method for ϕ. $\phi_{x'}$ is then the quark propagator,

$$G_\psi(x; x') = M^{-1}_{xx'}. \tag{6.16}$$

To calculate a connected correlator one employs the following method. We can make use of the γ_5 hermiticity of the naive fermion matrix to derive

$$M^{-1}_{x'x} = \gamma_5 (M^{-1}_{xx'})^\dagger \gamma_5, \tag{6.17}$$

or

$$G_\psi(x'; x) = \gamma_5 G^\dagger_\psi(x; x')\gamma_5 \tag{6.18}$$

This means that one only has to calculate the propagator from one point on the lattice to all other points and use the relationship (6.18) to obtain the propagator from any other point back to the original point. It is usual to calculate the propagator from the origin to all other points on the lattice. So, one sets up a source which is 1 at the origin and zero at all other sites, $\xi = \delta_{x,0}$. Using the conjugate gradient method to solve (6.15) gives us $G_\psi(0; x)$. This is the simplest way to calculate a quark propagator in lattice simulation. One should be aware that there are other sources that one can use to suit the needs of a particular calculation. We shall discuss some other sources later.

One can illustrate the use of (6.18) by considering the case of the flavour non-singlet pseudoscalar meson consisting of two light quarks, the pion. The operator which creates a state with the quantum numbers of a pion (0^{-+}) is $\overline{\psi}\gamma_5\psi$, where we have dropped the flavour index on the quarks. The correlation function for the pion is then

$$G_\pi(t) = \sum_{\mathrm{x}} \langle \overline{\psi}(\mathrm{x}, t)\gamma_4\gamma_5\gamma_4\psi(\mathrm{x}, t)\overline{\psi}(0, 0)\gamma_5\psi(0, 0)\rangle \tag{6.19}$$

One can write this in terms of quark propagators. Since we are calculating the flavour non-singlet pion correlator, we can use (6.6) or (6.10) to obtain

$$\begin{aligned}
G_\pi(t) &= -\sum_{\mathrm{x}} \mathrm{Tr}(G_\psi(0,0;\mathrm{x},t)\gamma_4\gamma_5\gamma_4 G_\psi(\mathrm{x},t;0,0)\gamma_5) \\
&= \sum_{\mathrm{x}} \mathrm{Tr}(G_\psi(0,0;\mathrm{x},t)\gamma_5 G_\psi(\mathrm{x},t;0,0)\gamma_5) \\
&= \sum_{\mathrm{x}} \mathrm{Tr}(G_\psi(0,0;\mathrm{x},t)\gamma_5^2 G_\psi^\dagger(0,0;\mathrm{x},t)\gamma_5^2) \\
&= \sum_{\mathrm{x}} \mathrm{Tr}|G_\psi(0,0;\mathrm{x},t)|^2. \qquad (6.20)
\end{aligned}$$

This method is not sufficient however, when calculating disconnected correlations. When dealing with these correlations one needs to calculate the propagator from a lattice site to itself. One also needs to calculate this at all lattice sites to be able to carry out the contraction in (6.9). To do this one employs stochastic techniques. We create volume sources of random noise, ξ^i using either a Gaussian or Z_2 distribution of random numbers. For each source one solves

$$M_{xx'}\phi^i_{x'} = \xi^i_x. \qquad (6.21)$$

By using a Gaussian or Z_2 distribution of random numbers in the sources, one ensures that the sources have the normalisation $\langle \xi^{i*}_a \xi^i_b \rangle = 1$ if $a = b$ and zero otherwise where a and b contain the site, spin and colour indices and the average is taken over the total number of noise sources used. Of course this is only true in the limit of infinite number of sources. This ensures that one can obtain estimates for the quark propagator from

$$M^{-1}_{xx'} = \frac{1}{N}\sum_{i=1}^{N}(\xi^i_{x'})^*\phi^i_x, \qquad (6.22)$$

where N is the number of sources. This is because

$$\phi_x = M^{-1}_{xy}\xi_y, \qquad (6.23)$$

so therefore,

$$\begin{aligned}
\xi^*_{x'}\phi_x &= \xi^*_{x'}M^{-1}_{xy}\xi_y \\
&= \xi^*_{x'}M^{-1}_{xx'}\xi_{x'} + \xi^*_{x'}M^{-1}_{x'y}\xi_y, \qquad (6.24)
\end{aligned}$$

where $y \neq x'$.

The second term of (6.24) is zero when averaged over an infinite number of sources due to the random distribution of the sources leaving us with the propagator we want, namely $M^{-1}_{xx'}$. This technique enables us to calculate a stochastic estimator of the propagator from any lattice site to any other lattice site. So for the calculation of a disconnected correlation one can pick out the propagator from a site, x, to itself by taking the scalar product $\xi^*_x \phi_x$. We must consider here the effect of using a finite number of noise sources. The normalisation of the sources, that we described earlier, only holds if $N \to \infty$ and so by using a finite N we do not ensure that the second term of (6.24) is zero. Therefore there are spurious contributions from other propagators which manifest themselves as statistical noise in our measured quantities. One must make sure to use enough noise samples to ensure that these contributions are small.

The variance in the measurements of $\xi^*_{x'} \phi_x$ tends to be large meaning that a reliable calculation of stochastic propagators can be a time consuming affair. To determine whether the statistical noise is making a significant contribution to our measurements there is a test one can perform. Let us consider the measurement of a disconnected loop operator

$$L(t) = \sum_{\mathrm{x}} \mathrm{Tr}(G_\psi(\mathrm{x}, t; \mathrm{x}, t)\Gamma), \tag{6.25}$$

where $G_\psi(\mathrm{x}, t; \mathrm{x}, t) = M^{-1}_{xx}$ and is given by (6.22) with $x = x'$. One can calculate the observed variance of these operators on a particular gauge configuration as follows;

$$\sigma^2_{obs} = \frac{1}{L_t} \sum_{t=1}^{L_t} (L(t) - \overline{L})^2. \tag{6.26}$$

Here L_t is the length of the lattice in the time direction and $\overline{L}$ is the average over timeslices of $L(t)$. So, we have L_t measurements of our disconnected loop operators and σ_{obs} is the variance of the operators with respect to timeslice. Of course $L(t)$ is an average of the loop operators, $L_i(t)$, calculated for each random source. Therefore one can estimate the standard deviation on the mean of these operators over the total number of noise samples and use this to calculate the variance due to the stochastic sources.

$$\sigma_{sto} = \frac{1}{L_t} \sum_{t=1}^{L_t} \frac{1}{\sqrt{N-1}} \, \sigma_L(t) \tag{6.27}$$

where

$$\sigma^2_L(t) = \frac{1}{N} \sum_{i=1}^{N} (L_i(t) - L(t))^2. \tag{6.28}$$

So, one now has an estimate of the observed variance in the operators and an estimate of the variance which is induced by the use of random noise sources. These can be used to calculate the real standard deviation of the loop operators on a gauge configuration,

$$\sigma_{gauge} = \sqrt{\sigma_{obs}^2 - \sigma_{sto}^2}. \tag{6.29}$$

By measuring these quantities it is possible to determine how much error is introduced into the loop calculations from the use of stochastic methods. Indeed if $\sigma_{sto} > \sigma_{gauge}$ then this would imply that our observed variance has a larger contribution from the noise sources than it does from the true physics error. One can reduce the value of σ_{sto} by including more noise sources into the calculation. Ideally we would like to use enough sources so that σ_{sto} is negligible but more sources means more inversions which, as we have already seen, means the calculation becomes a lot more time consuming.

When deciding on how many stochastic sources to use, an absolute limit should be that enough sources are used so that $\sigma_{sto} < \sigma_{gauge}$. This would then ensure that the largest contribution to the observed variance is from real physics and not from the stochastic techniques employed. This will be discussed in more detail when we consider exactly which operators we will be measuring.

6.4 Staggered Operators

We have seen how to calculate correlations of mesonic operators using naive fermions. We must now consider staggered fermions and in particular how one goes about constructing operators in this formalism. One can recall from chapter 3 the definition of staggered fermions, χ,

$$\psi(x) = \Omega(x)\chi(x). \tag{6.30}$$

These have only one spin component and so to be able to reconstruct continuum objects with four spin components one must work in the *spin* $\otimes$ *taste* basis. Therefore one must use the extended quark fields defined in (3.15) to construct mesonic operators which will have the correct spin and flavour content in the continuum. One also has to take into account the four extra tastes of staggered fermions.

In the staggered formalism an operator which creates a meson of given spin and taste is [33]

$$\mathcal{O} = \overline{Q}(\Gamma_S \otimes \Gamma_T)Q, \tag{6.31}$$

where $\overline{Q}$ and Q are defined in (3.15). Here the Γ_S and Γ_T act on the spin and taste indices of the quark fields respectively and are defined as follows;

$$\begin{aligned} \Gamma_S &= \prod_{\mu=1}^{4}(\gamma_\mu)^{S_\mu}, \\ \Gamma_T &= \prod_{\mu=1}^{4}(\gamma_\mu)^{T_\mu}. \end{aligned} \tag{6.32}$$

Here we have represented the spin and taste content as four vectors whose components are defined modulo 2. In terms of the staggered χ fields these operators can be written as

$$\mathcal{O} = \sum_{\eta,\eta'} \bar{\chi}(2y+\eta)\mathrm{Tr}(\Gamma_\eta^\dagger \Gamma_S \Gamma_{\eta'} \Gamma_T^\dagger)\chi(2y+\eta'). \tag{6.33}$$

It is obvious that inserting this into (6.2) will lead to a very complicated derivation of the correlation functions. Fortunately one can simplify things by considering the relationship between the staggered fermion propagator and the naive fermion propagator. The naive fermion propagator was defined earlier to be

$$G_\psi(x;x') = \langle \overline{\psi}(x')\psi(x) \rangle. \tag{6.34}$$

Using (6.30), one can rewrite this as follows [74];

$$\begin{aligned} G_\psi(x;x') &= \langle \overline{\chi}(x')\Omega^\dagger(x')\Omega(x)\chi(x) \rangle \\ &= G_\chi(x;x')\Omega(x)\Omega^\dagger(x'), \end{aligned} \tag{6.35}$$

where $G_\chi(x;x')$ is the staggered propagator. This shows that if one can write staggered operators in terms of naive fermions, it is possible to write down correlators for these naive operators and use (6.35) to derive the staggered correlators.

To derive the correlators one firstly has to consider how the trace in the operator (6.33) is going to give a non-zero value. One begins by choosing a Γ_S which will give the correct spin quantum numbers of the particle of interest. For example for a pseudoscalar particle one would use $\Gamma_S = \gamma_5$ and for a scalar particle $\Gamma_S = 1$. One now has to consider which choice to make for Γ_T. There are sixteen possible choices for this matrix, which correspond to the sixteen tastes of particle produced by the four tastes of staggered fermion as described in section 3.3.2.

One can write down all of the possible representations of a particular meson in the $\Gamma_S \otimes \Gamma_T$ basis. Since this thesis is mainly concerned with scalar mesons, we shall consider them here. In [33] all the representations for the pseudoscalar and vector mesons were written down. Here we follow [33] and write this down for the scalar meson.

$$\begin{aligned}
\mathbf{15} \quad &\rightarrow \quad (1 \otimes \gamma_i) \oplus (1 \otimes \gamma_i\gamma_4) \oplus (1 \otimes \gamma_i\gamma_5) \oplus (1 \otimes \gamma_i\gamma_4\gamma_5) \\
&\qquad \oplus (1 \otimes \gamma_4) \oplus (1 \otimes \gamma_5) \oplus (1 \otimes \gamma_4\gamma_5) \\
\mathbf{1} \quad &\rightarrow \quad (1 \otimes 1). \qquad (6.36)
\end{aligned}$$

Here the **15** and **1** are the continuum $SU(4)$ representations that the mesons lie in and $i = 1, 2$ or 3. In principle all of these sixteen representations correspond to particles of identical mass but as discussed in section 3.3.2 taste symmetry is broken at finite lattice spacing and these particles have different masses. The final choice for Γ_T that will be used in a specific calculation will be discussed later.

Getting back to the main consideration here, which is how to obtain a non-zero value of the trace in (6.33), it is convenient to define a hypercube vector $\delta = S + T$ where the addition is carried out modulo 2. Let us now try to calculate this trace for a general Γ_S and Γ_T,

$$\mathrm{Tr}(\Gamma_\eta^\dagger \Gamma_S \Gamma_{\eta'} \Gamma_T^\dagger) = \mathrm{Tr}(\Gamma_\eta^\dagger \Gamma_{\eta'} \Gamma_S \Gamma_T^\dagger)\ \zeta(\eta', S), \qquad (6.37)$$

where $\zeta(\eta', S)$ is a phase which arises from commuting the gamma matrices in $\Gamma_{\eta'}$ through those in Γ_S. Now since $S + T = \delta$ one can write

$$\begin{aligned}
\mathrm{Tr}(\Gamma_\eta^\dagger \Gamma_{\eta'} \Gamma_S \Gamma_T^\dagger)\ \zeta(\eta', S) &= \mathrm{Tr}(\Gamma_\eta^\dagger \Gamma_{\eta'} \Gamma_{\delta-T} \Gamma_T^\dagger)\ \zeta(\eta', S) \\
&= \mathrm{Tr}(\Gamma_\eta^\dagger \Gamma_{\eta'} \Gamma_\delta \Gamma_T \Gamma_T^\dagger)\ \zeta(\eta', S)\ \zeta'(\delta, T) \\
&= \mathrm{Tr}(\Gamma_\eta^\dagger \Gamma_{\eta'-\delta})\ \zeta(\eta', S)\ \zeta'(\delta, T)\ \zeta''(\eta', \delta) \\
&= 4\delta_{\eta,\eta'-\delta}\ \zeta(\eta', S)\ \zeta'(\delta, T)\ \zeta''(\eta', \delta) \qquad (6.38)
\end{aligned}$$

So, in general, the trace is only non-zero for the cases where $\eta' + \eta = \delta$, where again the addition is modulo 2.

Substituting this into (6.33), one obtains

$$\mathcal{O} = \sum_{\eta} \bar{\chi}(2y+\eta)\chi(2y+\eta+\delta)\ \zeta'(\eta,S)\ \zeta'(\delta,T)\ \zeta''(\eta,\delta). \tag{6.39}$$

Therefore for a particular Γ_S, operators which create mesons with different taste content will have differing distances between the $\overline{\chi}$ and the χ fields across a hypercube and a different phase. Of course these operators are not gauge invariant so one must either include gauge links in the operators or work in a fixed gauge such as the Coulomb gauge. Calculations in this thesis involving non-local operators have been carried out in the Coulomb gauge, following the lead of the MILC collaboration [56]. For details on how one fixes the gauge to the Coulomb gauge, the reader is referred to the discussion in [15].

Summing up, the situation is that to create a meson in a particular $\Gamma_S \otimes \Gamma_T$ representation one must use an operator in which the $\overline{\chi}$ and χ fields are, in general, at different sites. The distance between the sites is given by $\delta = S + T$. The operator also has an associated phase which, for a given Γ_S and Γ_T, depends on η and δ. To arrive at the expressions for the correlators one needs to perform the complicated trace as above for the particular representation one wishes to study and do the Wick contractions. This can be a complicated and arduous calculation. However one can derive the staggered correlators alternatively using naive fermionic operators [74], in which the $\overline{\psi}$ and ψ fields are at different sites where the distance between the sites is governed by δ, and making use of (6.35).

In the *spin* $\otimes$ *taste* basis the naive operators are [75]

$$\overline{\psi}(x)\Gamma_S\psi(x+\delta). \tag{6.40}$$

Using these non-local operators in (6.2) and performing the Wick contraction as in section 6.2, one obtains the connected correlation

$$C = -\mathrm{Tr}(M^{-1}_{xy'}\overline{\Gamma}_S M^{-1}_{yx'}\Gamma_S), \tag{6.41}$$

where we have created the meson at a site x and destroyed it at a site y. Here $x' = x + \delta$ and $y' = y + \delta$. One can rewrite this as

$$C \;=\; -\mathrm{Tr}(G_\psi(x;y')\overline{\Gamma}_S G_\psi(y;x')\Gamma_S)$$

$$
\begin{aligned}
&= -\mathrm{Tr}(G_\chi(x;y')\Omega(x)\Omega^\dagger(y')\overline{\Gamma}_S G_\chi(y;x')\Omega(y)\Omega^\dagger(x')\Gamma_S) \\
&= -\mathrm{Tr}(G_\chi(x;y')G_\chi(y;x'))\mathrm{Tr}(\Omega(x)\Omega^\dagger(y')\overline{\Gamma}_S\Omega(y)\Omega^\dagger(x')\Gamma_S). \qquad (6.42)
\end{aligned}
$$

Here the trace of the staggered propagators is over colour only as they don't contain spin indices. One can also derive the staggered version of (6.18) here.

$$
\begin{aligned}
G_\psi(y;x) &= \gamma_5 G_\psi^\dagger(x;y)\gamma_5 \\
\Rightarrow G_\chi(y;x)\Omega(y)\Omega^\dagger(x) &= G_\chi^\dagger(x;y)\gamma_5\Omega(y)\Omega^\dagger(x)\gamma_5. \qquad (6.43)
\end{aligned}
$$

Commuting a γ_5 through the Ω matrices gives

$$
G_\chi(y;x) = (-1)^{\sum_\mu(x_\mu+y_\mu)}G_\chi^\dagger(x;y). \qquad (6.44)
$$

Substituting this into (6.42) leads to a correlator of the form

$$
-(-1)^{\sum_\mu(x'_\mu+y_\mu)}\mathrm{Tr}(G_\chi(x;y')G_\chi^\dagger(x';y))\mathrm{Tr}(\Omega(x)\Omega^\dagger(y')\overline{\Gamma}_S\Omega(y)\Omega^\dagger(x')\Gamma_S). \qquad (6.45)
$$

This equation illustrates the main difference between a staggered correlator calculation and a naive correlator calculation. In section 6.3 it was described how one could calculate a naive correlator using a point source at the origin and only calculating one propagator. In the analogous staggered calculation, except for the case when $\Gamma_S = \Gamma_T$, one would have to calculate two staggered propagators, one from the origin to all other points on the lattice and one from the site δ to all other points on the lattice. This is not too much of a hindrance however, since the computational cost of computing a staggered propagator is at least a factor of four cheaper than any other fermion formalism. The correlator of a meson created at the origin and destroyed at a point y is

$$
-(-1)^{\sum_\mu(\delta_\mu+y_\mu)}\mathrm{Tr}(G_\chi(0;y')G_\chi^\dagger(\delta;y))\mathrm{Tr}(\Omega^\dagger(y')\overline{\Gamma}_S\Omega(y)\Omega^\dagger(\delta)\Gamma_S). \qquad (6.46)
$$

All connected staggered correlators studied in this thesis have been derived using (6.46).

The disconnected correlator that arises from using this method is

$$
D = \mathrm{Tr}(G_\psi(x';x)\overline{\Gamma}_S)\mathrm{Tr}(G_\psi(y';y)\Gamma_S), \qquad (6.47)
$$

where again $x' = x+\delta$ and $y' = y+\delta$. Writing this in terms of staggered propagators, one obtains

$$
D = \mathrm{Tr}(G_\chi(x';x)\Omega(x')\Omega^\dagger(x)\overline{\Gamma}_S)\mathrm{Tr}(G_\chi(y';y)\Omega(y')\Omega^\dagger(y)\Gamma_S). \qquad (6.48)
$$

One must consider here whether, for a particular Γ_S, D is non-zero for all sixteen choices of Γ_T. Now since

$$\Omega(x') = \Gamma_\delta \Omega(x) \zeta(\delta, x) \tag{6.49}$$

then considering just the piece of (6.48) involving y we have

$$\begin{aligned} \mathrm{Tr}(G_\chi(y';y)\Omega(y')\Omega^\dagger(y)\Gamma_S) &= \zeta(\delta,y)\mathrm{Tr}(G_\chi(y';y)\Gamma_\delta\Gamma_S) \\ &= \zeta(\delta,y)\zeta'(\delta,S)\mathrm{Tr}(G_\chi(y',y)\Gamma_T), \end{aligned} \tag{6.50}$$

where again the ζ's are phases which arise from commuting γ matrices with each other (for examples of explicit calculations of these phases see appendix B). From this one can see that this will only be non-zero if Γ_T is the identity matrix because all other choices for Γ are traceless. This means that for a staggered meson correlator to have a disconnected contribution then the meson must be a taste singlet and lie in the representation $\Gamma_S \otimes 1$.

This simplifies things a bit in that to carry out a calculation involving disconnected loops then the choice of Γ_T is automatic. For the calculation of the singlet scalar the operator that one would use would lie in the $1 \otimes 1$ representation. In this case we have $\Gamma_S = \Gamma_T$ which means that $\delta = 0$. Therefore the operator which creates this state is simply

$$\mathcal{O} = \overline{\psi}(x)\psi(x). \tag{6.51}$$

If one wished to study the singlet pseudoscalar, the operator would lie in the $\gamma_5 \otimes 1$ representation. In this case the operator is

$$\mathcal{O} = \overline{\psi}(x)\gamma_5\psi(x+\delta), \tag{6.52}$$

where $\delta = (1,1,1,1)$. Here lies a problem one must confront in a calculation involving the η'. In calculations of the pion spectrum using staggered fermions, the taste breaking effects are large at lattice spacings presently used. One uses the lightest of the states as the true Goldstone pion. The operator for this state lies in the $\gamma_5 \otimes \gamma_5$ representation. The connected correlator that one would be using in an η' calculation is therefore not the Goldstone pion correlator and indeed corresponds to the heaviest of the pions.

6.5 Parity Partners

Another feature of calculating meson correlators with staggered fermions is the fact that an operator which creates a state that lies in the representation $\Gamma_S \otimes \Gamma_T$ also couples to a state that lies in the $\gamma_4\gamma_5\Gamma_S \otimes \gamma_4\gamma_5\Gamma_T$ representation. This state is named the oscillating parity partner of the $\Gamma_S \otimes \Gamma_T$ state. This is because the contribution from this state to a correlator oscillates in time, i.e. is positive on one time slice and negative on the next and so on. Thus a staggered correlator has the general form

$$C(t) = A_0 e^{-m(\Gamma_S\otimes\Gamma_T)} + (-1)^t A_1 e^{-m(\gamma_4\gamma_5\Gamma_S\otimes\gamma_4\gamma_5\Gamma_T)}. \tag{6.53}$$

The reason why this is the general form of the correlator is discussed later (in particular see (6.62) - (6.64)). In general pseudoscalars are partnered with scalars and vector particles are paired with pseudovectors. To resolve this when calculating masses, one must carry out a two exponential fit, allowing one exponential to oscillate.

In certain cases however, the parity partner of a particular particle will have exotic quantum numbers and so will not contribute to the correlator. In these cases a single, non-oscillating exponential fit will suffice. One can illustrate this by considering some of the pseudoscalar representations and their parity partners, as shown in table 6.1.

Pseudoscalar Representation	J^{PC}	Parity Partner	J^{PC}
$\gamma_5 \otimes \gamma_5$	0^{-+}	$\gamma_4 \otimes \gamma_4$	0^{+-}
$\gamma_4\gamma_5 \otimes \gamma_4\gamma_5$	0^{-+}	$1 \otimes 1$	0^{++}
$\gamma_5 \otimes \gamma_i\gamma_5$	0^{-+}	$\gamma_4 \otimes \gamma_i\gamma_4$	0^{+-}
$\gamma_4\gamma_5 \otimes \gamma_i\gamma_4\gamma_5$	0^{-+}	$1 \otimes \gamma_i$	0^{++}

Table 6.1: Local and one link pseudoscalar representations and their parity partners.

Of the two local pseudoscalar operators, one has a parity partner with exotic quantum numbers and one does not. This is also the case for the one link pseudoscalar operators. Indeed one can extend this to show that for half the pseudoscalars there is no oscillatory contribution to the correlators because of the exotic quantum numbers of their respective parity partners. This makes fitting to the pion correlators less complicated as one only needs to do a single exponential fit. This is especially advantageous since the Goldstone pion operator, namely that which lies in the $\gamma_5 \otimes \gamma_5$ representation, has an exotic parity partner.

This is not the case when considering the scalars however. The lightest scalar lies in the $1 \otimes 1$ representation and the corresponding operator is also that which we want to use for our taste singlet study. Looking at table 6.1 one can see that this state is partnered with the local non-Goldstone pion, which lies in the $\gamma_4\gamma_5 \otimes \gamma_4\gamma_5$ representation. This means that when studying the correlations of this operator one must include an oscillating exponential corresponding to the pion contribution. Alternatively if one was only interested in calculating the mass of the flavour non-singlet scalar, one could measure correlations of the operator corresponding to the $\gamma_4\gamma_5 \otimes \gamma_4\gamma_5$ representation and then the oscillating piece would be the scalar contribution. Extending this to consider all the scalar operators one can show that all scalar operators will give rise to an oscillating pseudoscalar state. Therefore for all fits to scalar correlators one must include an oscillating exponential in the fit function.

6.6 Details of Specific Calculations

In this section we will discuss the specific calculations that have been carried out for this thesis. The main calculation involves the study of the flavour/taste singlet and non-singlet scalar mesons. As a by product of this calculation we have calculated non-singlet pseudoscalar masses using the connected correlators. A small study of taste splitting in the mass spectrum of the scalar representations has also been carried out. We will describe the methods employed for this calculation first and then move on to the methods used for the singlet calculation. These discussions will include descriptions of the specific operators used, the corresponding quark sources that we chose to invert from and the correlators measured. It should be pointed out that for all the calculations we have generated quark propagators with the valence quark mass equal to the light sea quark mass.

This means that the quark mass that was used in the fermion matrix for the generation of the quark propagators is theoretically identical to that which was used in the generation of the gauge configurations themselves. One could choose to use a valence quark mass that was different from the sea quark mass if one wished. Adopting such an approach, one would be working in the so called partially quenched approximation. We have chosen not to work in this approximation, but to simulate full QCD as closely as possible by using equal sea and valence masses.

6.6.1 Methods for Calculating the Taste Splitting in the Scalars

The mass splitting between the different taste representations of pseudoscalar particles is a well known and well studied phenomenon, for example see [38, 57, 76, 77]. It is known to be an $O(a^2)$ effect and can be reduced by improving the action as described in chapter 3. What is less well reported in the literature is the mass differences between the different taste representations of other particles. A study by the MILC collaboration [56] reported that the taste symmetry breaking was smaller than the statistical errors on the masses of the vector particles. However, for the scalars they report that the splittings are large and may be correlated with the splittings of the pseudoscalars they are partnered with. We propose to carry out a mini study of this on the coarse lattices with light quark mass $am_q = 0.03$.

The sixteen different taste representations of a scalar meson are arranged into eight multiplets, which were written down earlier (6.36). Using the methods employed here one can calculate the masses of four of these representations. The eight multiplets can be described by the number of links between the quark and anti-quark in the operator. The eight choices are; a local operator, one, two and three link operators containing only spatial links, one, two and three link operators containing a temporal link and a four link operator. Instead of including the gauge links in the operators to ensure gauge invariance, we fix the gauge to the Coulomb gauge. This is a spatially fixed gauge and so we restrict ourselves to studying operators containing spatial links only. Therefore, the four scalar representations one can study are the local $1 \otimes 1$, the one link $1 \otimes \gamma_i$, the two link $1 \otimes \gamma_i\gamma_4\gamma_5$ and the three link $1 \otimes \gamma_4\gamma_5$. The pseudoscalar parity partners of these representations are $\gamma_4\gamma_5 \otimes \gamma_4\gamma_5$, $\gamma_4\gamma_5 \otimes \gamma_i\gamma_4\gamma_5$, $\gamma_4\gamma_5 \otimes \gamma_i$ and $\gamma_4\gamma_5 \otimes 1$ respectively.

A quantity that has been used as a measure of taste breaking for the pseudoscalar mesons is [57]

$$(m_\pi^2 - m_G^2)r_1^2. \tag{6.54}$$

Here m_G is the mass of the Goldstone pion and m_π is the mass of some other pseudoscalar representation. We propose to measure a similar quantity here as a measure of the mass splittings of the available scalar representations,

$$(m_{sc}^2 - m_{1\otimes 1}^2)r_1^2. \tag{6.55}$$

We will measure the values of (6.54) and (6.55) for each representation and investigate if indeed there is some connection between the splitting of the scalar and pseudoscalar masses.

To obtain the masses of the particles we measure correlators that have been derived using the methods of section 6.4. In particular, let us recall from (6.46) that the correlator for a meson created at the origin and destroyed at a point x, which lies in a $\Gamma_S \otimes \Gamma_T$ representation, is

$$C = -(-1)^{\sum_\mu(\delta_\mu + x_\mu)}\mathrm{Tr}(G_\chi(0;x')G_\chi^\dagger(\delta;x))\mathrm{Tr}(\Omega^\dagger(x')\overline{\Gamma}_S\Omega(x)\Omega^\dagger(\delta)\Gamma_S). \tag{6.56}$$

Since we are restricted to using operators containing no temporal links there are only eight possible choices for δ, which correspond to vectors pointing to the eight corners of cube on a timeslice. Therefore to calculate the masses of the local, one link, two link and three link scalar representations one must carry out eight inversions. We follow the methods of the MILC collaboration and use wall source [33] inversion methods for this calculation. The source is equal to one at the point δ in each of the cubes on the source timeslice and zero elsewhere. One ends up with eight propagators which can be contracted together in the correct ways to give the correlator required for each scalar representation.

Of course one also needs to calculate the trace involving the Ω, Γ_S and Γ_T matrices. This is a relatively straightforward calculation which gives a phase factor by which the correlator should be multiplied. Let us explicitly calculate this for the $1\otimes\gamma_4\gamma_5$ representation here. For this representation

$$\Gamma_S = 1 \quad , \quad \Gamma_T = \gamma_4\gamma_5, \tag{6.57}$$

therefore,

$$S = (0,0,0,0) \quad , \quad T = (1,1,1,0). \tag{6.58}$$

This means that

$$\delta = (S+T)\text{mod}2 = (1,1,1,0). \tag{6.59}$$

Now since $x' = x + \delta$, it follows that

$$\begin{aligned}\Omega(x') &= \gamma_1^{x_1+1}\gamma_2^{x_2+1}\gamma_3^{x_3+1}\gamma_1^{x_4} \\ &= (-1)^{x_2+x_4}\gamma_1^{x_1}\gamma_2^{x_2}\gamma_3^{x_3}\gamma_4^{x_4}\gamma_1\gamma_2\gamma_3 \\ &= (-1)^{x_2+x_4}\Omega(x)\Omega(\delta).\end{aligned} \tag{6.60}$$

We also have that $\Gamma_S = 1$, which implies that $\overline{\Gamma}_S = 1$. Substituting for these and $\Omega(x')$ in (6.56) gives

$$\begin{aligned}C_{1\otimes\gamma_4\gamma_5} &= (-1)^{\sum_\mu x_\mu}(-1)^{x_2+x_4}\text{Tr}(G_\chi(0;x')G_\chi^\dagger(\delta;x))\text{Tr}(\Omega^\dagger(\delta)\Omega^\dagger(x)\Omega(x)\Omega^\dagger(\delta)) \\ &= -(-1)^{x_1+x_3}\text{Tr}(G_\chi(0;x')G_\chi^\dagger(\delta;x)).\end{aligned} \tag{6.61}$$

Performing a two exponential fit to the above correlator with one exponential oscillating, one obtains the masses of the $1\otimes\gamma_4\gamma_5$ and $\gamma_4\gamma_5\otimes 1$ representations. The correlators for the other scalar representations considered here are derived in appendix B. One can also see the relationship between a particular representation and its parity partner here by deriving the correlator for the $\gamma_4\gamma_5\otimes 1$ pseudoscalar operator. For this operator $\Gamma_S = \gamma_4\gamma_5$ and $\Gamma_T = 1$. Therefore we have

$$S = (1,1,1,0) \quad , \quad T = (0,0,0,0) \tag{6.62}$$

and so δ and $\Omega(x')$ are as they were in (6.59) and (6.60) respectively. The difference here is that $\Gamma_S = \gamma_4\gamma_5$, which implies that $\overline{\Gamma}_S = \gamma_4\gamma_5$ also. So,

$$\begin{aligned}\text{Tr}(\Omega^\dagger(x')\overline{\Gamma}_S\Omega(x)\Omega^\dagger(\delta)\Gamma_S) &= (-1)^{x_2+x_4}\text{Tr}(\Omega^\dagger(\delta)\Omega^\dagger(x)\gamma_4\gamma_5\Omega(x)\Omega^\dagger(\delta)\gamma_4\gamma_5) \\ &= (-1)^{x_2}\text{Tr}(\Omega^\dagger(\delta)\gamma_4\gamma_5\Omega^\dagger(\delta)\gamma_4\gamma_5) \\ &= (-1)^{x_2}.\end{aligned} \tag{6.63}$$

Substituting into (6.56) gives

$$\begin{aligned}C_{\gamma_4\gamma_5\otimes 1} &= (-1)^{x_1+x_3+x_4}\text{Tr}(G_\chi(0;x')G_\chi^\dagger(\delta;x)) \\ &= -(-1)^{x_4}C_{1\otimes\gamma_4\gamma_5}.\end{aligned} \tag{6.64}$$

One can see that the correlator for a particular representation oscillates in time with respect to the correlator of its parity partner. In this case if one measures the correlator for the scalar operator, then the oscillating piece is the pseudoscalar contribution. Conversely, if one calculates the correlator for the pseudoscalar operator, the oscillating piece is the scalar contribution. This gives two equivalent ways of calculating a particle's mass: using the operator for that particle or its parity partner. For this study we calculate the correlators for the four scalar representations listed above and also the Goldstone pion correlator. This has been done on a subset of 205 of the coarse lattices with light quark mass $am_q = 0.03$. To increase the statistics we use two source timeslices per configuration, separated by equal distances. These are at $t = 0$ and $t = 32$.

6.6.2 Methods for Singlet Calculations

As in the previous section one must derive the correlators one needs to calculate for the singlet calculation. As we are interested in the scalar we are forced to use the operator for the $1 \otimes 1$ representation. For the scalar taste singlet one must consider both connected and disconnected correlations as described in sections 6.2 and 6.4. The connected correlator for this operator has been derived in appendix B and is given by (B.5). In the singlet calculation we must use a different technique than in the previous section for calculating the connected correlator. This follows from the requirement that one must use the same methods for calculating the disconnected and connected correlations. Since one would like to use volume source techniques to generate point-like quark propagators for the disconnected calculation, one must also use a point source inversion to generate the quark propagators for the connected calculation. The source we use for this calculation is simply equal to one at the origin and zero elsewhere.

To derive the disconnected correlator, one can recall from (6.48) that the disconnected correlator for a staggered meson is

$$D = \mathrm{Tr}(G_\chi(x';x)\Omega(x')\Omega^\dagger(x)\overline{\Gamma}_S)\mathrm{Tr}(G_\chi(y';y)\Omega(y')\Omega^\dagger(y)\Gamma_S), \tag{6.65}$$

where, as is now customary, $x' = x + \delta$ and $y' = y + \delta$. For the $1 \otimes 1$ operator, one has

$\Gamma_S = \Gamma_T = 1$. Therefore $S = T$ and

$$\delta = S = T = (0, 0, 0, 0). \tag{6.66}$$

This means that $x' = x$ and $y' = y$. Also, $\overline{\Gamma}_S = 1$ and so

$$D = \mathrm{Tr}(G_\chi(x; x))\mathrm{Tr}(G_\chi(y; y)) \tag{6.67}$$

To calculate this quantity one calculates the fermion loops

$$L(t) = \sum_{\mathrm{x}} \mathrm{Tr} G_\chi(\mathrm{x}, t; \mathrm{x}, t), \tag{6.68}$$

using the methods described in section 6.3. We used Gaussian volume sources for our inversions. An analysis has been carried out for ensembles A, B and C listed in table 4.1. To make a choice of the number of stochastic sources to use, one calculates σ_{obs} and σ_{sto}. These were defined in (6.26) and (6.27) respectively. A very small scale calculation of these quantities on five configurations of ensemble A revealed that by using 48 and 100 sources we have $\sigma_{sto} < \sigma_{gauge}$, as is shown in table 6.2. This is the condition that is necessary to ensure that the variance in our results is due to physics rather than the stochastic sources, as was explained in section 6.3.

Nsrc	σ_{obs}	σ_{sto}	σ_{gauge}
48	29.6	15.3	25.2
100	27.8	10.6	25.8

Table 6.2: Investigation of stochastic noise on five configurations of ensemble A.

The number of sources we therefore decided to use was 48. The main factor in this decision was one of time. A doubling of the number of sources results in a doubling of computer time but only a $\frac{1}{\sqrt{2}}$ reduction in σ_{sto}. We felt we could gain more by analysing more configurations than using more sources. Analysing more configurations means that we have a better determination of the correlations of the operators. As has been pointed out before, we deem that our operators are determined well enough if $\sigma_{sto} < \sigma_{gauge}$. As one can see by looking at table 6.3, 48 sources is enough to ensure that $\sigma_{sto} < \sigma_{gauge}$ for all the ensembles that we chose to measure. One can also see that as one decreases the light quark mass the noise due to the stochastic sources increases. However, it does not increase so much that we should be too worried about increasing the number of sources.

Ensemble	σ_{obs}	σ_{sto}	σ_{gauge}
A	29.3	15.3	24.9
B	31.2	17.2	26.0
C	35.3	21.8	27.7

Table 6.3: Stochastic variance versus true variance for 48 sources calculated using all the configurations of each ensemble.

Once one has calculated the fermion loops then one can construct the disconnected correlators and form the combination $C + 2D$, which corresponds to the two flavour taste singlet correlator as described in section 6.2. Now is the time to discuss yet another vagary of calculations with staggered fermions. The taste singlet scalar operator has as its parity partner the $\gamma_4\gamma_5 \otimes \gamma_4\gamma_5$ pseudoscalar operator. Now, this operator is not taste singlet and so has no disconnected piece. We can show this by calculating (6.65) for this operator. Since $\Gamma_S = \Gamma_T = \gamma_4\gamma_5$, then $\delta = 0$. So, for this operator we have,

$$D = \mathrm{Tr}(G_\chi(x;x)\gamma_4\gamma_5)\mathrm{Tr}(G_\chi(y;y)\gamma_4\gamma_5). \tag{6.69}$$

Since the trace here is over spin and colour and the staggered propagator has no spin indices, this will be zero.

So, one has the situation that the connected piece of the scalar taste singlet has an oscillating contribution from its parity partner, while the disconnected piece does not. Therefore the only oscillating contribution to $C + 2D$ comes from C. Ideally we would like to remove the oscillating contribution from the connected correlator. To deal with this we have chosen to proceed as follows. One first performs an oscillating fit to the connected correlator alone. This allows one to determine the mass of the oscillating component of the correlator and also the non-singlet scalar mass. Once the parameters of the oscillating component have been found, one then fixes these parameters in a fit to $C + 2D$. This procedure amounts to effectively subtracting the oscillating contribution from the connected correlator. As a result of this analysis one obtains the masses of the local non-Goldstone pion, the non-singlet scalar and the singlet scalar.

6.7 Improving the operators

As was the case for the glueball calculation, the singlet calculation suffers from the fact that the signal to noise ratio of the disconnected correlations is quite poor. As a result one is forced to carry out the fits to the data at small time values and also short time regions. At these small values of t it is not clear that the excited state contributions are negligible. One can perform a multi exponential fit to the data to allow for the excited state contributions. However it may be the case that doing so is not enough to resolve the problem. In this case it is usual to use improved operators in the calculation. A common way to improve the operators is by so called fuzzing [78].

Fuzzed operators have the advantage that they tend to have an increased coupling to the ground state when compared to local operators. They also have a different coupling to excited states. By using these operators along with local operators one is able to make a better estimate of the ground state mass along with the mass of excited states. A fuzzed operator differs from a local operator in that the quark and anti-quark are not at the same site. This is not to be confused with the non-local staggered operators described earlier. Here we are creating an operator which couples to the same state as the original local operator.

A fuzzed operator has the form

$$\mathcal{O} = \overline{\psi}(x)\Gamma P(x, x + n\mu)\psi(x + n\mu), \tag{6.70}$$

where P is a product of gauge links separating the quark and anti-quark and n is an integer which is called the fuzzing width and represents how many gauge links are included in the path P. To ensure that J^{PC} values are not affected, one must make this operator spatially symmetric by summing over the six spatial directions on the lattice. Therefore, the operator is

$$\mathcal{O} = \frac{1}{6}\sum_{\mu=1}^{6}\overline{\psi}(x)\Gamma P(x, x + n\mu)\psi(x + n\mu). \tag{6.71}$$

The term fuzzing arises here because of the fact that one does not use the original gauge links in the path P but so called fuzzed links. These fuzzed links are obtained by a number of iterations of APE smearing [47]. This procedure gives an operator a spatial extension which one would hope would result in a greater overlap with the ground state wavefunction of the particular state one is interested in. One can tune the operators by varying the number of iterations of APE smearing, the parameters of the smearing itself and also n, which we call the fuzzing width.

In principle one can use any value of n when creating a fuzzed operator. However one must be careful when considering fuzzing in the case of staggered fermions. The value of n used in the fuzzing must be even for two reasons. Firstly, one has to ensure that there is no contamination from different taste representations. By using an even fuzzing width the quark in the fuzzed operator will be at the same position, albeit in a different hypercube, as in the original unfuzzed operator. If the fuzzing width was odd then the quark would be one link away from the corresponding quark in an unfuzzed operator. This would lead to contributions from different taste representations in the correlators. The other reason for using an even fuzzing width is to ensure that the Kogut-Susskind phases (3.11) at the site at which the quark in the fuzzed operator lies are the same as in the unfuzzed operator.

6.8 Calculating with Fuzzed Operators

In this thesis the fuzzed links are created using five iterations of APE smearing. Each iteration replaces an initial link with by 2.5 times itself added to a sum of the spatial staples surrounding the link, followed by a projection back onto $SU(3)$ as in [78]. When creating the fuzzed operators a fuzzing width of 2 is used. Using these fuzzed operators in conjunction with local operators, where by local we mean unfuzzed, four correlations can be studied. One can use a local operator to both create and destroy a state, a fuzzed operator to both create and destroy a state, a local operator to create a state and a fuzzed operator to destroy it, or a fuzzed operator to create a state and a local operator to destroy it. We refer to these correlations as LL, FF, LF and FL respectively.

Each of these correlations will have differing amounts of ground and excited state contributions. They can be studied separately to determine which correlation gives the best estimate of the ground state mass or whatever one is interested in. Usually the LF correlator is not studied. This is because this is essentially the same correlator as the

FL correlator because of the periodic boundary conditions of the lattice. However, since the FL correlator contains a propagator calculated with a fuzzed source we are actually using more samples of the propagator than in the LF correlator where the propagators are calculated using local sources. This leads to smaller errors in the FL correlators when compared to the LF correlators and so the FL correlator is used rather than the LF correlator.

As well as studying the correlations separately, one can study them simultaneously by carrying out what is called a factorizing fit to a 2×2 matrix of correlations. If we consider for now a state with no oscillating component in the correlator, this amounts to performing a fit to the function

$$C_{ij}(t) = \sum_{n=0}^{N} c_i^n c_j^n e^{-m_n t}, \tag{6.72}$$

where i and j can be L or F, and n labels the state with $n = 0$ being the ground state. So, for instance, if one was performing a two exponential fit to the correlators then the FL correlator would be fitted to

$$C_{FL}(t) = c_F^0 c_L^0 e^{-m_0 t} + c_F^1 c_L^1 e^{-m_1 t}. \tag{6.73}$$

For comparison, the FF correlator would be fitted to

$$C_{FF}(t) = c_F^0 c_F^0 e^{-m_0 t} + c_F^1 c_F^1 e^{-m_1 t}. \tag{6.74}$$

In this work we study the effect of using fuzzed operators for staggered fermions. We shall consider fuzzed operators in the context of the singlet calculation. An aim here will be to see if one gains anything by using the fuzzed operators. We shall also be able to test whether using fuzzed operators helps with the resolution of excited states in the non-singlet scalar channel and also the Goldstone pion channel, which we obtain from the same inversions that were carried out for the connected scalar correlator. Here we can see if the problems encountered by the MILC collaboration [57, 79] in trying to extract excited states from meson correlators created using wall sources are resolved by our use of point sources.

6.9 Summary

In this chapter we have discussed all the methods and techniques that have been used in the calculation of singlet and non-singlet meson masses in this thesis. Particular attention has been paid to the understanding of staggered operators in an attempt to highlight the major difference between hadron spectroscopy with staggered fermions and other discretizations, that of oscillating contributions to correlators from the parity partner of a particular state. Now that this has been emphasised and how one deals with the parity partner contribution, especially in the singlet calculation, has been discussed we can move on and discuss the results of the calculations.

Chapter 7

Results And Discussions

This chapter contains the results of the calculations involving staggered mesons that have been carried out. The chapter will be structured as follows. We will first discuss the findings of the small taste splitting study of the staggered scalar meson that was undertaken using the $\beta = 6.81$ data set listed in table 4.1. This will be followed by a discussion of calculations of the non-singlet scalar mass and excited state contributions to the local scalar and Goldstone pion correlators. The findings of those calculations will then be utilised along with disconnected loop calculations in the next section, where the results of the singlet calculations will be presented.

7.1 Taste Splitting Results

Here we present the results of our fits to correlators calculated using the methods described in section 6.6.1. As was previously discussed, these scalar correlators also have an oscillating contribution from their pseudoscalar parity partners. Therefore one has to take this into account in the fitting function. One also takes into account the backward propagating states in the fit. Therefore for the correlators listed in appendix B, one uses the fitting function

$$C(t) = A_0(e^{-m_{sc}t} + e^{-m_{sc}(T-t)}) + (-1)^t A_1(e^{-m_{osc}t} + e^{-m_{osc}(T-t)}), \tag{7.1}$$

where m_{sc} is the mass of the scalar representation under consideration, m_{osc} is the mass of the corresponding pseudoscalar parity partner and T is the temporal extent of the lattice, which in this case is 64. We don't feel that we need to include any extra terms to account for excited states because wall sources have been used in the calculation.

It is here that we should introduce the idea of correlated fits [80, 81] and how we utilise them. The idea of using correlated fits comes about from the fact that the methods we employ in generating quark propagators mean that the correlators we calculate are correlated in t. If one does not allow for these correlations in the fit and calculates χ^2, then one can, in general, obtain a rather low number. This would lead to the conclusion that the quality of the fit to the data was rather good, when this may not be the case. A fitting procedure that takes into account the correlations in the correlators leads to a larger χ^2 as was shown in [80]. While a larger value of χ^2 is undesirable, using a correlated fit gives a more reliable value of χ^2 because of the fact that it allows for correlations in the data. This means that a low value of χ^2 from a correlated fit is indeed a good indicator of a good quality fit to correlated data.

However, using correlated fits introduces bias into the fit because of the finite number of samples available to us. This can lead to bias in the amplitudes and masses which arise from the fit, as was discussed in [81]. It was also found in this work that using uncorrelated fits actually leads to a better estimation of the parameters of the fit, which in this case is our masses and amplitudes. So, as a result, the procedure we use is as follows. We use a correlated fit to calculate χ^2 while searching for a suitable fitting region. When performing the final fit to calculate the masses and amplitudes we will use an uncorrelated fit to determine the fit parameters and a bootstrap analysis to calculate the errors.

To decide on the fitting region to use, a number of correlated fits were carried out using different values of the minimum and maximum values of t. The aim is to find a fit region, $t_{min} \leq t \leq t_{max}$, which gives a good χ^2 and also where the masses appear to have reached a plateau as a function of t_{min}. The choice of the minimum value of t is the most critical decision one has to make as errors on the correlators tend to be less at smaller t and also any plateaux in the masses may be short. Up to a certain point, the choice of the maximum value of t has little effect on the mass values and so is not as important.

Of course one can not just arbitrarily choose a maximum t. One has to include enough points in the fit to make sure one is not throwing away useful information and that the fit is reliable. The effects of varying t_{min} and t_{max} can be seen in figures 7.1 and 7.2. These plots show the results of fits to the $1 \otimes 1$ correlators, the former showing the result of varying t_{min} with $t_{max} = 21$ and the latter with $t_{min} = 4$ and t_{max} varying.

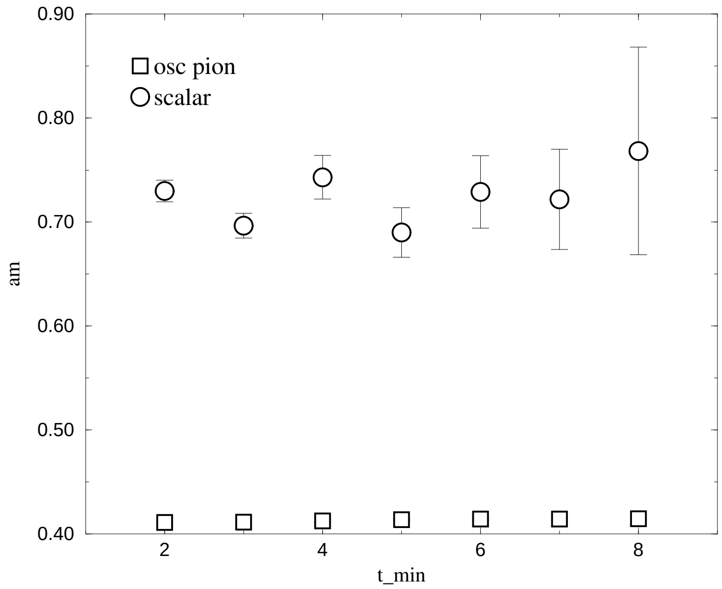

Figure 7.1: Scalar and oscillating pion masses with $t_{max} = 21$.

Looking at these figures, one can clearly see that changing t_{max} has almost no effect on the fitted mass values, while varying t_{min} has a significant effect on the scalar mass. One should also note that the mass of the oscillating pseudoscalar parity partner is very precisely determined in both cases, with the error bars being smaller than the symbol size. Also the effects of changing t_{min} in the fits does not have a large effect on the pseudoscalar mass. Fits to the $1 \otimes \gamma_i$, $1 \otimes \gamma_i \gamma_4 \gamma_5$ and $1 \otimes \gamma_4 \gamma_5$ correlators also display the same behaviour. To decide on the final fit region to use here we took into account the values of χ^2 for each fit and also the errors on the fitted mass values and on the corresponding amplitudes. It was found that increasing the value of t_{max} for a fixed t_{min} resulted in higher values of $\chi^2/d.o.f$, where $d.o.f$ is the number of degrees of freedom in the fit. Also, the errors on the masses and amplitudes tended to increase with increasing t_{max}. This was most noticeable for the amplitude of the scalar contribution. In some cases the error on this quantity was

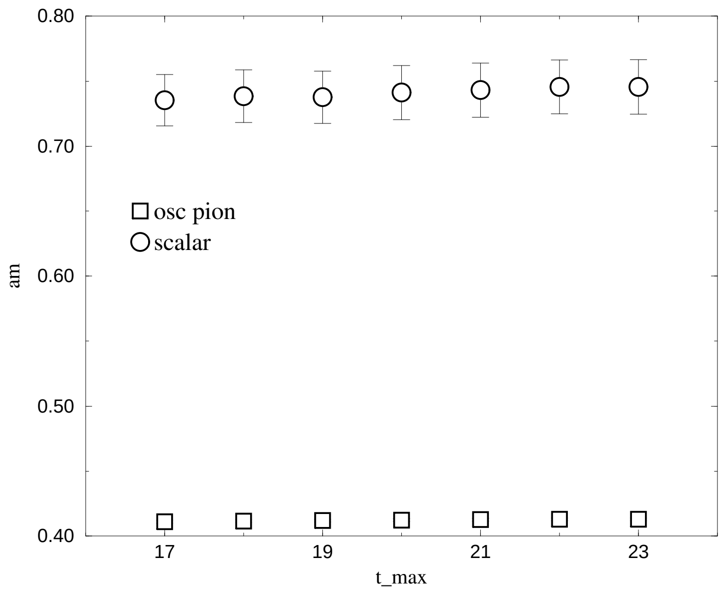

Figure 7.2: Scalar and oscillating pion masses with $t_{min} = 4$.

significantly more than 10%.

As the choice of t_{max} does not have any effect on the masses of the particles, we chose a value of t_{max} so as to try and achieve an error of less than 10% on the scalar amplitude and to keep χ^2 to a reasonable value. Once this was decided, we looked at plots similar to figure 7.1 to determine the value of t_{min} to be used. In general, t_{min} was chosen so that the scalar mass appeared to lie on a plateau like one can see in figure 7.1. Other factors that were taken into account were again χ^2 and the overall errors on the masses and amplitudes. Once t_{min} and t_{max} had been decided on, uncorrelated fits were carried out using these values to calculate masses. The results of these fits are shown in table 7.1, while the fit regions and the corresponding $\chi^2/d.o.f$ are listed in table 7.2. The errors quoted here are statistical errors. They have been calculated via a bootstrap analysis with 100 bootstrap samples.

Where quantities have been converted into units of r_1 rather than a, we have used the smoothed r_1 values from [57]. The errors on $(m_\pi^2 - m_G^2)r_1^2$ or $(m_{sc}^2 - m_{1\otimes 1}^2)r_1^2$ have been estimated by adding the errors on $m^2 r_1^2$ in quadrature. It should be pointed out that this results in an over-estimation of the error. Using these numbers as a measure of

Operator	am_π	am_{sc}	m_{sc}/m_π	$(m_\pi^2 - m_G^2)r_1^2$	$(m_{sc}^2 - m_{1\otimes 1}^2)r_1^2$
$\gamma_5 \otimes \gamma_5$	0.37956(58)	-	-	-	-
$1 \otimes 1$	0.4106(12)	0.718(25)	1.749(60)	0.1740(74)	-
$1 \otimes \gamma_i$	0.4310(12)	0.772(27)	1.793(61)	0.2957(77)	0.577(392)
$1 \otimes \gamma_i\gamma_4\gamma_5$	0.4470(13)	0.814(27)	1.821(60)	0.3952(90)	1.042(402)
$1 \otimes \gamma_4\gamma_5$	0.4632(17)	0.852(35)	1.839(75)	0.4997(118)	1.489(495)

Table 7.1: Scalar and pion masses for the different taste representations.

Operator	Fit Region	$\chi^2/d.o.f$
$\gamma_5 \otimes \gamma_5$	$14 - 26$	17.9/11
$1 \otimes 1$	$4 - 17$	15.1/10
$1 \otimes \gamma_i$	$4 - 17$	20.0/10
$1 \otimes \gamma_i\gamma_4\gamma_5$	$4 - 17$	14.7/10
$1 \otimes \gamma_4\gamma_5$	$4 - 17$	15.9/10

Table 7.2: Fitting regions and χ^2 for each operator.

taste splitting is motivated by the fact that for the pion $(m_\pi^2 - m_G^2)r_1^2$ is approximately independent of quark mass. Therefore it is a reliable measure of taste splitting for a particular lattice size or spacing. So, it is reasonable to calculate this for only one quark mass. Now, there is no reason to believe that $(m_{sc}^2 - m_{1\otimes 1}^2)r_1^2$ is insensitive to quark mass. If the squared mass of the lightest scalar, i.e. that which lies in the $1 \otimes 1$ representation, is linear in quark mass then this certainly would be true.

The thing to notice here is that this quantity is larger for the scalar than it is for the pion for this particular quark mass. One can assume that this would be the case for all quark masses, using the arguments above. This indicates that the taste splitting in the scalar channel is large, as was mentioned in [56], and we definitely find that the mass splittings are larger than the statistical errors, which is not the case in the vector channel. To what extent the taste symmetry breaking for the scalars is correlated with that of the corresponding parity partners, one can not be certain without analysis of other ensembles. However the indications are that there is some correlation. Since the masses of the four different taste representations considered here are all approximately 1.8 times the masses of their parity partners then it is plausible that this will be reflected in the taste splitting. One would expect the scalar splittings to be as large, if not larger, than the pseudoscalar splittings.

It is difficult to make a direct comparison with other calculations here since there are no published results on the scalar taste splittings. We are also using different fitting techniques to those used by the MILC collaboration in [56, 57]. We are using uncorrelated fits to determine our fit parameters once we have found a suitable fit region, whereas MILC use correlated fits. This does not make a difference for the pion masses, where both methods give consistent results. However, if we look at the mass of the $1 \otimes 1$ representation in table 7.1 we find that this differs from the mass published in [56] by two standard deviations. This is an indication that bias is introduced into the correlated fits. Our corresponding correlated fit gives a mass which is consistent with that in [56] within the statistical errors.

In conclusion, we find that the taste splitting in the scalar channel is as dramatic as in the pseudoscalar channel. Of course this is a rather small study but it is still an interesting one. One would expect from looking at these results that if the taste symmetry breaking was reduced for the pseudoscalars that this would also be reflected in the splittings for the scalar. The simplest way to test this hypothesis in the future would be to measure the scalar masses on the finer set of lattices. This would allow one to see if the reduction in the pion splittings in going to a smaller lattice spacing that was shown in [57] was reflected in the scalar splittings also.

7.2 Non-Singlet Scalar Masses, the Goldstone Pion and Excited States

In this section we will consider correlators that have been calculated using quark propagators that have been generated using point sources rather than wall sources, which were discussed in the previous section. As was mentioned earlier, we used point sources so that we would have connected correlators which were calculated using the same type of source as was used for the disconnected loop calculation. The two correlators which we have have calculated using this method are those of the $1 \otimes 1$ and $\gamma_5 \otimes \gamma_5$ representations. These have been calculated for ensembles A, B and C of table 4.1. The main goal here is to determine the non-singlet scalar mass, but as a by-product of the inversions we will also be able to measure the Goldstone pion mass. This will be used as a check against the pion masses calculated in [56, 57] to ensure our methods give consistent results for the pion.

Since we have used point sources, we expect that there will be more excited state contributions in these correlators than in correlators calculated using wall source methods. This is because wall sources are specifically designed to reduce excited state contributions [33]. This has led to us considering fuzzed operators also in an effort to resolve the states. We have attempted to calculate the masses of the excited pion and excited scalar using the unfuzzed and fuzzed operators. This has involved carrying out fits to the LL, FL and FF correlators and also performing factorizing fits to the 2×2 correlation matrices as described in section 6.8. The section will be structured as follows. Firstly we will present results from the simple fits to the LL, FL and FF correlators. Then we will consider the factorizing fits and try to see whether using these gives a better estimate of the ground and excited state masses. We shall first discuss the scalar fits and then move on to the pseudoscalar fits.

7.2.1 Fits to LL, FL and FF Scalar Correlations

To determine scalar masses, fits were carried out using the fit function defined in (7.1). When looking for excited states we have also performed fits to functions similar to this but with extra terms included. The three other functions that have been used are,

$$\begin{aligned} C(t) &= A_0(e^{-m_{sc}t} + e^{-m_{sc}(T-t)}) + (-1)^t A_1(e^{-m_{osc}t} + e^{-m_{osc}(T-t)}) \\ &+ A_2(e^{-m_{sc^*}t} + e^{-m_{sc^*}(T-t)}), \end{aligned} \tag{7.2}$$

$$\begin{aligned} C(t) &= A_0(e^{-m_{sc}t} + e^{-m_{sc}(T-t)}) + (-1)^t A_1(e^{-m_{osc}t} + e^{-m_{osc}(T-t)}) \\ &+ (-1)^t A_2(e^{-m_{osc^*}t} + e^{-m_{osc^*}(T-t)}), \end{aligned} \tag{7.3}$$

$$\begin{aligned} C(t) &= A_0(e^{-m_{sc}t} + e^{-m_{sc}(T-t)}) + (-1)^t A_1(e^{-m_{osc}t} + e^{-m_{osc}(T-t)}) \\ &+ A_2(e^{-m_{sc^*}t} + e^{-m_{sc^*}(T-t)}) + (-1)^t A_3(e^{-m_{osc^*}t} + e^{-m_{osc^*}(T-t)}), \end{aligned} \tag{7.4}$$

where m_{sc^*} and m_{osc^*} are the masses of an excited scalar and excited oscillating pion respectively.

The same procedures used in the taste splitting analysis were carried out in order to determine the optimal fitting regions for each quark mass and fit function. Since one of the goals of using fuzzed operators is to obtain a greater overlap with the ground state, one would naively expect that the best determination of the ground state mass would come from a fit to the FF correlators. One would similarly expect that a fit to the LL correlators would give the best determination of any excited state contributions to the correlators. These are some of the things that we have investigated.

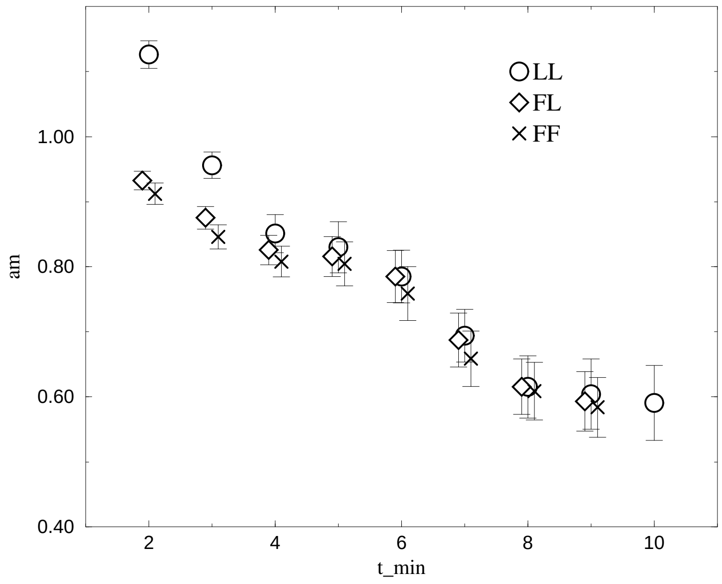

Figure 7.3: Scalar masses from two state fits for ensemble A with $t_{max} = 19$.

Figures 7.3 - 7.5 show the results of fits to LL, FL and FF correlators using the fit function defined in (7.1). In all these fits we have chosen $t_{max} = 19$ and studied the effect of varying t_{min}. The fits to all three correlators have been plotted together for each quark mass to emphasize the effect of using fuzzed operators. On all three plots one can clearly see that for small t_{min} the LL correlations give a higher mass than the FL correlations which in turn give a higher mass than the FF correlations. At larger t_{min}, where any excited state contributions are expected to have decayed away, the masses from

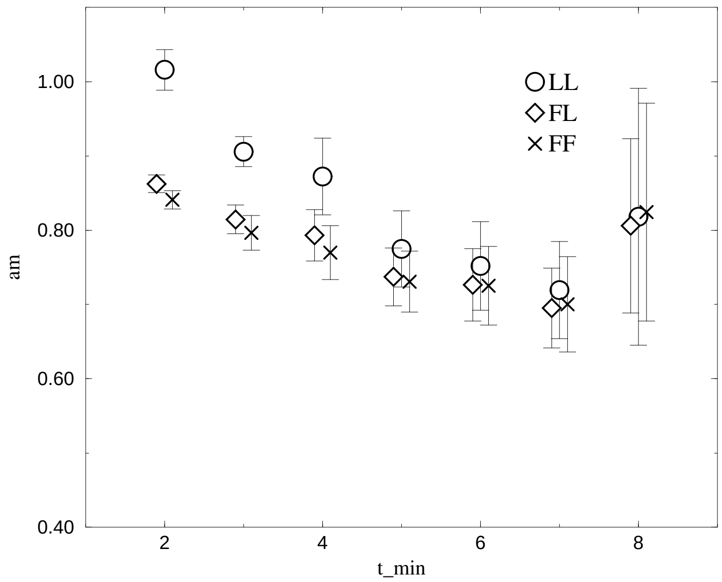

Figure 7.4: Scalar masses from two state fits for ensemble B with $t_{max} = 19$.

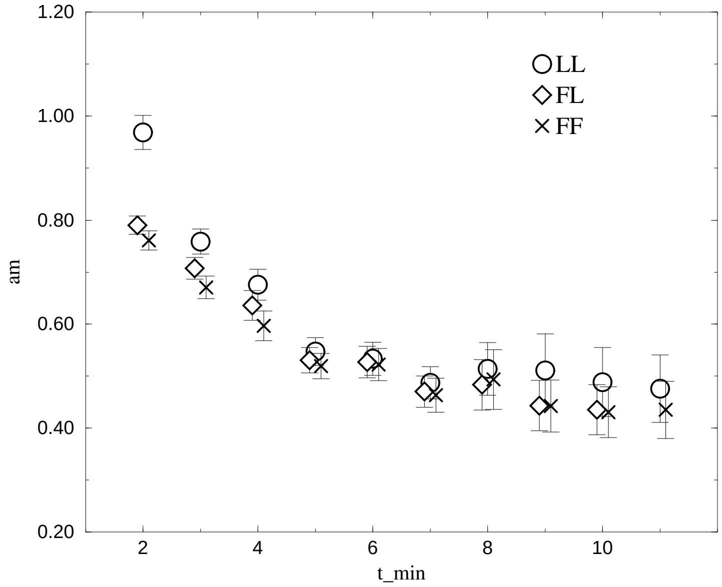

Figure 7.5: Scalar masses from two state fits for ensemble C with $t_{max} = 19$.

the three correlators are comparable. This confirms the expectations that the use of fuzzed operators reduces the contamination from excited states. This will be useful later for the singlet calculations, where we are constrained to use small t_{min}.

Perhaps the most striking thing about these plots however is the apparent existence of two plateaux. This feature is most obvious in the plot for ensemble A, which has the heaviest quark mass. Looking at figure 7.3 one can see a plateau forming, at least for the FF correlator, from $t_{min} = 3 - 5$. This then drops away and another plateau forms from $t_{min} = 8$ onwards. For the other two ensembles this does not seem to be the case. There is just one, albeit rather short plateau in figure 7.4 from $t_{min} = 4 - 7$. Figure 7.5 shows slight evidence of a very short plateau from $t_{min} = 5 - 6$ which drops into a larger one from $t_{min} = 7 - 11$, although it could be interpreted as being only one plateau.

This behaviour has been noted before in fits to staggered correlators, but in the context of the $J^{PC} = 1^{-+}$ hybrid mesons [82]. In that context, this was attributed to contributions from lighter states, in particular a two meson state where the two mesons are particles into which the hybrid meson can decay. This is a very similar argument to the one that we used to attempt to explain the behaviour of our scalar glueball effective mass plots in section 5.4.1.

What is puzzling though is that we do not see this behaviour in figure 7.1, which shows the mass of the scalar with the same quark mass as in figure 7.3. The difference between these two plots is of course that the former is from correlators which have been calculated using wall sources whereas the latter has been calculated using point sources. As a further comparison we plot the mass of the oscillating pion for ensembles A, B and C with $t_{max} = 19$ and t_{min} varying. The $\beta = 6.81$ (ensemble A) data is identical to that in figure 7.1 in that the mass is very well determined and does not change as we vary t_{min}.

This is reassuring as it shows that the data from the two different sources is consistent for the lowest mass particle, which one would expect to be the most accurately determined state. Moreover, the masses of the pseudoscalar parity partner states are consistent with what one would expect them to be when looking at the Goldstone pion masses, which are calculated in section 7.2.3, and combining these with the taste breaking measure calculated

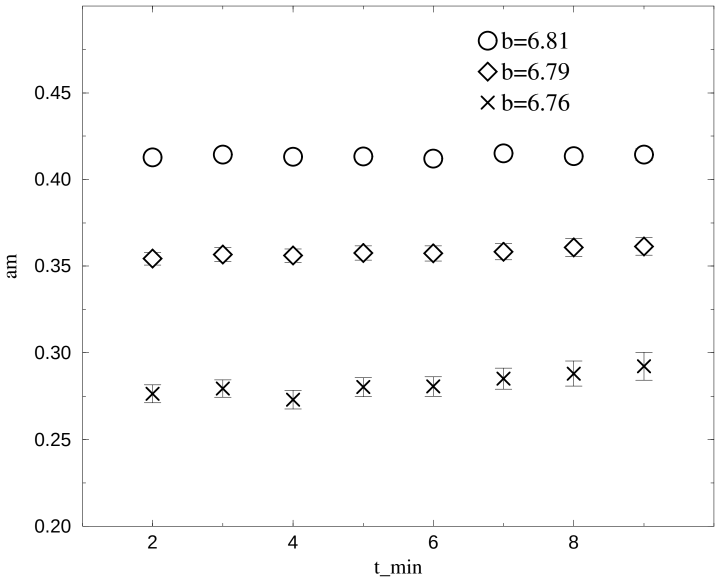

Figure 7.6: Oscillating pion masses from two state fits to the FF correlators for all three ensembles with $t_{max} = 19$.

earlier. This is a sound way to estimate the mass of the parity partner as the pseudoscalar taste breaking measure is approximately independent of quark mass.

In previous attempts to calculate the scalar mass in the staggered formalism [56, 57], it was found that the mass calculated in the dynamical theory was much lower than the quenched mass for lighter quarks. It was also much smaller than was expected from extrapolations from calculations using heavy quarks. This was put down to the decay of the scalar into $\pi + \eta$ so that what was in fact being measured was the mass of the $\pi\eta$ intermediate state in the scalar correlator. If this indeed the case, then to measure the scalar mass one would need to include extra non-oscillating exponentials in the fit, i.e. use the fit function (7.2) or (7.4).

Of course another reason for the badly behaved correlators could just be statistical limitations. We are only using point sources here as opposed to wall sources, as well as only using one source time slice as opposed to two in the taste splitting study and eight in [56]. This means that as well as not calculating as many propagators, we can also expect a smaller overlap with the ground state scalar. However, we do not really expect this to be a major problem and are reassured by the fact that the oscillating parity partner is well determined and also that the Goldstone pion is extremely well determined as we shall see in the next section.

It is most likely that what we are seeing here does have something to do with the decay of the scalar. To try and resolve this without having access to the $\pi\eta$ operator we can perform fits to the fitting function (7.2) and see whether we can determine two distinct masses in the non-oscillating exponentials. These two masses could then be interpreted as the mass of the $\pi\eta$ state and the mass of the scalar (a_0). Another strategy we can adopt is to fit to this fitting function but fix one of the masses in the non-oscillating exponentials to be the sum of the masses of the pion and the eta. The mass of the eta can be estimated using the Gell-Mann-Okubo formula, which is

$$m_\eta^2 = \frac{1}{3}m_\pi^2 + \frac{2}{3}m_{s\bar{s}}^2. \tag{7.5}$$

To calculate this we use the values listed in table III of [56]. The estimates of the $\pi + \eta$ mass are shown in table 7.3.

Ensemble	$am_\pi + am_\eta$
A	0.8321
B	0.7499
C	0.6482

Table 7.3: Estimates of the mass of $\pi + \eta$.

We should also consider the other decay channels of the a_0 here. As well as $\pi\eta$ the a_0 also decays into $\pi\eta'$ and $K\overline{K}$. We must ask whether these states will be heavier than the $\pi\eta$ state or not. We don't have any information on the η' mass but it is reasonable to say that the $\pi\eta'$ state will be heavier than the $\pi\eta$ state. We can use the Kaon masses published in [56] to estimate the mass of a $K\overline{K}$ two-body state on the ensembles considered here. These are listed in table 7.4. Comparing these numbers with those in table 7.3, one can see that the $K\overline{K}$ state will be heavier on these ensembles than the $\pi\eta$ mass. Since this is the case it is reasonable to expect the mass we are measuring to be the mass of the $\pi\eta$ state because we are fitting at reasonably large values of t and so expect to be measuring the mass of the lightest state. For this reason we neglect the $\pi\eta'$ and $K\overline{K}$ states in the following analysis and concentrate on fits where we shall try and interpret a state as the $\pi\eta$ state.

Ensemble	$am_{K\overline{K}}$
A	0.8723
B	0.8197
C	0.7667

Table 7.4: Estimates of the mass of a $K\overline{K}$ state.

Before considering such fits, we can look back at figures 7.3 - 7.5 and try to see if there is any evidence of the fits giving masses consistent with those in table 7.3. Looking at the fit results for ensemble A, it appears that the first plateau is consistent with the estimate of $m_\pi + m_\eta$ but the subsequent dropping off of the plateau gives a mass much less than this. The ensemble B results are certainly consistent with the estimate in that the plateau from $t_{min} = 3 - 5$ lies around $am = 0.75$. The errors on the results in this case are rather large though. Finally, the results for ensemble C seem to indicate a mass which is a lot smaller than the estimate of $am_\pi + am_\eta$.

We shall use the three exponential fits to see whether this unexpectedly small mass is because a fit function with only one non-oscillating exponential can not match the data very well. This may be the case although it should be pointed out that for the larger t_{min} values, we get an indication that the data is well matched to the two exponential fit function from the values of χ^2. This is shown in table 7.5. Firstly, we shall consider the fits where we did not fix the mass of one of the states to be the estimate of $am_\pi + am_\eta$.

t_{min}	3	4	5	6	7	8	9	10
$\chi^2/d.o.f$	46.6/13	34.9/13	18.0/11	18.0/10	12.2/9	11.3/8	9.5/7	9.3/6

Table 7.5: $\chi^2/d.o.f$ for fits to scalar correlators from ensemble C.

To get reasonable fits using the fitting function (7.2), with two non-oscillating terms and one oscillating term, we have to consider smaller values of t_{max} than we have previously used. This is because we are looking for a higher mass state and so we want to ensure that we are not so far out in t that the signal is dominated by the lighter states. The values of

t_{min} that can be used are also restricted for similar reasons. If a large value of t_{min} was used then any contribution from the heavier states would have begun to drop away.

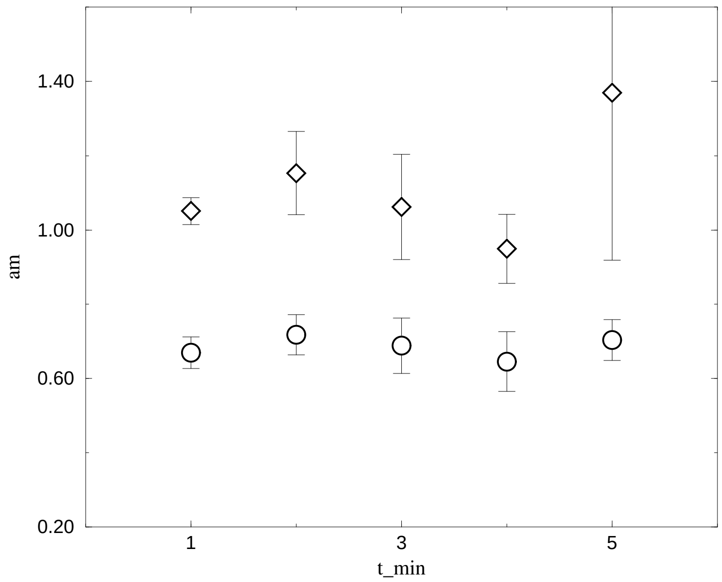

Figure 7.7: Results of three state fits for ensemble A with $t_{max} = 13$ and all fit parameters free.

In all three cases it was found that reasonable fits could only be obtained using $t_{min} \leq 5$. The results of the best of these fits are shown in figures 7.7 - 7.9. In these plots the circles show the mass of the lowest lying 0^{++} state, which we have hypothesised may be a two meson state, and the diamonds represent the mass of a heavier 0^{++} state which we would believe to be the a_0.

The main problem was in accurately determining all the parameters in these fits. In all three cases we found that the oscillating 0^{-+} mass and amplitude were very well determined. The problems arose with the 0^{++} contributions. The mass of the lowest lying 0^{++} state is reasonably well determined and we don't see evidence of the two plateau behaviour which was exhibited in the two exponential fits. The mass of the state which we may expect to be the a_0 meson is not very well determined from these fits. There is evidence of a plateau in the mass of this state in figure 7.7, but things are not so clear in figures 7.8 and 7.9. The best fits were actually those from the FF correlators, indicating

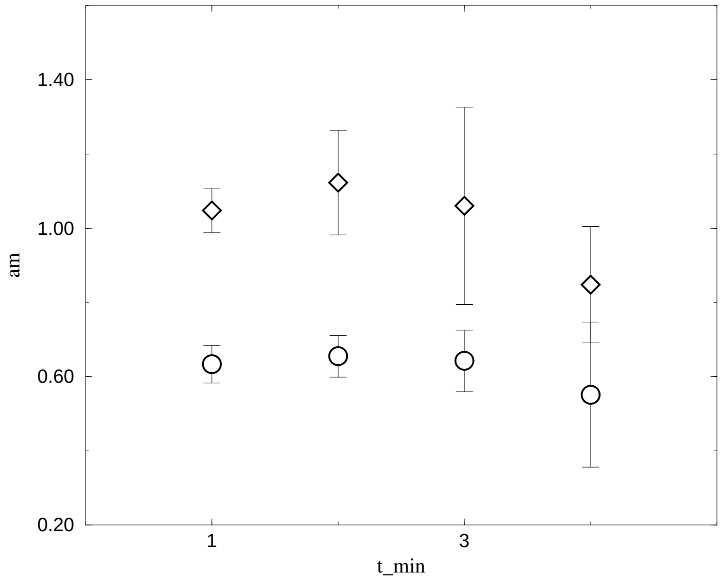

Figure 7.8: Results of three state fits for ensemble B with $t_{max} = 11$ and all fit parameters free.

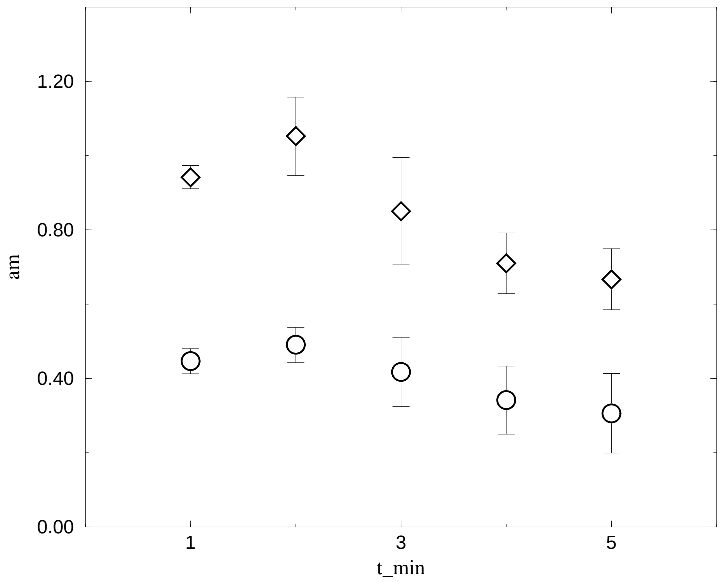

Figure 7.9: Results of three state fits for ensemble C with $t_{max} = 13$ and all fit parameters free.

that for these fit regions there are contributions from higher excited states in the LL correlators which are affecting the fits.

The main cause for concern in the fits was in the amplitudes of the 0^{++} states. These were determined very poorly in the fits, especially the amplitude of the lowest mass state. The errors on this quantity, as calculated using the jackknife method, are very large. In some cases the error was as large as 100%. This tended to occur in the fits where $t_{min} = 4$ or 5. The amplitudes of the heavier mass state were also quite poorly calculated but not to the same extent as the lighter state, with the errors being typically around $10\% - 35\%$. Another observation was that for smaller quark mass, the fits tended not to be as good as for the heaviest quark mass and the errors on the amplitudes were much larger.

Comparing these fits to the estimates of $am_\pi + am_\eta$ in table 7.3, one can clearly see than the mass of the lowest lying state is much smaller that this estimate for all three ensembles. This mirrors what was found in the two state fits earlier. It appears then that the mass calculated from the two state fits was not poorly determined because the fit function could not match the data very well, which we earlier stated may be the case. However we did show that the values of χ^2 arising from the two state fits indicated a good match to the data for t_{min} around five and greater. The values of χ^2 for the three state fits indicate good matches to the data for t_{min} around five and less. Of course the fits for $t_{min} = 5$ in this case are plagued by huge errors, but nevertheless we have evidence that, for quite a large spread of fit ranges, the mass of the lightest state is smaller than the mass of the lightest expected state with 0^{++} quantum numbers.

We also attempted to fit the data using the fit functions defined in (7.3) and (7.4), thus allowing for an excitation in the oscillating state. These attempts proved to be fruitless in that we could not determine an excited oscillating state. Such fits proved to be very sensitive to the input fit parameters and tended to result in the masses of the oscillating states coming out to be equal or one of the masses coming out to be so large that the value of e^{-mt} was negligible. This has led us to believe that there is no contribution from the excitation of the oscillating state.

Earlier we said we could also try fixing one of the non-oscillating masses in the fits to be equal to the estimates of $am_\pi + am_\eta$ given in table 7.3. Attempts to do this have proven to be spectacularly unsuccessful. A plot showing some results of these fits for the two heavier quark mass ensembles is shown in figure 7.10. This plot shows the mass of the state one would expect to be the a_0, if indeed the lightest state is the $\pi\eta$ two meson state. As one can see there is no evidence of plateaux in this plot and the errors are huge. There are no data plotted here for the lightest quark mass ensemble because we could not get any reasonable fits while fixing one of the masses.

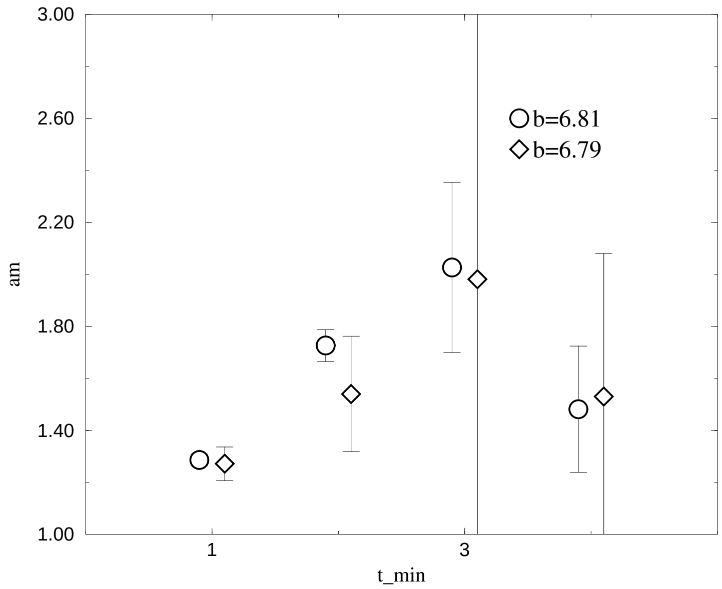

Figure 7.10: Results of fits to the LL correlators with one mass fixed to be $am_\pi + am_\eta$ with $t_{max} = 13$.

One could conclude from these findings that there is no state contributing to the scalar correlators which has the mass of the intermediate $\pi\eta$ state. One can say this because we have attempted to fit the data with this mass as a fixed parameter in the fits and found that the fits were unreliable and poor in fact. Allowing all the parameters to be free in the fits gave a mass which was much lighter than one would expect and the amplitude of this state was extremely poorly determined. These conclusions can be further tested by the factorizing fits described in the next section.

7.2.2 Factorizing Fits to the Scalar Correlators

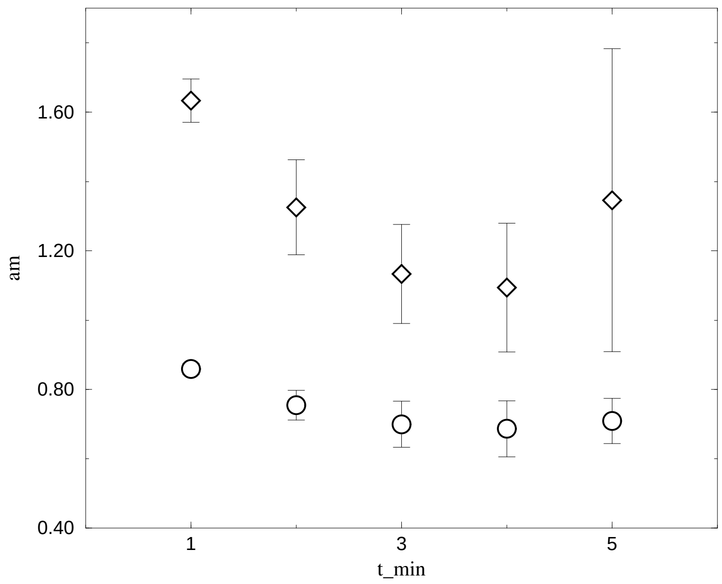

Figure 7.11: Results of factorizing fits for ensemble A with $t_{max} = 13$.

The factorizing fits to the scalar correlators are actually no better than the fits to the FF correlators presented in figures 7.7 - 7.9. Looking at figures 7.11 - 7.13, where again the circles and the diamonds show the mass of what one may expect to be the two meson state and the a_0 respectively, one can see that things look similar for the lowest mass state but not for the higher mass state. There is less indication of any plateau in the masses of the higher state from the factorizing fits and the errors on the masses are certainly larger. This may be a reflection of the fact that we found that fits to the LL correlators were not of a high quality. This carries over into the factorizing fits and lowers the quality of the fits.

However, one can again see an indication that the mass of the lighter state is lower than the estimates in table 7.3. We also found that the errors on the coefficients which describe the amplitude of this state were large, in agreement with the findings of the earlier fits. Again this adds evidence to our observation that we have a state with a poorly determined amplitude which has a mass which is not what one should expect. Attempts to perform fits with an extra oscillating exponential and also with one mass fixed to the estimate of

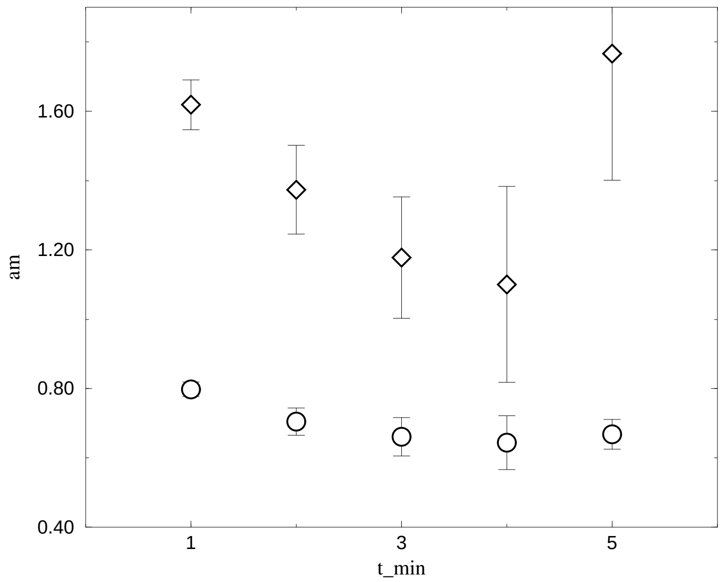

Figure 7.12: Results of factorizing fits for ensemble B with $t_{max} = 11$.

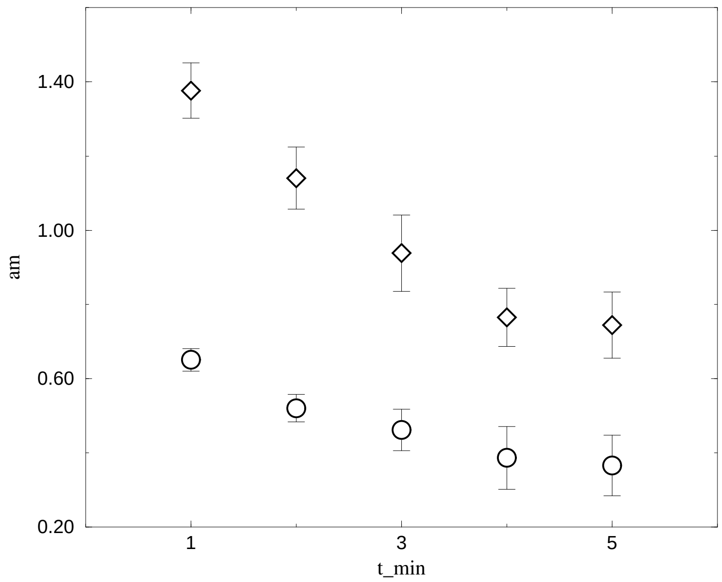

Figure 7.13: Results of factorizing fits for ensemble C with $t_{max} = 11$.

$am_\pi + am_\eta$ were again unsuccessful.

One must ask why we do not find a state with the mass of the $\pi\eta$ state in our fits, or at least a mass larger than it for our lowest state. It is certainly the case that this is the lightest state with 0^{++} quantum numbers that the a_0 can decay into and we should not find a mass lower than this. In quenched Lattice QCD it has been shown [83] that the scalar correlator gets a negative contribution from quenched chiral loop effects. Moreover this contribution is larger for lighter quarks. This study, using the clover improved Wilson fermion discretization for the valence quarks, found that for light quarks the scalar correlator in fact becomes negative.

In order to determine properly the scalar meson mass in this case the data was fit to a fit function which took the chiral loop contribution into account. The negative chiral loop contribution was said to demonstrate clearly that working in the quenched approximation violates unitarity. A more recent study of scalar correlators [84] has been carried out. This study is an unquenched study utilizing two flavours of domain wall fermions in the sea. They consider both full dynamical correlators, where the valence quark masses are equal to the sea quark mass, and also partially quenched correlators, where $m_{val} \neq m_{sea}$.

The study concludes that the dynamical correlators can be fit to a simple exponential fit function and also to a function which allows for partially quenched chiral loop effects, with no difference in the fits. They find that the partially quenched correlators suffer from the same problems as in the quenched study [83]. The fits to these correlators must take into account the unphysical partially quenched chiral loop contributions. This illustrates the point that in unitarity breaking theories, the scalar correlator is affected by unphysical contributions.

Now in dynamical staggered simulations, such as the ones considered in this thesis, there is the problem that unitarity may be violated as we touched upon in section 4.3. This is because of the differing treatment of the sea and valence quarks. To ensure one has the correct number of flavours in the vacuum, one removes the extra tastes by taking fractional powers of the fermion determinant. However the valence quark action that is used is the full four taste action. The correct taste structure is obtained by using an operator which projects into the required taste representation. This leads to a mismatch of sea and valence quarks lines which, as discussed in [53], may break unitarity.

This is a possible explanation for the results of our a_0 calculation. If unitarity is broken then one would expect that the scalar correlator would be plagued by unphysical contributions. We would argue that we are seeing evidence of an unphysical state contributing to our scalar correlators. Something which we would like to be able to check is whether the scalar correlator is negative. Since there is a contribution to the correlator from the pseudoscalar parity partner this is difficult to do. The correlators are certainly negative for some larger values of t but this is due to the large negative contribution from the light parity partner. If one was able to obtain the scalar contribution alone and it was negative then this could lead one to assume that in the dynamical staggered theory, simulated with the present day methods, is in fact a partially quenched theory.

7.2.3 Fits to LL, FL and FF Pseudoscalar Correlations

To calculate the Goldstone pion mass we performed fits to a simple, single exponential fitting function. As was discussed in section 6.5 the Goldstone pion has a parity partner with exotic quantum numbers, so there is no need to include an oscillating exponential in the fit function. We have also attempted fits to a two exponential fitting function in the hope of calculating any excited state mass with which to compare with [57]. This will show whether using fuzzed and unfuzzed point sources gains you anything over using wall sources when attempting to calculate excited state masses in the staggered formalism.

Figure 7.14 shows the by now usual plot of the effects of varying t_{min} in the fits while keeping t_{max} fixed at 25. These fits were one exponential fits to the LL correlators. One can clearly see that the Goldstone pion mass is extremely well determined, as should be expected. We are far enough out in t that there are no excited state contributions and this is reflected in the long plateau. In fits to the correlators from ensemble C we found that the plateau extended back to $t_{min} = 6$, although for small t_{min} the value of χ^2 was quite large. Again we have used correlated fits to determine a suitable fitting range and uncorrelated fits to determine the fit parameters. The errors are statistical errors, calculated using 400

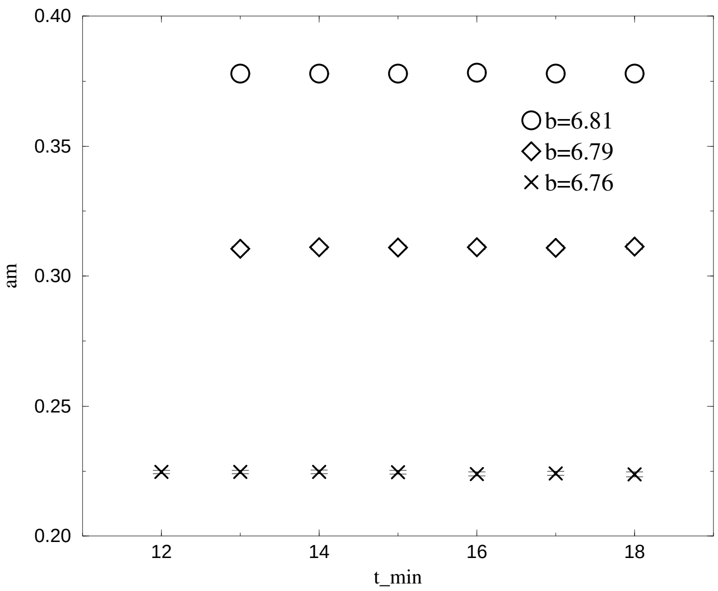

Figure 7.14: Goldstone pion masses from fits to the LL correlators for all three ensembles with $t_{max} = 25$.

bootstrap samples. Comparing table 7.6 with the pion masses in [56], one can see that the masses calculated here are consistent with the previous results. This shows that the point sources employed in this thesis give the same results as for wall sources, without the extra effort needed in fixing the gauge. The only difference is that we have larger errors which is understandable when you consider that we only use one source time slice as opposed to eight.

Ensemble	am_π	Fit Region	$\chi^2/d.o.f$
A	0.37820(72)	17 - 27	7.5/9
B	0.31109(71)	14 - 27	15.5/12
C	0.22455(85)	13 - 25	20.2/11

Table 7.6: Goldstone pion masses.

When attempting to calculate the mass of any excited state contribution to the correlators it is necessary to choose t_{min} to be small enough that any contribution is significant. One also must take care not to choose t_{max} to be so large that the contribution has decayed away. Figure 7.15 shows the results of two state fits to the LL pseudoscalar correlators for ensemble A. Again one can see that the ground state mass is very well determined, with error bars smaller than the size of the symbol. The excited state mass is less well determined. The mass is reasonably well determined for small t_{min}, but as it is increased the errors increase and it becomes difficult to obtain a good fit with a definite excited state.

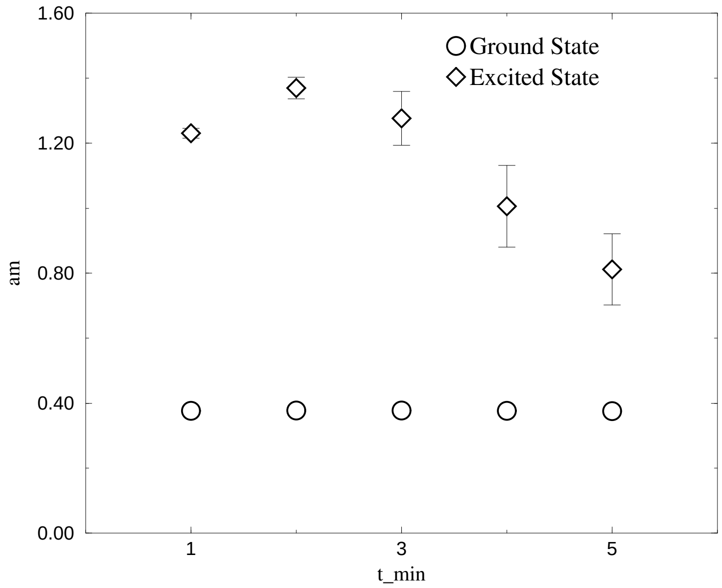

Figure 7.15: Ground and excited state pion masses from fits to the LL correlators for ensemble A with $t_{max} = 15$.

This is not unreasonable when you consider that the excited state mass appears to be above $am = 1$ and so the value of $e^{-m_{exc}t}$ rapidly becomes much smaller than the contribution from the ground state. Indeed if t_{min} is increased any further in the fits we just get the masses of both states equal to the ground state mass, showing that the excited state contribution has decayed away. The behaviour of fits for the other two ensembles mirrors that of ensemble A in that we start off with reasonable fits at small t_{min} and the fits get worse as we increase t_{min} until we can no longer determine two definite states.

We also found that it was possible to obtain reasonable two state fits to the FF correlators. In fact we find that fits to the FF correlators indicate that the mass of the excited state is not as large as one would conclude from the LL correlators. This can be seen from looking at figure 7.16. This is the same plot as figure 7.15 but with the excited state mass calculated using the FF correlators also included. This would indicate that at the small values of t_{min} used in these fits that there is still some significant contribution to the LL correlators from higher excited states, as was the case for the fits to the scalar correlators. Unfortunately, attempts to fit the LL correlators to a three exponential fitting function have been unsuccessful. We can use the fact that there are differing excited state contributions to the correlators in the next section when we consider the factorizing fits.

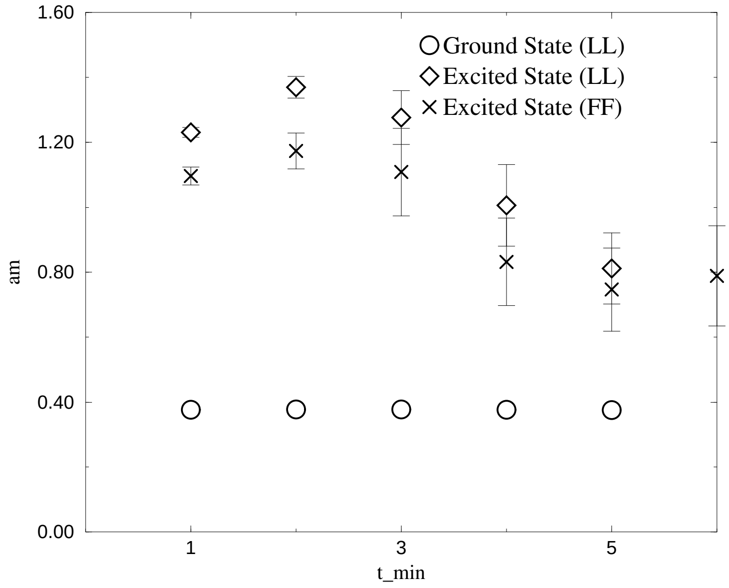

Figure 7.16: Ground and excited state pion masses from fits to the LL and FF correlators for ensemble A with $t_{max} = 15$.

Table 7.7 lists our best shot estimates for the excited pseudoscalar mass using fits to the FF correlators. The first error quoted on the excited state mass is statistical and calculated via a bootstrap with 400 samples. The second error is a systematic error, which is estimated by looking at the mass value if t_{min} is varied by one unit in either direction. The fit region was $2 - 15$ in all cases. Since any plateau in the excited state mass were difficult to determine, the fit range was chosen by taking into account a mixture of a reasonable χ^2, apparent plateau within the statistical errors and the errors on the mass and amplitude. This is reflected in the rather large systematic errors, which are as large as 25% for our smallest sized ensemble.

Ensemble	am_{GS}	am_{exc}
A	0.3775(10)	$1.103(56)^{+0}_{-0.159}$
B	0.3131(12)	$1.342(57)^{+0}_{-0.328}$
C	0.2227(8)	$1.095(90)^{+0.011}_{-0.086}$

Table 7.7: Estimates of excited pseudoscalar masses.

7.2.4 Factorizing Fits to the Pseudoscalar Correlators

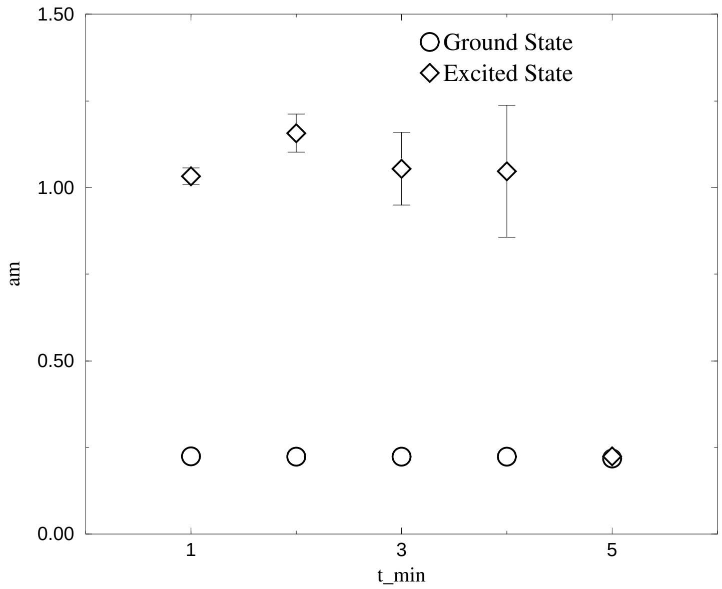

Figure 7.17: Ground and excited state pion masses from factorizing fits for ensemble C with $t_{max} = 14$.

Things improve slightly when carrying out factorizing fits to the 2×2 correlation matrices. There is definite evidence of a plateau in the excited state mass for ensemble C, as can be seen in figure 7.17. The plateau is small however and the signal from the excited state quickly dies away. Looking at figure 7.18, one can see that the excited state plateau is definitely a lot flatter than in figure 7.16. In the case of ensemble B, it is difficult to say that we can definitely determine an excited state mass from the data, as can be seen

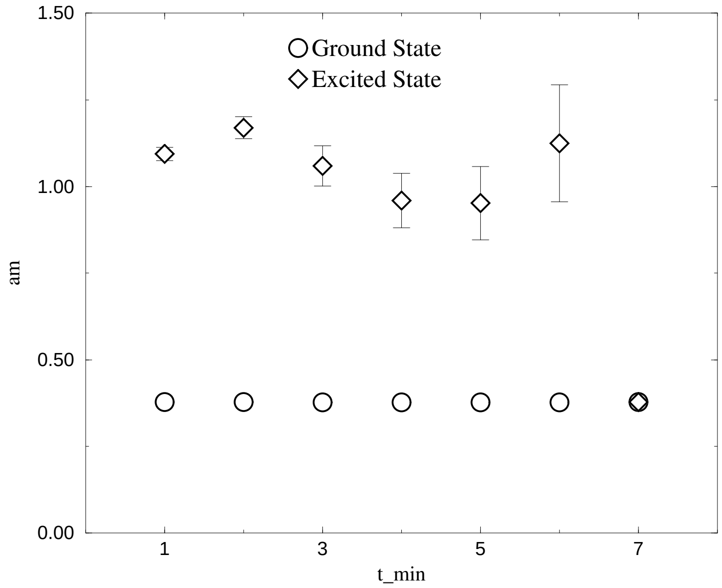

Figure 7.18: Ground and excited state pion masses from factorizing fits for ensemble A with $t_{max} = 17$.

in figure 7.19.

Ensemble	am_{GS}	am_{exc}
A	0.3774(6)	$1.060(54)^{+0.110}_{-0.100}$
B	0.3110(9)	$1.026(88)^{+0.158}_{-0.260}$
C	0.2236(8)	$1.054(106)^{+0.103}_{-0.008}$

Table 7.8: Estimates of excited pseudoscalar masses from factorizing fits.

A summary of the pseudoscalar masses calculated from the factorizing fits can be seen in table 7.8. The value of the excited state mass for ensemble B is a very crude estimate however since there was no evidence of a plateau in the plots of t_{min} versus am for this ensemble. This is the reason for the huge systematic error on the mass for that particular data set. The use of fuzzed operators has certainly helped in this calculation, as has the use of point sources. We can obtain reasonable fits to the data using values of t_{min} up to five or even six on the coarse lattices. If we compare this with the fits presented in [57], where fits to data from the finer lattices were only considered to be reasonable up to

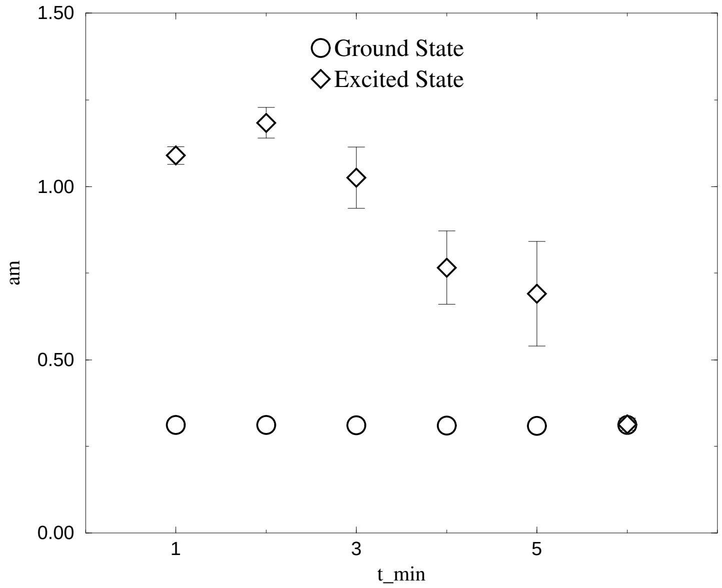

Figure 7.19: Ground and excited state pion masses from factorizing fits for ensemble B with $t_{max} = 15$.

$t_{min} = 6$, we see that our methods are as good if not better for calculating excited state masses in the pseudoscalar channel. This is because we expect to be able to fit at larger values of t_{min} for the finer lattices.

7.3 Flavour Singlet Scalar Results

We now move on to discuss the calculation of the flavour singlet scalar mass. Again, this calculation has been carried out for ensembles A, B and C of those listed in table 4.1. When carrying out the fits to the data here we have to consider different factors than we did in the previous two sections. As touched upon in section 6.6.2 there is the problem of the connected correlation having an oscillating contribution, whereas the disconnected correlation does not. This leads to the need for two fits per calculation, firstly to the connected correlator to determine the oscillating contribution and secondly to $C + 2D$ with the oscillating fit parameters fixed.

To determine fitting regions in this context we have to consider the quality of the signal we have from our disconnected loops. As was the case for the glueball calculation, the disconnected correlation is noisy and we do not have to go out very far in t before the signal has died away. Consequently, we don't have as much scope for choosing a fit region as we did in the previous sections and are, to some extent, forced to consider short time regions. This is entirely governed by the quality of the signal in the disconnected correlations. There is no point in choosing a large t_{max} with a small t_{min} for a fit to $C + 2D$ since there will be no contribution from D at the larger t values except for noise. Conversely if one chooses a too large value of t_{min} then there is little chance of getting a significant contribution from D to $C + 2D$ since the signal will have begun to disappear. So, we are resigned to using small values for both t_{min} and t_{max} and so may need to allow for excited states in the fits.

When determining the fit ranges to use we look first at the disconnected correlations only. This is because if we looked at the $C + 2D$ correlators we may have been misled about the quality of the overall fit. If the contribution to $C + 2D$ from D is only noise for a certain t range then the fitting code may be able to produce a good fit to the data but it will be fitting to $C + noise$. As such, the mass determined by such a fit will not be the singlet mass but more or less the non-singlet mass. The strategy we adopted was to inspect the disconnected correlations to see when the signal becomes completely swamped by noise. We deem that the upper limit on the value to use for t_{max} in the fits is the largest value of t where the noise is less than signal. This can be determined by considering the average correlators on an ensemble and their variance.

Table 7.9 shows the LL disconnected correlations and the corresponding standard deviations for all three ensembles. The notation here is $\overline{D}_A$ and σ_A stand for the average correlator and the standard deviation for ensemble A and similarly for ensembles B and C. To calculate these correlators we use the methods described in sections 6.3 and 6.6.2. We use a Gaussian distribution of random numbers to create a volume source and use this source to invert the fermion matrix $M = 2m + \not{D}$[1], where m is the quark mass and $\not{D}$ is the Asqtad $\not{D}$ operator. We then estimate the quark propagator using (6.22) with $x = x'$ and calculate the disconnected loop operator using (6.68), where the trace is over colour.

[1]We use $M = 2m + \not{D}$ rather than $m + \frac{1}{2}\not{D}$ (which was how we defined the fermion matrix in (3.10)) in all our inversions to conform with the conventions of the MILC collaboration.

t	$\overline{D}_A(t)$	$\sigma_A(t)$	$\overline{D}_B(t)$	$\sigma_B(t)$	$\overline{D}_C(t)$	$\sigma_C(t)$
2	374.5	8.3	454.5	11.2	568.0	11.1
3	243.7	7.4	319.4	10.3	406.9	10.4
4	142.9	6.9	210.9	9.5	286.7	10.0
5	83.0	6.6	140.2	9.0	192.1	9.9
6	40.5	6.6	78.0	9.1	119.1	9.9
7	16.8	6.8	46.6	9.0	76.3	10.0
8	-2.5	7.0	22.9	8.9	40.3	9.7
9	-1.8	7.1	16.0	8.8	34.1	9.7
10	-11.3	7.1	6.0	8.8	21.9	9.7

Table 7.9: Disconnected correlations and their standard deviations for all three ensembles.

The disconnected correlations are then given by

$$D(t) = L^*(t)L(0), \tag{7.6}$$

along with a vacuum subtraction as in the glueball case.

When we come to combine the disconnected correlators with the connected correlators we include a $1/V$ normalisation factor, where V is the lattice volume. This is to account for the fact that the source used to calculate the disconnected loops filled all sites whereas the source used for the connected quark propagators only filled one site. There is also an extra normalisation factor of 1/2. This is because when creating our sources we filled both the real and imaginary parts with random numbers. This means that the our sources normalise to 2 rather than 1 and so we need to account for this.

One can see from table 7.9 that for decreasing quark mass the signal decays into noise at larger values of t. Therefore we can choose a larger t_{max} for the lighter quark mass ensembles. Reading off from the table one would conclude that the largest values of t_{max} that should be used are 7, 9 and 10 for ensembles A, B and C respectively. We must now think what to use for t_{min}, bearing in mind that we have to fit to the connected correlations alone to obtain the oscillating contribution. We should also keep in mind that we don't want to be using too large a value of t_{min} to ensure the disconnected correlations with the smallest errors are include in the fits.

We have carried out fits to the LL and FF correlators, along with factorizing fits to the 2×2 matrix of correlations using both fuzzed and un-fuzzed operators. We have differing conditions for choosing the fit region for each case. As we saw in section 7.2.1, fits to the connected correlators for small t_{min} are poor using a fit function with one oscillating exponential and one non-oscillating exponential, i.e equation (7.1). Therefore we must carry out our fits to the connected correlators using (7.2). These fits have six free parameters and we must ensure that the number of degrees of freedom in the fits is greater than zero. Ideally we would like the number of degrees of freedom in the fits to be $\gg 1$ so that the fits are unconstrained. However, the quality of the signal from the disconnected loop calculation means, that at least for the fits to the LL and FF correlators, we may not be able to ensure that this is so. Therefore we say that the minimum requirement must be that the number of degrees of freedom must be ≥ 1.

For the fits to LL and FF correlators the number of degrees of freedom is the number of fit parameters subtracted from the length of the fit region. Therefore we must use fit regions of length seven or greater in our fits to the connected correlators. This gives us a slight problem in that for ensemble A we are only allowed one fit region for fits to the LL and FF correlators, namely $t = 1 - 7$, since we don't want to be using $t_{min} = 0$. For the factorizing fits this is not a problem since the number of degrees of freedom in the fits are four times the fit length less the number of parameters in the fits. We would like to consider more than one fit region for each ensemble to see if there is much fit region dependence in the fits so we also have allowed fits for ensemble A with $t_{max} = 8$, which means the maximum value of t_{min} we can use is 2. For ensembles B and C we can safely use up to $t_{min} = 3$ and still have a positive number of degrees of freedom in the fits to the LL and FF correlators. We should point out that we use uncorrelated fits here since the volume source methods used to calculate the disconnected loops do not lead to correlations in the disconnected correlators.

Once we had carried out fits to the connected correlators at all the time ranges allowed by the above criteria, we then took the oscillating amplitudes and masses from the fits and used them to fix the oscillating parameters in the full fits to $C + 2D$. For these fits we used the fit function defined in equation (7.1). We found that fits using equation (7.2) either did not converge or gave a mass for the excited state to be so large that e^{-mt} was negligible. This was not entirely unexpected given the limited statistics here for a singlet calculation. With more statistics we expect we may be able to resolve any excited state contributions.

		LL		FF	
t_{min}	t_{max}	am	$\chi^2/d.o.f$	am	$\chi^2/d.o.f$
1	7	0.682(13)	9.2/3	0.578(12)	3.4/3
1	8	0.683(13)	12.1/4	0.580(12)	9.1/4
2	8	0.655(20)	5.5/3	0.597(20)	6.8/3

Table 7.10: Estimates of flavour singlet scalar mass from fits to LL and FF correlators on ensemble A.

t_{min}	t_{max}	am	$\chi^2/d.o.f$
1	7	0.598(12)	294/15
2	6	0.607(17)	22.8/9
2	7	0.611(19)	28.6/12
2	8	0.616(19)	47.1/15

Table 7.11: Estimates of flavour singlet scalar mass from factorizing fits for ensemble A.

Tables 7.10 and 7.11 show the results of the fits for ensemble A. What is clear from these tables is that the fits to the $\beta = 6.81$ data are not very reliable. There is a large discrepancy between the results from the LL and FF correlators, which indicates a large excited state contribution to the LL correlators. This is to be expected at the small values of t we are working at. How much we can read into these results is unclear given that using $t_{max} = 8$ means we are already using regions where the disconnected correlation is completely overtaken by noise. The factorizing fits don't give us much insight either since the values of χ^2 indicate that we are not matching the data very well.

We can be more certain of the better quality of the results for the $\beta = 6.79$ data which is presented in tables 7.12 and 7.13. One can see from table 7.10 that for the LL

		LL		FF	
t_{min}	t_{max}	am	$\chi^2/d.o.f$	am	$\chi^2/d.o.f$
1	7	0.587(14)	23/3	0.496(12)	1.9/3
1	8	0.586(15)	23/4	0.500(13)	7.2/4
2	8	0.541(19)	2.8/3	0.508(19)	7.6/4
2	9	0.541(20)	2.8/4	0.510(20)	6.7/3
3	9	0.524(28)	1.6/3	0.518(29)	7.4/3

Table 7.12: Estimates of flavour singlet scalar mass from fits to LL and FF correlators on ensemble B.

correlators there is a decrease in the mass as we increase t_{min} indicating a drop off in the excited state contributions. For the FF correlations the mass does not seem to have much fit region dependence. This is also the case for the factorizing fits, which indicates we have a large coupling to the ground state for this quark mass. The values of χ^2 also indicate that we have a good match with the data from our fits with $t_{min} = 2$ and 3.

t_{min}	t_{max}	am	$\chi^2/d.o.f$
1	7	0.517(12)	222/15
2	6	0.511(16)	16.4/9
2	7	0.513(17)	17.1/12
2	8	0.518(18)	26.2/15
2	9	0.519(19)	27.8/18
3	8	0.515(28)	16.4/12
3	9	0.518(26)	17.9/15

Table 7.13: Estimates of flavour singlet scalar mass from factorizing fits for ensemble B.

The results of the fits to the $\beta = 6.76$ data are presented in tables 7.14 and 7.15. These results are comparable with the $\beta = 6.79$ results in that there is no fit region dependence for the factorizing fits and the fit to the FF correlators, whereas the mass is decreasing as we increase t_{min} in the fits to the LL correlators. Again the values of χ^2 give an indication that the data matches the fit function reasonably well. This leads to the belief that we

		LL		FF	
t_{min}	t_{max}	am	$\chi^2/d.o.f$	am	$\chi^2/d.o.f$
1	8	0.516(11)	31.5/4	0.435(10)	6.2/4
2	8	0.479(14)	4.4/3	0.440(14)	6.1/3
2	9	0.477(15)	4.5/4	0.440(15)	6.0/4
2	10	-	-	0.441(15)	6.9/5
3	9	0.458(21)	1.5/3	0.440(21)	6.0/3
3	10	-	-	0.442(21)	6.9/4

Table 7.14: Estimates of flavour singlet scalar mass from fits to LL and FF correlators on ensemble C.

are coupling well to the ground state. The errors quoted in all these tables are statistical errors that have been calculated via a jackknife analysis.

There is also a systematic error which comes about from the uncertainty in the calculation of the oscillating parameters in the connected fits, which are then fixed in the fits to $C + 2D$. However, these parameters are very well determined as we have seen in previous chapters and the errors on them are very small. We have checked that changing the fixed oscillating parameters by an amount equal to the errors on them does not induce a change in the singlet mass larger than the statistical errors and so we do not quote this systematic error.

We must now ask what this ground state is. What we hope to be measuring here is the flavour singlet scalar (f_0) meson. Of course, since we have not included any valence strange quarks in our calculations, this is not strictly the case. Our work has been mainly carried out with the goal of developing methods to calculate singlet quantities using staggered fermions and as such the singlet calculations presented here should be treated as an exploratory calculation.

What we can definitely say is that these simulations show that the mass of the flavour singlet scalar meson in this two quark approximation is lighter than the flavour non-singlet meson. This is in agreement with [62]. We expect that this will still be the case when the

t_{min}	t_{max}	am	$\chi^2/d.o.f$
1	7	0.456(9)	258/15
2	6	0.451(12)	24.6/9
2	7	0.451(13)	24.8/12
2	8	0.455(13)	32.4/15
2	9	0.451(14)	32.1/18
2	10	0.455(15)	33.2/21
3	8	0.449(19)	15.5/12
3	9	0.449(20)	15.1/15
3	10	0.449(21)	16.3/18

Table 7.15: Estimates of flavour singlet scalar mass from factorizing fits for ensemble C.

valence strange quark is included in the analysis. This is because, if we believe that the non-singlet mass is given by the largest mass from the fits to the FF correlators in section 7.2.1, the glueball masses we estimated earlier are also lower than the non-singlet masses and we expect that the flavour singlet scalar mass should be comparable with the glueball mass.

As with the glueball and non-singlet calculations we should also think about what other 0^{++} states we could be picking up here. It is certainly the case that the f_0 decays into two pions and the mass indicated by our fits for ensemble C are certainly consistent with twice the pion mass for this ensemble. One can see this by comparing the numbers in table 7.15 with twice the pion mass for this ensemble, which is ≈ 0.448. The indications are that for ensembles A and B the mass measured here is less than twice the pion mass for those data sets. Again, how much one can read into this is open for debate because we have not included the strange quark in our analysis and we also do not have as high statistics as we would like.

We believe that with the methods used for the flavour singlet calculation here that with more data it would be possible to obtain better fits and also maybe to resolve excited state contributions. It seems to be the case that the disconnected correlations are less noisy for lighter quark masses and so a lot more configurations would be needed for heavier quark mass runs than light quark mass runs. We could also reduce the noise in the operators themselves by using more noise source inversions in the operator calculation. This is certainly a prospect for future work, with greater computing power becoming available to the lattice community. This future work should also include the strange quark in the analysis.

7.4 Note On Error Analysis.

As was the case for the glueball calculations we did not bin the data while carrying out the error analysis on the results in this chapter. In retrospect, we must ask if this was the correct thing to do. A further analysis of the disconnected correlations which were listed in table 7.9 revealed that binning the data had the effect of increasing the errors on the correlations. Binning the data into bin sizes of six increased the errors on the correlators in table 7.9 by around 25% for ensemble A, 40% for ensemble B and 30% for ensemble C. While this means that the errors quoted in this chapter may be underestimated by up to 40%, it does not alter any of the mass values or any of the criteria for choosing fit regions. Accounting for the increased errors, we would still choose the same fit regions for the flavour singlet fits using the criteria adopted in the previous section. However, any further analysis or other calculations should take this into account to make sure errors are not underestimated.

We have also checked the effects of binning the data on a subset of the fits to the scalar correlators described in sections 7.2.1 and 7.2.2. We found that there was very little change to the errors on the scalar masses and amplitudes and so don't believe that this will change the statistical significance of our findings in these sections.

Chapter 8

Summary and Outlook

In thesis we have presented an exploratory study of the light $J^{PC} = 0^{++}$ states in the framework of Lattice QCD using dynamical staggered fermions. We have also highlighted a number of problems associated with attempting to study states with these quantum numbers. Firstly we presented results of the calculation of the scalar glueball mass. Despite the fact that in quenched studies thousands of configurations were needed to obtain a high quality estimate of the glueball mass, we showed, in agreement with [60], that in dynamical simulations it is possible to obtain reasonable results from much smaller ensembles. These results are not totally satisfactory however and would benefit greatly from larger ensembles, the use of better improved operators or variance reduction techniques [62]. A better understanding of mixing with two pion states and also the scalar meson operators is also needed for a more complete study. This would also be helped by a larger quantity of data.

At the outset of this work, a primary goal was to study the mixing of the scalar glueball and the flavour singlet scalar meson directly by considering fits to a matrix of correlations including both gluonic and fermionic operators. However, our attempts to do this have proved unsuccessful. Unfortunately, the values of t where the glueball correlators become completely swamped by noise are the values of t where we are just starting to obtain reasonable fits to the flavour singlet meson correlators, namely $t = 3$. This meant that we could not get any good fits to such correlation matrices. This investigation would definitely benefit from larger ensembles and/or large improvements in glueball operators. Such a study should be carried out when UKQCD's QCDOC machine comes online, as we shall discuss later.

We have established methods for calculating the flavour singlet scalar meson mass using staggered fermions using fermionic operators only. We have shown that the oscillating contribution to the connected correlator need not be a major problem in the calculation of singlet quantities. It has been pointed out that this was only to be treated as an exploratory study to establish the methods and gain some insight into the number of stochastic sources that one would need to use. This has been done and we have obtained a reasonable signal for the lighter quark masses with 48 sources. Future studies should be focused on introducing the strange quark into the analysis, mixing with the glueball as mentioned above and a treatment of decays.

Perhaps the most interesting part of the thesis is concerned with the non-singlet scalar. We showed that the taste splitting in the scalars is large and can not be ignored as is the case for other heavier particles. The study of the lightest scalar, that lies in the $1 \otimes 1$ representation has thrown up some striking results. It seems that there is a non-physical contribution to this correlator which is resulting in a mass which is much lighter than is expected. This mass is much too light to be the mass of the a_0 meson and also its decay products. This may be a place where some suspicions about the unitarity and locality violating properties of staggered fermions are proved to be correct.

We have compared our study with quenched [83] and partially quenched [84] studies, where unphysical contributions to the scalar correlators had to be dealt with by analysing the correlators in chiral perturbation theory. Future work on the a_0 meson using staggered fermions should probably involve a study of the scalar correlator in staggered chiral perturbation theory and also partially quenched staggered chiral perturbation theory, using the framework of Aubin and Bernard [85]. This would enable one to account for any unphysical chiral loop contributions which may be affecting the correlators as a result of partial quenching. The three point correlation function which involves the $\pi\eta$ intermediate state should also be studied in order to gain a better understanding of the decay of the a_0.

We have also considered the effects of using point sources in staggered propagator calculations instead of the wall sources that are typically used in staggered calculations [33, 56]. It was shown that equivalent results are obtained for the Goldstone pion mass and equivalent behaviour was found in the scalar correlators. The downside of using point sources is that the statistical errors are larger and there are extra contributions from excited states. These can be reduced however by using fuzzed operators, as long as one takes care not to mix up the taste representations by using an odd fuzzing width. An added bonus of adopting this approach is that one does not need to fix the gauge and one can more readily resolve excited state masses, at least for the pseudoscalar. Using the fuzzing procedure also helped in our disconnected loop calculations in that fits to $C + 2D$ were shown to be more stable when using the FF correlators and factorizing fits.

To summarise, this thesis has attempted to answer a lot of questions about the 0^{++} states in QCD. Some of these questions have been answered and new questions have arisen which could be answered in the near future. The singlet calculation will benefit from the extra computing power that is becoming available to UKQCD in the form of the QCDOC machine now installed at Edinburgh. This will enable us to carry out simulations with much greater statistics, indeed one of the first runs on this machine should produce a staggered ensemble around ten times larger than those considered in this thesis. This will help greatly in that we could improve the signal of our glueball operators to a level where it would be possible to carry out reasonable fits to a correlation matrix which involves both gluonic and fermionic operators.

We feel that the greatest influence the QCDOC machine will have on the singlet calculation will be in the large number of configurations that will be generated. An ensemble ten times larger than those considered in this thesis would result in the errors on correlators being reduced by a factor of $\approx \frac{1}{\sqrt{10}}$. This would mean that the glueball correlators would not be swamped by the noise as quickly and we would have correlators at more values of t to include in factorizing fits to the correlation matrices described above. Since we have shown that a reasonable signal can be obtained for the disconnected fermion loop with 48 noise sources per configuration, then we conclude that it is more configurations not more sources that will improve the calculation.

Of course, once the configurations have been generated the computing power can be used to calculate with more sources if one wished. One could also study other 0^{++} operators, such as two pion operators, $\overline{K}K$ operators and non-zero momentum operators. The non-singlet calculation should also benefit in that more operators and differing fuzzing levels can be studied. One could also decrease the errors in the non-singlet calculation by using sources at more than one timeslice, as we did in the taste splitting study. It is hoped that the non-singlet calculation will help confirm or dispel some of the doubts concerning the use of staggered fermions.

Appendix A

Euclidean Gamma Matrices

The γ matrices used in this thesis from chapter 2 onwards lie in the Euclidean representation and are defined as follows;

$$\gamma_1 = \begin{pmatrix} 0 & 0 & 0 & i \\ 0 & 0 & i & 0 \\ 0 & -i & 0 & 0 \\ -i & 0 & 0 & 0 \end{pmatrix}, \quad \gamma_2 = \begin{pmatrix} 0 & 0 & 0 & 1 \\ 0 & 0 & -1 & 0 \\ 0 & -1 & 0 & 0 \\ 1 & 0 & 0 & 0 \end{pmatrix}, \quad \gamma_3 = \begin{pmatrix} 0 & 0 & i & 0 \\ 0 & 0 & 0 & -i \\ -i & 0 & 0 & 0 \\ 0 & i & 0 & 0 \end{pmatrix},$$

$$\gamma_4 = \begin{pmatrix} 1 & 0 & 0 & 0 \\ 0 & 1 & 0 & 0 \\ 0 & 0 & -1 & 0 \\ 0 & 0 & 0 & -1 \end{pmatrix}, \quad \gamma_5 = \begin{pmatrix} 0 & 0 & 1 & 0 \\ 0 & 0 & 0 & 1 \\ 1 & 0 & 0 & 0 \\ 0 & 1 & 0 & 0 \end{pmatrix}.$$

These are hermitian matrices which satisfy the following relationships;

$$\{\gamma_\mu, \gamma_\nu\} = 2\delta_{\mu\nu} \tag{A.1}$$

$$\frac{1}{4}\mathrm{Tr}\,(\gamma_\mu\gamma_\nu) = 1 \tag{A.2}$$

$$\gamma_5 = \gamma_1\gamma_2\gamma_3\gamma_4 \tag{A.3}$$

Appendix B

Scalar Correlators

Here we derive the connected correlators for the scalar representations used in section 6.6.1. For all these representations $\Gamma_S = 1$ and so therefore

$$\overline{\Gamma}_S = \gamma_4 \Gamma_S \gamma_4 = 1 \quad \text{and} \quad S = (0,0,0,0). \tag{B.1}$$

The general form of a staggered correlator is

$$C = -(-1)^{\sum_\mu(\delta_\mu + x_\mu)} \mathrm{Tr}(G_\chi(0;x')G_\chi^\dagger(\delta;x))\mathrm{Tr}(\Omega^\dagger(x')\overline{\Gamma}_S\Omega(x)\Omega^\dagger(\delta)\Gamma_S). \tag{B.2}$$

where $\delta = (S+T)\mathrm{mod}2$. So for these scalar representations we obtain,

$$C = -(-1)^{\sum_\mu(\delta_\mu + x_\mu)} \mathrm{Tr}(G_\chi(0;x')G_\chi^\dagger(\delta;x))\mathrm{Tr}(\Omega^\dagger(x')\Omega(x)\Omega^\dagger(\delta)). \tag{B.3}$$

B.1 $1 \otimes 1$ Correlator

For this representation one has $\Gamma_S = \Gamma_T = 1$. Therefore,

$$T = S = (0,0,0,0), \tag{B.4}$$

which means that $\delta = (0,0,0,0)$ and so $x' = x$ and $\Omega(\delta) = 1$. The correlator for this representation is then just simply

$$C_{1\otimes 1} = -(-1)^{\sum_\mu x_\mu} \mathrm{Tr}(G_\chi(0;x)G_\chi^\dagger(0;x)). \tag{B.5}$$

B.2 $1 \otimes \gamma_i$ Correlators

In this section we shall consider the one-link operators.

B.2.1 $1 \otimes \gamma_1$

Here one has $\Gamma_T = \gamma_1$ which implies that $T = (1,0,0,0)$ and so $\delta = (1,0,0,0)$. It then follows that $x' = x + (1,0,0,0)$ and so,

$$\begin{aligned} \Omega(x') &= \gamma_1^{x_1+1}\gamma_2^{x_2}\gamma_3^{x_3}\gamma_4^{x_4} \\ &= (-1)^{x_2+x_3+x_4}\Omega(x)\Omega(\delta). \end{aligned} \tag{B.6}$$

Substituting this into (B.3) one obtains,

$$\begin{aligned} C_{1\otimes\gamma_1} &= (-1)^{\sum_\mu x_\mu}(-1)^{x_2+x_3+x_4}\mathrm{Tr}(G_\chi(0;x')G_\chi^\dagger(\delta;x)) \\ &= (-1)^{x_1}\mathrm{Tr}(G_\chi(0;x')G_\chi^\dagger(\delta;x)). \end{aligned} \tag{B.7}$$

B.2.2 $1 \otimes \gamma_2$

Here one has $\Gamma_T = \gamma_2$ which implies that $T = (0,1,0,0)$ and so $\delta = (0,1,0,0)$. It then follows that $x' = x + (0,1,0,0)$ and so,

$$\begin{aligned} \Omega(x') &= \gamma_1^{x_1}\gamma_2^{x_2+1}\gamma_3^{x_3}\gamma_4^{x_4} \\ &= (-1)^{x_3+x_4}\Omega(x)\Omega(\delta). \end{aligned} \tag{B.8}$$

Substituting this into (B.3) one obtains,

$$\begin{aligned} C_{1\otimes\gamma_2} &= (-1)^{\sum_\mu x_\mu}(-1)^{x_3+x_4}\mathrm{Tr}(G_\chi(0;x')G_\chi^\dagger(\delta;x)) \\ &= (-1)^{x_1+x_2}\mathrm{Tr}(G_\chi(0;x')G_\chi^\dagger(\delta;x)). \end{aligned} \tag{B.9}$$

B.2.3 $1 \otimes \gamma_3$

Here one has $\Gamma_T = \gamma_3$ which implies that $T = (0,0,1,0)$ and so $\delta = (0,0,1,0)$. It then follows that $x' = x + (0,0,1,0)$ and so,

$$\Omega(x') = \gamma_1^{x_1}\gamma_2^{x_2}\gamma_3^{x_3+1}\gamma_4^{x_4}$$

$$= (-1)^{x_4}\Omega(x)\Omega(\delta). \quad \text{(B.10)}$$

Substituting this into (B.3) one obtains,

$$\begin{aligned} C_{1\otimes\gamma_3} &= (-1)^{\sum_\mu x_\mu}(-1)^{x_4}\mathrm{Tr}(G_\chi(0;x')G_\chi^\dagger(\delta;x)) \\ &= (-1)^{x_1+x_2+x_3}\mathrm{Tr}(G_\chi(0;x')G_\chi^\dagger(\delta;x)). \end{aligned} \quad \text{(B.11)}$$

So, in general, the correlator for the $1\otimes\gamma_i$ representation is,

$$C_{1\otimes\gamma_i} = (-1)^{\sum_{\mu\leq i} x_\mu}\mathrm{Tr}(G_\chi(0;x')G_\chi^\dagger(\delta;x)). \quad \text{(B.12)}$$

B.3 $1\otimes\gamma_i\gamma_4\gamma_5$ Correlators

In this section we shall consider the two-link operators.

B.3.1 $1\otimes\gamma_1\gamma_4\gamma_5$

Here one has $\Gamma_T = \gamma_1\gamma_4\gamma_5$ which implies that $T = (0,1,1,0)$ and so $\delta = (0,1,1,0)$. It then follows that $x' = x + (0,1,1,0)$ and so,

$$\begin{aligned} \Omega(x') &= \gamma_1^{x_1}\gamma_2^{x_2+1}\gamma_3^{x_3+1}\gamma_4^{x_4} \\ &= (-1)^{x_3}\Omega(x)\Omega(\delta). \end{aligned} \quad \text{(B.13)}$$

Substituting this into (B.3) one obtains,

$$\begin{aligned} C_{1\otimes\gamma_1\gamma_4\gamma_5} &= (-1)^{\sum_\mu x_\mu}(-1)^{x_3}\mathrm{Tr}(G_\chi(0;x')G_\chi^\dagger(\delta;x)) \\ &= (-1)^{x_1+x_2+x_4}\mathrm{Tr}(G_\chi(0;x')G_\chi^\dagger(\delta;x)). \end{aligned} \quad \text{(B.14)}$$

B.3.2 $1\otimes\gamma_2\gamma_4\gamma_5$

Here one has $\Gamma_T = \gamma_2\gamma_4\gamma_5$ which implies that $T = (1,0,1,0)$ and so $\delta = (1,0,1,0)$. It then follows that $x' = x + (1,0,1,0)$ and so,

$$\begin{aligned} \Omega(x') &= \gamma_1^{x_1+1}\gamma_2^{x_2}\gamma_3^{x_3+1}\gamma_4^{x_4} \\ &= (-1)^{x_2+x_3}\Omega(x)\Omega(\delta). \end{aligned} \quad \text{(B.15)}$$

Substituting this into (B.3) one obtains,

$$\begin{aligned} C_{1\otimes\gamma_2\gamma_4\gamma_5} &= (-1)^{\sum_\mu x_\mu}(-1)^{x_2+x_3}\mathrm{Tr}(G_\chi(0;x')G_\chi^\dagger(\delta;x)) \\ &= (-1)^{x_1+x_4}\mathrm{Tr}(G_\chi(0;x')G_\chi^\dagger(\delta;x)). \end{aligned} \tag{B.16}$$

B.3.3 $1\otimes\gamma_3\gamma_4\gamma_5$

Here one has $\Gamma_T = \gamma_3\gamma_4\gamma_5$ which implies that $T = (1,1,0,0)$ and so $\delta = (1,1,0,0)$. It then follows that $x' = x + (1,1,0,0)$ and so,

$$\begin{aligned} \Omega(x') &= \gamma_1^{x_1+1}\gamma_2^{x_2+1}\gamma_3^{x_3}\gamma_4^{x_4} \\ &= (-1)^{x_2}\Omega(x)\Omega(\delta). \end{aligned} \tag{B.17}$$

Substituting this into (B.3) one obtains,

$$\begin{aligned} C_{1\otimes\gamma_3\gamma_4\gamma_5} &= (-1)^{\sum_\mu x_\mu}(-1)^{x_2}\mathrm{Tr}(G_\chi(0;x')G_\chi^\dagger(\delta;x)) \\ &= (-1)^{x_1+x_3+x_4}\mathrm{Tr}(G_\chi(0;x')G_\chi^\dagger(\delta;x)). \end{aligned} \tag{B.18}$$

B.4 $1\otimes\gamma_4\gamma_5$ Correlator

This correlator has been derived in section 6.6.1.

Bibliography

[1] W. N. Cottingham and D. A. Greenwood, *An Introduction to the Standard Model of Particle Physics.* (Cambridge University Press, 1998).

[2] J. Ellis, hep-ph/0203114.

[3] R. J. Szabo, hep-th/0207142.

[4] S. Weinberg, Phys. Rev. Lett. **19**, 1264 (1974)

[5] S. Glashow, J. Iliopoulos and L. Maiani, Phys. Rev. **D2**, 1285 (1970).

[6] M. Gell-Mann, Phys. Lett. **8**, 214 (1964).

[7] H. Yukawa, Proc. Phys. Math. Society of Japan, **17**, 48 (1935).

[8] G. Zweig, CERN Rep. 8419/TH 412.

[9] R. P. Feynman, *QED. The Strange Theory of Light and Matter* (Princeton University Press, 1998).

[10] R. P. Feynman, Rev. Mod. Phys. **20**, 267 (1948).

[11] D. J. Gross and F. Wilczek, Phys. Rev **D8**, 3497 (1974).

[12] K. Schilling, Nucl. Phys. B (Proc. Suppl.) **83**, 140 (2000).

[13] I. Montvay and G. Münster, *Quantum Fields on a Lattice.* (Cambridge University Press, 1994).

[14] H. J. Rothe, *Lattice Gauge Theories, An Introduction* (World Scientific, 1992).

[15] R. Gupta, hep-lat/9807028.

[16] K. G Wilson, Phys. Rev. **D10**, 2445 (1974).

[17] M. Di Pierro, hep-lat/0009001.

[18] H. B. Nielson and M Ninomiya, Phys. Lett **B105**, 219 (1981).

[19] K. Symanzik, Nucl. Phys. **B226**, 187 (1983).

[20] P. Weisz, Nucl. Phys. **B212**, 1 (1983).

[21] M. Lüscher and P. Weisz, Nucl. Phys. **B185**, 250 (1985).

[22] G. P. Lepage and P. B. Mackenzie, Phys. Rev. **D48**, 2250 (1993).

[23] M. Alford *et al.*, Phys. Lett. **B361**, 87 (1995).

[24] K. G. Wilson, in *New Phenomena in Subnuclear Physics*, ed. A. Zichichi (Plenum Press, 1977).

[25] J. Kogut and L. Susskind, Phys. Rev. **D11**, 395 (1975).

[26] D. B. Kaplan, Phys. Lett. **B288**, 342 (1992).

[27] H. Neuberger Phys. Lett. **B417**, 141 (1998).

[28] B. Sheikholesami and R. Wohlert, Nucl. Phys **B259**, 572 (1985).

[29] P. H. Ginsparg and K. G. Wilson Phys. Rev **D25**, 2649, (1985).

[30] L. Susskind, Phys. Rev. **D16**, 3031 (1977).

[31] M. F. L Golterman and J. Smit, Nucl. Phys. **B245**, 61 (1984).

[32] C. Bernard *et al.*, Nucl. Phys. B (Proc. Suppl.) **119**, 233 (2003).

[33] R. Gupta *et al.*, Phys. Rev. **D43**, 2003 (1991).

[34] H. Kluberg-Stern, A. Morel, O. Napoly and B. Petersson, Nucl. Phys. **B220**, 447 (1983).

[35] C. T. H. Davies, private communication.

[36] T. Blum *et al.*, Phys. Rev. **D55**, 1133 (1997).

[37] J. F. Lagaë and D. K. Sinclair, Nucl. Phys. B (Proc. Suppl.) **63**, 892 (1998).

[38] MILC Collaboration, K. Orginos and D. Toussaint, Phys. Rev. **D59**, 014501 (1999).

[39] MILC Collaboration, K. Orginos, D. Toussaint and R. L. Sugar, Phys. Rev. **D60**, 054503 (1999).

[40] G. P. Lepage, Phys. Rev. **D59**, 074502 (1999).

[41] S. Naik, Nucl. Phys. **B316**, 238 (1989).

[42] G. P. Lepage, Nucl. Phys. B (Proc. Suppl.) **60A**, 267 (1998).

[43] MILC Collaboration, C. Bernard *et al.*, Phys. Rev. **D61**, 111502 (2000).

[44] A. Hasenfratz and F. Knechtli, Phys. Rev. **D64**, 034504 (2001).

[45] HPQCD Collaboration, E. Follana *et al.*, Nucl. Phys. B (Proc. Suppl.) **129**, 447 (2004).

[46] E. Follana, hep-lat/0409062

[47] M. Albanese *et al.*, Phys. Lett. **B192**, 103 (1987).

[48] E. Follana, private communication.

[49] S. Duane, A. D. Kennedy, B. J. Pendleton and D. Roweth, Phys. Lett. B **195**, 216 (1987).

[50] D. H. Weingarten and D. N. Petcher, Phys. Lett. B **99**, 333 (1981).

[51] S. Gottlieb *et al.*, Phys. Rev. **D35**, 2531 (1987).

[52] T. DeGrand, Int. J. Mod. Phys. **A119**, 1337 (2004).

[53] B. Bunk *et al.*, Nucl. Phys. **B697**, 343 (2004).

[54] F. Maresca and M. Peardon, hep-lat/0411029.

[55] D. Adams, hep-lat/0411030.

[56] MILC Collaboration, C. Bernard *et al.*, Phys. Rev. **D64**, 054506 (2001).

[57] MILC Collaboration, C. Bernard *et al.*, Phys. Rev. **D70**, 094505 (2004).

[58] G.S. Bali *et al.*, Phys. Lett. **B309**, 378 (1993).

[59] C. Morningstar and M. Peardon, Phys. Rev. **D60**, 034509, (1999).

[60] A. Hart and M. Teper, Phys. Rev. **D65**, 034502 (2002).

[61] G.S. Bali *et al.*, Phys. Rev. **D62**, 054503 (2000).

[62] UKQCD Collaboration, C. McNeile and C. Michael, Phys. Rev. **D63**, 114503 (2001).

[63] W. Lee and D. Weingarten, Phys. Rev. **D61**, 014015 (2000).

[64] Particle Data Group, S. Eidelman *et al.*, Phys. Lett. **B592**, 1 (2004).

[65] R. Jaffe, Phys. Rev. **D15**, 267 (1977).

[66] B. Berg and A. Billoire, Nucl. Phys. **B221**, 109 (1983).

[67] C. Michael and M. Teper, Nucl. Phys. **B314**, 347 (1989).

[68] M. Teper, Phys. Lett. **B187**, 345, (1987).

[69] M. Lüscher and P. Weisz, Nucl. Phys. **B240**, 349 (1984).

[70] S. Necco, Nucl. Phys. **B683**, 137 (2004).

[71] UKQCD Collaboration, C.R. Allton *et al.*, Phys. Rev. **D65**, 054502 (2002).

[72] R. Sommer, Nucl. Phys. **B411**, 839 (1994).

[73] M. Wingate *et al.*, Phys. Rev. Lett. **92**, 162001 (2004).

[74] M. Wingate *et al.*, Phys. Rev. **D67**, 054505 (2003).

[75] C. T. H. Davies, private communication.

[76] W. Lee and S. R. Sharpe, Phys. Rev. **D60**, 114503 (1999).

[77] JLQCD Collaboration, S. Aoki *et al.* Phys. Rev. **D62** 094501 (2000).

[78] UKQCD Collaboration, P. Lacock *et al.*, Phys. Rev. **D51**, 6403 (1995).

[79] MILC Collaboration, C. Bernard *et al.*, Nucl. Phys. B (Proc. Suppl.) **129**, 230 (2004).

[80] C. Michael, Phys. Rev. **D49**, 2616 (1994).

[81] C. Michael and A. McKerrell, Phys. Rev. **D51**, 3745 (1995).

[82] MILC Collaboration, C. Bernard *et. al.*, Phys. Rev. **D68**, 074505 (2003).

[83] W. Bardeen *et al.*, Phys. Rev. **D65**, 014509 (2002).

[84] S. Prelovsek *et al.*, Phys. Rev. **D70**, 094503 (2004).

[85] C. Aubin and C. Bernard, Phys. Rev. **D68**, 034014 (2003).